Mémoire

Auteur : Dethye, Cyril
Promoteur(s) : Van Grootel, Valérie; 21406
Faculté : Faculté des Sciences
Diplôme : Master en sciences spatiales, à finalité approfondie
Année académique : 2022-2023
URI/URL : http://hdl.handle.net/2268.2/18725

University of Liège
Faculty of Science

Master Thesis: Investigating survivor planets around hot subdwarfs using the Kepler data

Supervisors: Valérie Van Grootel & Francisco J. Pozuelos

Author: Cyril Dethye

Academic Year: 2022-2023

Contents

Abstract

In this work, I will use data from the Kepler mission to investigate hot subdwarfs and the possibility of exoplanets transiting these stars. The goal is to detect transits and constrain by observations the hypothesis of the existence of planets that survived the RGB phase. With planetary formation being more and more understood, this work's goal is to better understand the death, or survival, of planetary systems after their host star has undergone severe changes upon leaving the main sequence. Note that no planets have been confirmed to orbit hot subdwarfs yet. From simulations and theories, it is unclear if such survivors are possible.

Using the SHERLOCK pipeline, I retrieved and investigated many signals in the light curves of hot subdwarfs, and this work will focus on the most promising of such candidates. I focused on detecting short-period planetary candidates, objects that may have survived the RGB phase of their host stars and might have been engulfed in the star's outer layers during this process.

1 Science background

1.1 Stellar evolution

After their formation, stars burn Hydrogen into Helium for millions or billions of years, depending on their masses. This stable portion of stellar evolution is called the main sequence. Helium continuously accumulates in the stellar core as a result of this process, hampering core hydrogen fusion. At some point, the H is exhausted in the core, leaving only He, with the hydrogen now distributed as a shell around the helium core. The temperature for helium fusion is much higher than the one needed for hydrogen fusion, hence the helium core experiences no nuclear reaction at this stage. Therefore, the pressure from the core drops, breaking the hydrostatic equilibrium. The absence of energy from the core allows gravity to take over, leading to gravitational contraction. This gravitational energy is converted to heat, increasing the temperature in the core but also in the hydrogen shell around it, which is now hot enough to undergo fusion. This is the H-shell burning phase. As most stars typically produce more energy by H-shell burning than they did for H-core burning, their luminosity increases. This extra energy also leads to the outer layer's expansion and the surface temperature drops. Hence the creation of a bigger, more luminous, and cooler star; this is the red giant phase. This evolution is illustrated in Fig. 1, where the increase in radius and decrease in surface temperature are clearly visible.

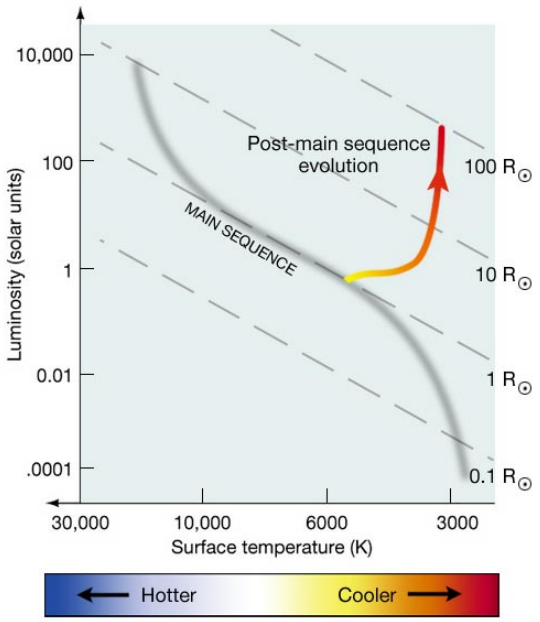

Fig. 1: Illustration of the red giant phase in an HR diagram. Credit: Penn State Astronomy & Astrophysics

Upon entering the red giant phase, a sun-like star would experience an expansion of the order of 100 to 1000 solar radii. This drastic change will greatly affect any planetary system around the host star. In the sun's case, for example, Mercury and Venus are expected to be completely engulfed during the red giant phase, while the Earth's future is still uncertain (see Fig. 2).

At the very end of the red giant phase, the temperature in the core, that had pursued its contraction, is high enough to initiate helium fusion. This ignition creates the so-called helium flash, the energy of which rapidly expels the outer layers and causes the star to lose a more or less high amount of mass, depending on the star. In some cases, so much of the envelope has been expelled that the H-shell burning can no longer be supported, and only the He burning core remains [1]. We are left with relatively small and really hot He-burning stars with an extremely thin H-rich envelope: the hot subdwarfs, the subject of this work.

While the vast majority of stars eventually end up as white dwarfs, one could think the study of these objects would be a more sensible approach to getting information about the fate of post-RGB phase planetary systems. It is worth noting, however, that white dwarfs are typically the result of two giant phases, the RGB, of course, but also a subsequent AGB phase. The latter will significantly affect any surviving exoplanetary system [2]. Hence the study of white dwarfs is deemed inappropriate to the study of RGB effects alone, which is the aim of this work.

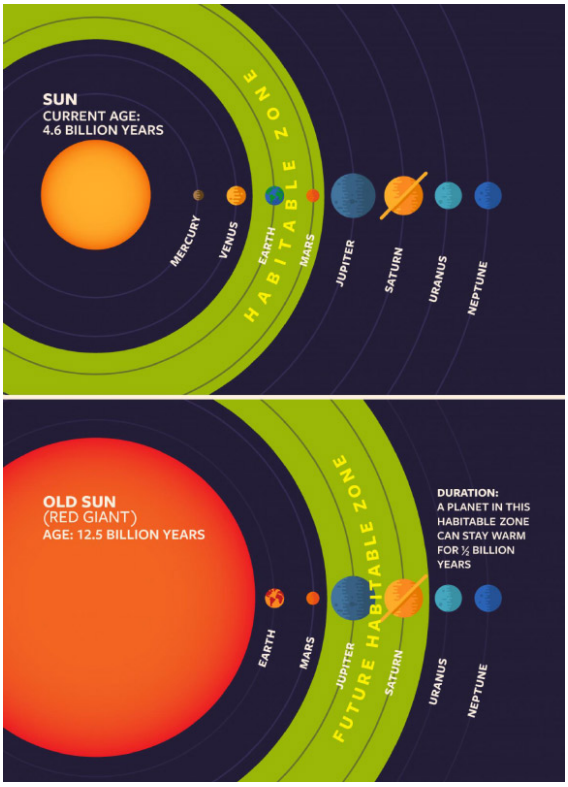

Fig. 2: The sun and our planetary system before and after the red giant phase. Credit: Cornell University

1.2 Hot subdwarfs

Now that we have introduced hot subdwarfs as a possible evolution after the red giant phase let us talk more about these objects and their properties. They are also called subluminous stars since they are below the main sequence for stars of the same spectral type. Stars in the main sequence being referred to as dwarfs, we end up with the subdwarfs classification. Hot Subwarfs (sdO/B) are located in the Extreme Horizontal Branch (EHB) in the HR diagram (see Fig. 3).

In this work, I investigated many types of subdwarf stars, namely sdB, sdO, sdOB, and He-sdOB. These are purely spectral types, giving information about the effective temperature, surface gravity, and some He bands in the atmosphere. These categories don't give any direct information about the star's internal structure. However, this structure is relatively well-known via asteroseismology for some types (namely, the sdBs and sdOs associated with them). In this next session, I will briefly discuss each type of subdwarf.

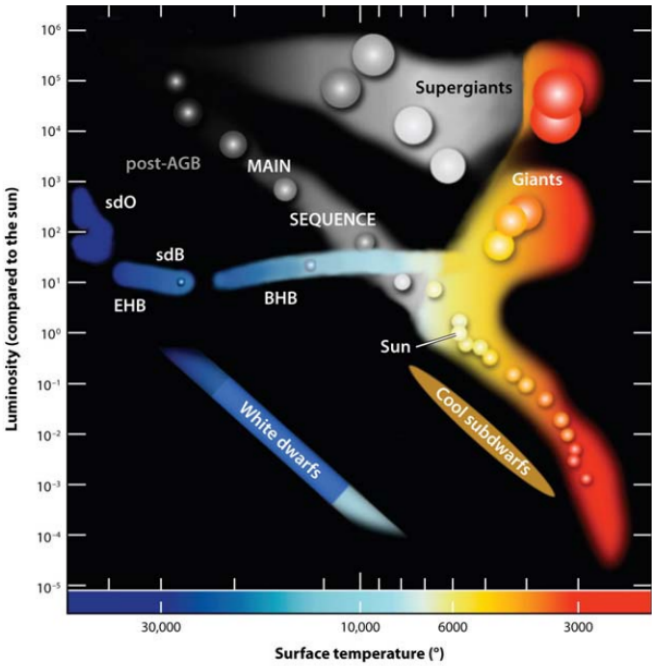

Fig. 3: HR Diagram, with the EHB visible (Heber 2009) [1]

sdB: They are core Helium burning stars, with a thin H-rich envelope and an H-rich atmosphere in most cases ($n_{He}/n_H \leq 0.01$). Helium-rich sdB (He-sdB) are rare, and I did not investigate any such object in this work. Objects from this family have a typical mass of $\sim 0.5 M_\odot$ and effective temperatures ranging between 20,000K and 40,000K. sdB stars have radii typically between 0.1 and $0.2 R_\odot$. One of the most promising theories to account for the formation of sdBs is through the binary formation scenario, and many sdBs are indeed observed in binary systems [1]. Their surface gravity (log g) lies between 5.0 and 6.2 [1] [3]. The internal structure of these objects is relatively well known, thanks to the study of pulsating sdBs [4]. Note that sdBs are a relatively uniform class, unlike the much more diverse sdOs.

sdO: We attribute many origins to sdOs; while some of them are simply the evolution of sdBs, with an O and C accumulating in the core as a result of He burning, leading to He-shell burning, others are the results of post-RGB, post-AGB, mergers, ... Apart from the descendants of sdBs, the internal structure of most sdOs is still subject to speculation. Their mass is similar to sdBs but they have a much higher effective temperature (40,000-80,000K) [5] with a surface gravity typically between 5.0 and 6.5. About 2/3 of sdOs have a He-dominated atmosphere, as opposed to the H-rich atmospheres found in most sdBs. Some sdOs are simply the evolution of sdB stars, they have a surface gravity comparable with sdBs and will be investigated in this work. The internal structures of both sdBs and their sdOs progenies are compared in Fig. 4. Since some sdOs may be post-AGB objects, I won't study any such stars in this work, for the same reason I excluded white dwarfs previously. Post-AGB sdOs are easily recognizable by their lower surface gravity ($\log(g)<5.0$).

sdOB: These are objects exhibiting sdB-like spectra but with weak He II lines. Similarly to previous types, He-sdOBs are Helium-rich sdOBs; a decent amount of these objects were investigated in this work. sdOBs correspond to hot sdBs, with effective temperatures in the 35,000-40,000K range. These stars constitute the transition between sdBs and sdOs.

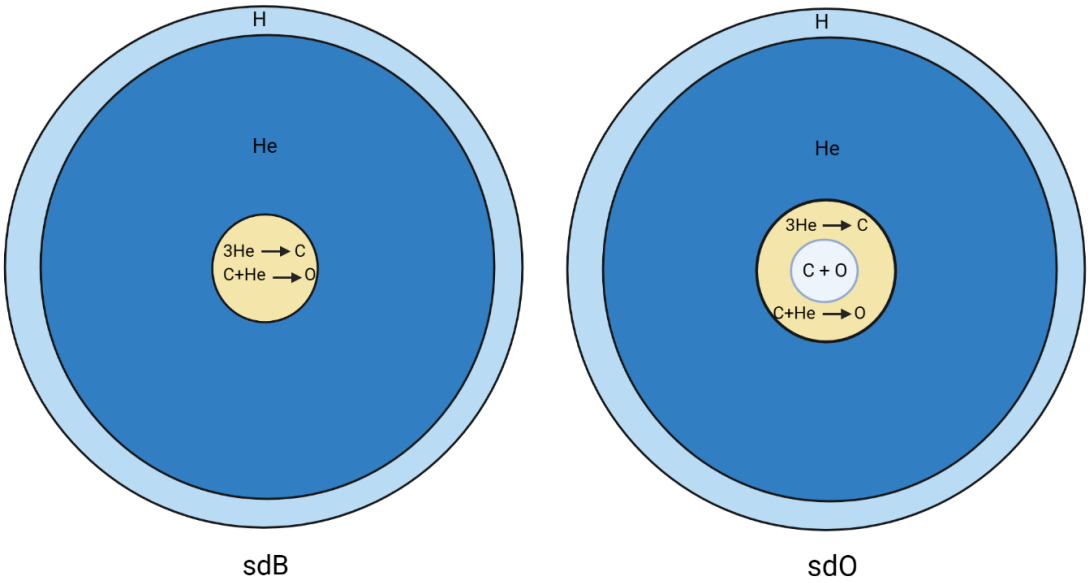

Fig. 4: Internal structure of sdB and their progenies sdO stars. Made with BioRender.

1.3 sdB formation scenarios

We know that hot subdwarfs are the result of extreme mass loss after the RGB phase, leading to the almost complete depletion of the Hydrogen envelope. The mechanisms behind such phenomenon are not yet fully understood, the formation of stars in the EHB is, therefore still an active field of research.

The main formation scenarios explaining this removal of the hydrogen envelope assume a stellar companion. Indeed, when a star is in a close binary system and reaches the RGB phase, its expansion can trigger an unstable mass transfer to its companion. If the companion cannot accrete all this material, a common envelope is formed around the two stellar cores. The two cores spiral inwards, transferring angular momentum to the envelope. This excess of energy will trigger further expansion from the now common envelope which might lead to the near-complete ejection of its material, thus explaining the mass-loss necessary to form hot subdwarfs [6]. This is the common envelope (CE) scenario, one of the main formation scenarios for objects in the EHB. Subdwarfs produced via this formation channel are expected to be in close binaries with an orbital period of only a few days, or even a few hours, as a direct result of the transfer of angular momentum. About 1/3 of hot subdwarfs seem to be in close binary systems [7], which suggests that a CE phase might indeed be responsible for their formation.

Another formation channel occurs when the mass transfer is stable, this is the Roche Lobe

OverFlow (RLOF) scenario. In that case, the companion can accrete the expelled material from the soon-to-be subdwarf and no common envelope is formed. Due to the absence of angular momentum transfer, the binary's orbital period remains unchanged and the end result is a subdwarf in a not-so-close binary system. Orbital periods for subdwarfs formed through such a channel are typically between 20 and 2000 days [8].

Both scenarios explain the vast range of subdwarfs in binary systems but fail to provide an explanation for single EHB objects which account for 1/3 of sdB stars. To account for these stars, a third formation scenario was proposed: the double helium white dwarfs merger. In such a case, two white dwarfs in a close binary system are losing orbital angular momentum via gravitational wave radiation. Once the two white dwarfs eventually merge, a helium ignition occurs and the resulting star is a He-burning sdB [9].

This last scenario explains the existence of single sdBs, but the conditions to have such WD mergers are hard to meet and this formation channel is expected to be rare. Moreover, single sdBs are slow rotators, while the products of such mergers are expected to have a fast rotation.

In this work, I am particularly interested in another formation scenario for single sdBs: substellar interaction. It has been proposed that brown dwarfs and massive planets might contribute to the envelope ejection of their host stars in the red giant phase. We know several systems with sdB + brown dwarf already [10]. In this context, the detection of planetary survivors around single sdBs would put more credit on this specific formation scenario, helping us to better understand how such stars came to be.

1.4 Planetary systems

The effects of the RGB phase on surrounding bodies are still unclear. While it is expected that nearby planets will be engulfed within the giant's envelope, which leads to decreasing orbit, the fate of these engulfed objects is still unknown. It is entirely possible that they are completely destroyed during the interaction but there exists a chance of a least partial survival [11], in particular when the stellar envelope is ejected at some point, which is the case for hot subdwarfs. One could imagine the disintegration of a planet's outermost layers while the planetary core survives. This phenomenon is illustrated in Fig. 5. Some studies also investigate exoplanets accreting material from the stellar envelope, leading to the formation of a binary system with low mass secondary [12]. This phenomenon could explain the extreme mass loss that characterizes the formation of single sdBs, and binary systems of sdBs and brown dwarfs.

It is worth noting that when some planets' orbits decrease due to tidal effects, others can be expelled toward the system's outer regions due to the host star's extreme mass loss [13] [14]. The whole system is also expected to be tremendously destabilized due to changes in orbital resonances. Hence the fate of exoplanetary systems orbiting a star in its RGB phase is a complex thing to predict, and more data concerning potential post-RGB exoplanets is essential. To date, no such planetary system around an sdB star has been detected, although some promising candidates await confirmation.

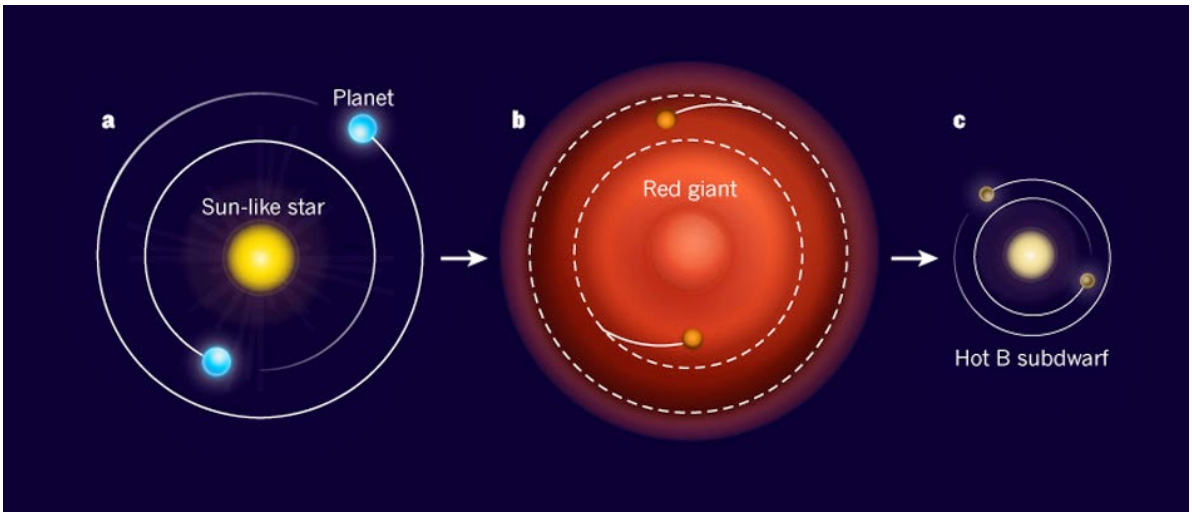

Fig. 5: Schematic evolution of a star and its planetary system before, during, and after the RGB phase leading to a hot sdB. We assume two gas giants (a), from which the outer layers were expelled during the RGB phase (b), leading to two rocky remains closely orbiting the resulting sdB (c). [15]

1.5 Binary systems

Out of the 54 hot subdwarfs investigated in this work, 20 are considered part of a binary system. This is to be expected since about 2/3 of hot subdwarfs are found in binary systems (and among our candidates, some may be unidentified binaries). This configuration often leaves an imprint on the light curves and is to be taken into consideration when trying to find exoplanetary candidates. Unwanted periods can be introduced by the companion (variability, moving stellar spots, etc...) or by the binarity itself, the most obvious example being eclipsing binaries. In most cases, the orbital period of the system is known, allowing us to determine if a signal is a promising candidate for a substellar object or simply the result of artifacts from the binarity. The detrending for such systems is detailed more thoroughly in section 5.

Most of these binary systems exhibit a very typical sinusoidal shape in their raw light curves. Let us take the case of KIC1868650 (aka KBS13), a well-known sdB+dM binary system, with an orbital period of 0.29d [16]. This system is one of our targets and consists of a reflection binary [17]. Reflection binaries occur when one star, here the M dwarf, is much less luminous than the other. In this case, the M dwarfs have a typical luminosity of $\sim 10^{-5} L_\odot$ while the sdB is around $20 - 30 L_\odot$ for a similar size. The M dwarf is illuminated by the sdB, and this illumination depends on the phase, leading to the sinusoidal shape we see on the light curve in Fig. 6. We can easily obtain useful plots for this kind of system, as well as their main parameters, using the Kepler Eclipsing Binary Catalog[1]. The folded light curve in such cases is typically as seen in Fig. 6.

[1] `http://keplerebs.villanova.edu/`

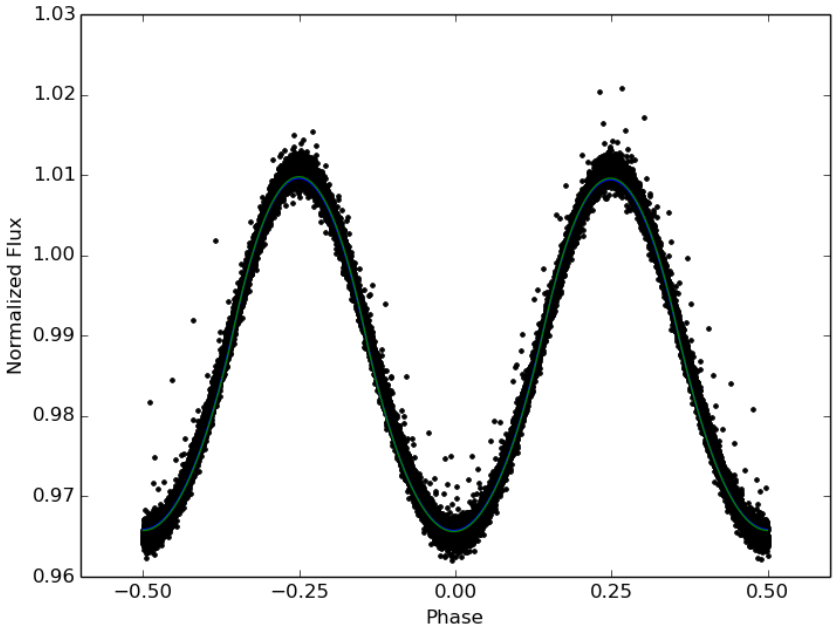

Fig. 6: Folded light curve of KIC1868650, a typical example of a binary system I often encountered in this work. The sinusoidal pattern is clearly visible. Taken from the Kepler Eclipsing Binary Catalog, here using the LC data.

Another example of binary systems with a significant impact on their light curve is KIC7975824 aka KPD 1946+4340, a sdOB+WD eclipsing binary with an orbital period of ≈ 0.40 days. The sdB is deformed by the white dwarf, resulting in an ellipsoidal (rugby-ball) shape. This specific target also exhibits a strong Doppler beaming effect, leading to asymmetry in the ellipsoidal modulations seen in the light curve [18]. This phenomenon is clearly visible in the light curve seen in Fig. 7, as well as the obvious eclipses.

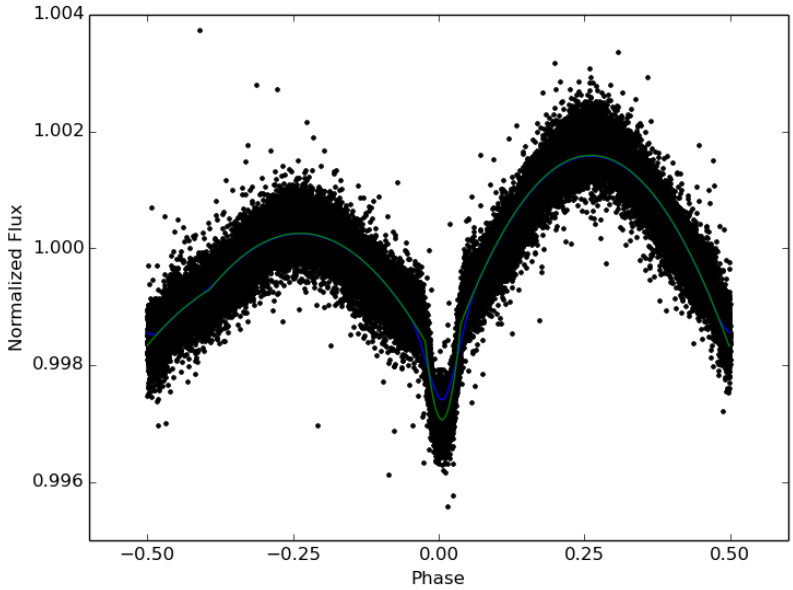

Fig. 7: Folded light curve of KIC7975824, taken from the Kepler Eclipsing Binary Catalog, using LC data. The effect of the ellipsoidal shape of the sdB is clearly visible, its beaming induced asymmetry as well; with the eclipse clearly visible. Note that this light curve is folded, and the different eclipse depths from white dwarf or sdB transit are not shown.

1.6 Scientific goals

In this last subsection, I will summarise the main scientific goals behind this work. As discussed before, the main idea here is to study the evolution of the planetary systems in the post-RGB phase. We put a particular emphasis on the survival of planetary objects that have been engulfed in their host star's outer layers during this RGB phase.

The choice of hot subdwarfs is particularly adapted for such work. We already know they are the direct descendant of stars that underwent this RGB phase, unlike the much more numerous white dwarfs which experienced an AGB phase as well. Hot subdwarfs are also relatively small objects, with a radius between $0.1R_{\odot}$ and $0.3R_{\odot}$. Which, as we know is particularly suited for the transit method (see section 3). These small radii allow the detection of smaller substellar objects, which is ideal for this work where the planets we aim to detect may be of modest sizes after their engulfment.

Finally, hot subdwarfs are short-lived, with a lifetime of ~100 million years for the sdBs and ~10-20 million years for the sdOs. These short lifetimes limit the chances of detecting second-generation planetary systems, or objects that migrated from the outer system, i.e. objects that were not engulfed in the red giant during this phase.

All these properties make the hot subdwarfs ideal targets to search for post-RGB planetary survivors.

2 The Kepler mission

Kepler is a space telescope launched by NASA with the explicit goal of detecting Earth-like planets orbiting a large sample of stars in the Milky Way. The primary Kepler mission took place between May 2009 and May 2013, when a second of its four reaction wheels experienced failure. The Kepler mission was then extended for several years as K2. In this work, I will focus only on targets observed during the primary mission.

The spacecraft continuously observed the same patch of the sky near the Cygnus constellation during the entirety of its primary mission, collecting brightness variations for about 200.000 stars. This region is shown in Fig. 8. However, Kepler only downloaded pixels around certain stars of interest, hence why many stars don't have data for the full duration of the mission. Kepler's pixel size is 27 x 27 microns, which corresponds to 3.98 arcseconds per pixel.

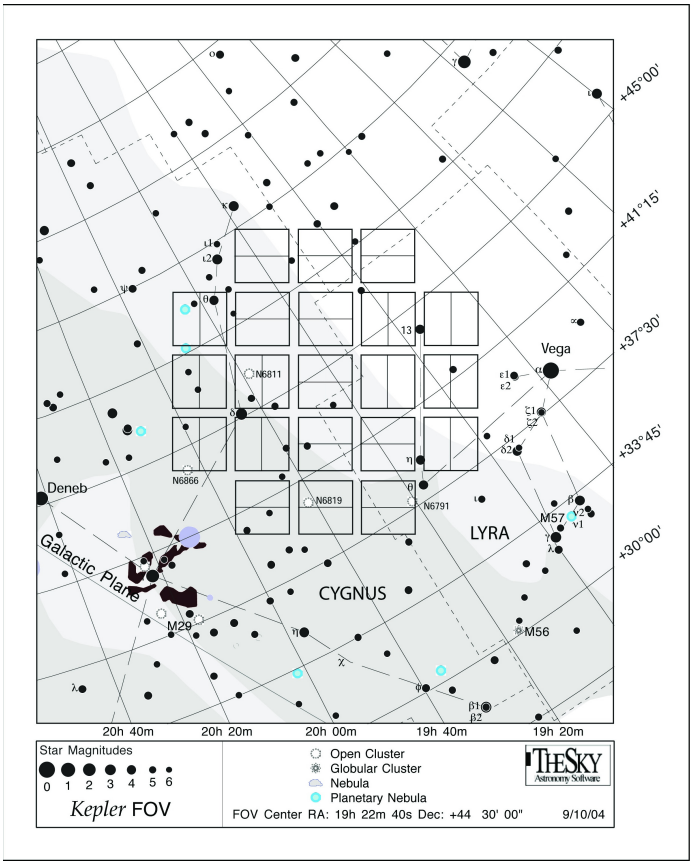

Fig. 8: Kepler's field of view. Credit: NASA AMES

2.1 Cadences

A set of coadded and stored pixels is referred to as a cadence. The Kepler Space Telescope operated at two distinct cadences: Short Cadence (SC) and Long Cadence (LC). Each

cadence consists of a series of frames consisting of 6.02s of exposure time and 0.52s of read-out time. The LC data consists of 270 frames, totaling exactly 1765.5s. Note that in our program, we indicate LC data as having an exposure time of 1800 seconds (see section4). The SC data consists of only 9 frames, for a total duration of 58.85s. Again, in our program, we indicate SC data by setting an exposure time of 60 seconds. These frames stacked together constitute a Full Frame Image (FFI). One can immediately see the difference in time resolution between these two cadences, and SC data will prove typically more useful to search for short-duration transits since we have roughly one data point per minute. The typical transit duration in front of an sdB star for a planet with an orbital period of 10 hours would be ~ 20 minutes, slowly increasing with the orbital period. LC data, with one data point roughly every 30 minutes, will prove to be more challenging to use for our transit search.

Light curves in short cadence are heavier in terms of raw data and are expected to take more computation time to analyze. In this work, however, targets observed in SC data were typically not observed for nearly as long as in LC data. This trade-off, a better time resolution for a shorter duration, allowed us to take advantage of this shorter cadence.

2.2 Quarters and Subquarters

The probe would rotate by 90 degrees every 90 days to keep its solar panels lit, interrupting observations for a few hours (see fig. 9). Hence the data from Kepler are typically divided into "Quarters" of 90 days each. The notable exceptions are Q0 which only lasted ten days, and Q1, with 33.5 days.

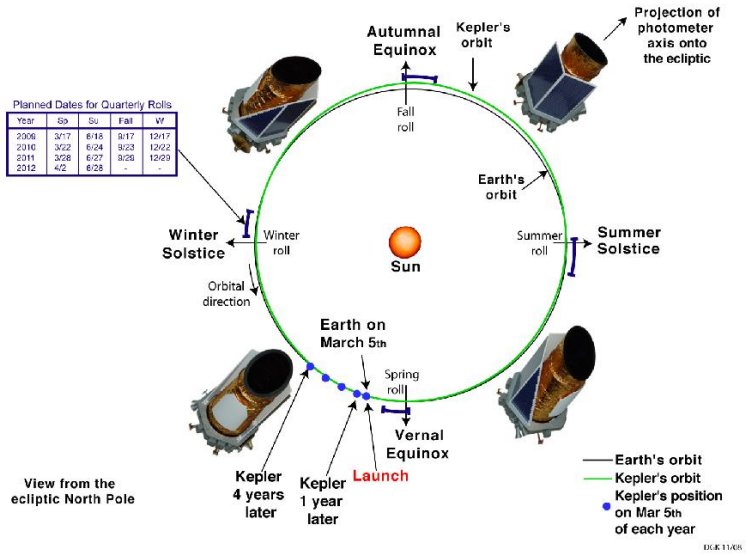

Fig. 9: Kepler's Earth-trailing orbit around the sun, during its primary mission. Source: NASA

The mission was nominal until Quarter 17, interrupted by the failure of a second reaction wheel. Furthermore, the short cadence allows us to switch targets every month; hence quarters in SC data are often divided into subquarters of one month each. Notations such as Q5.2; the second month of the 5th quarter, are therefore common when dealing with short cadence data.

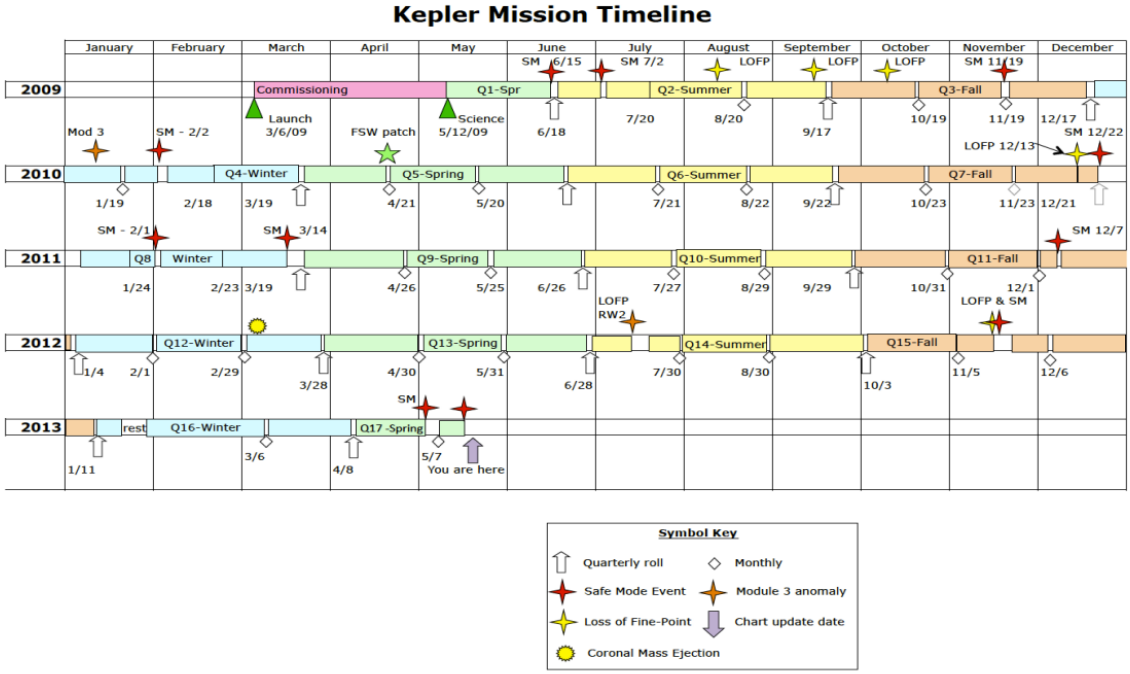

Fig. 10: Timeline of Kepler's primary mission, spanning all 17 quarters. Credit: Kepler Data Characteristics Handbook, 2016.

Figure 10 represents the entire timeline for Kepler's primary mission. The Quarterly rolls mentioned before are clearly visible every three months, as well as the subquarters. Data were downlinked every month, momentarily stopping data collection. The abrupt stop mid-quarter 17 is also represented. This figure is particularly useful to see the major anomalies that occurred during these four years, as these may have an impact on our data.

The Loss Of Fine Point (LOFP) corresponds to the spacecraft momentarily losing fine pointing control, leading to a decrease in photometric data. Affected cadences are usually masked.

Figure 10 clearly showcases many instances of gaps in the data. Some are expected, such as the aforementioned Quarterly rotations or data monthly downlinks. Others are due to the spacecraft unexpectedly entering safe mode for various reasons. Additionally, some cadences were manually removed in the MAST data, usually near gaps or discontinuity in the data that would make an automatic correction tedious, or due to LOFP. In this work, particular attention has to be given to these gaps, as many instances of transits seemingly cut in half can lead to false positives. Boundaries between quarters or data gaps also show behavior

that can lead to false detection if not well corrected. Specifically, it has been noted that the flux after an interruption in data collection often shows a "dip", which can be interpreted as a transit if not taken into account (see Fig. 11 and 12). Such regions are often manually masked if they pose an issue.

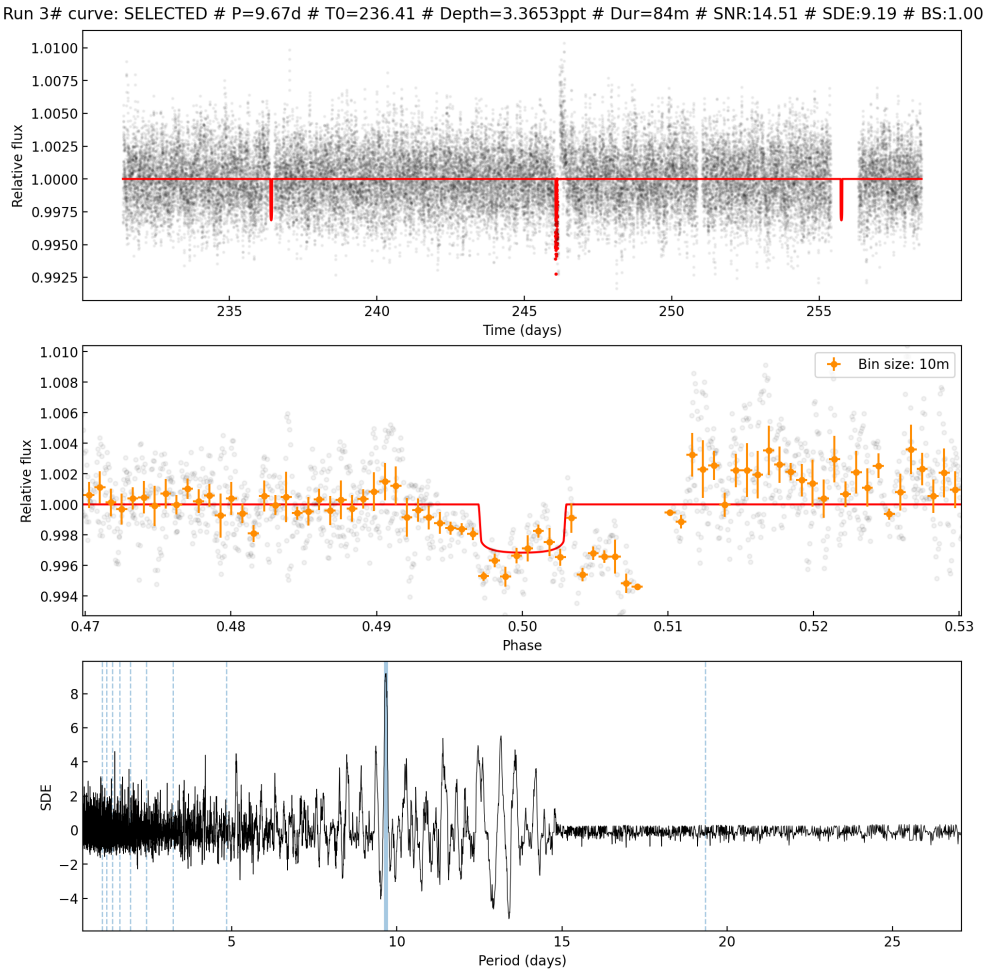

Fig. 11: Typical example of bad behavior near data gaps interpreted as a transit. Here for the hot subdwarf KIC8022110, in Q2.3 SC. The dip right before data interruption is clearly visible, both in the whole detrended light curve (top plot) and the middle plot. This candidate is obviously discarded.

2.3 Data

The data collected by Kepler are available for use on the MAST (Mikulski Archive for Space Telescopes[2]). The monthly FFI's and the light curves can be found in the archive. In this work, I am interested in these light curves, which can be found both in LC and SC when available. The light curve files consist of two parts, the SAP_Flux (Single Aperture Photometry), which corresponds to uncorrected light curves, and the systematic error-corrected

[2] `https://mast.stsci.edu/portal/Mashup/Clients/Mast/Portal.html`

PDCSAP_Flux (Pre-search Data Conditioning SAP). The SAP is contaminated by systematic artifacts and pointing drifts, making it a less-than-ideal option to study precise astrophysical phenomena such as shallow planetary transits. Such systematic errors are removed in the PDCSAP_Flux using the PDC pipeline [19]. Throughout the entirety of this work, the PDCSAP flux will be used.

The MAST allows us to visualize the light curve, which is particularly useful to manually check for obvious issues, such as stellar flares, bad photometry, too many data gaps, etc. This visualization is shown in Fig. 12.

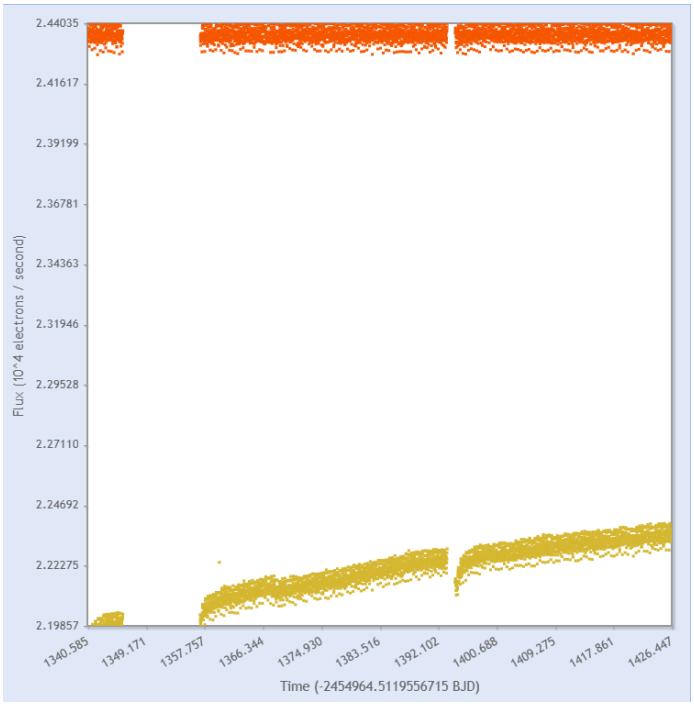

Fig. 12: Light curve as seen from the MAST. Here for KIC7975824, Q16 in LC. The yellow curve is the uncorrected SAP Flux, whereas the orange one is the PDCSAP Flux, showcasing clearly the corrections made by the PDC pipeline. Note that the data gaps seen here correspond perfectly to what is showcased in Fig. 10. The behavior aforementioned in data gap boundaries is also clearly visible in the SAP flux.

3 Method & data

3.1 Transit

There are various ways to detect substellar objects orbiting a nearby star, as a planet influences the signal we receive from its host star.

In this work, I will exclusively use the transit method, as it is the method employed by Kepler to detect exoplanets. This method is relatively straightforward and relies on the partial occlusion of the host star by a transiting planet, provided the observer is located

in the direction of the planet's orbital as illustrated in Fig. 13. The exoplanet blocking a portion of the star's light, a small decrease in its apparent brightness can be observed, allowing for the planet's detection.

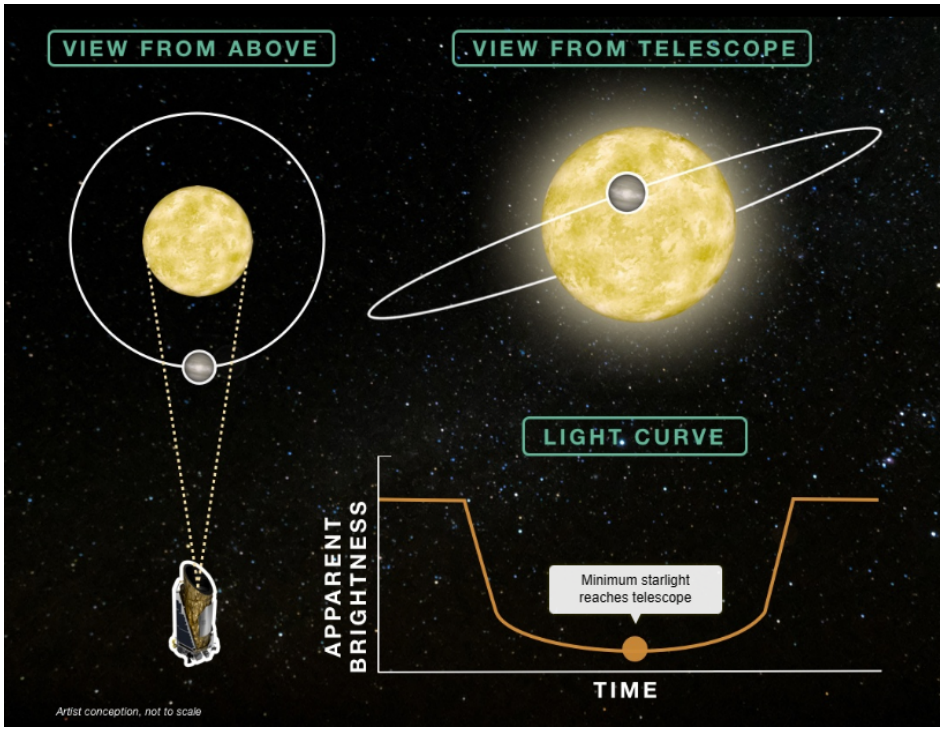

Fig. 13: Artist view of a transit event, conveniently showing observation from the Kepler Space Telescope as an example. Credit: Viewspace[3]

Using this method, we can expect two distinct changes in the flux: the transit itself, as well as the occultation, where the planet is masked by the star and its reflection no longer contributes to the total received flux, as represented in Fig. 14. Note however that the transit is typically much deeper than the occultation, making the latter difficult to observe.

[3] https://viewspace.org/interactives/unveiling_invisible_universe/detecting_other_worlds/transiting_exoplanet

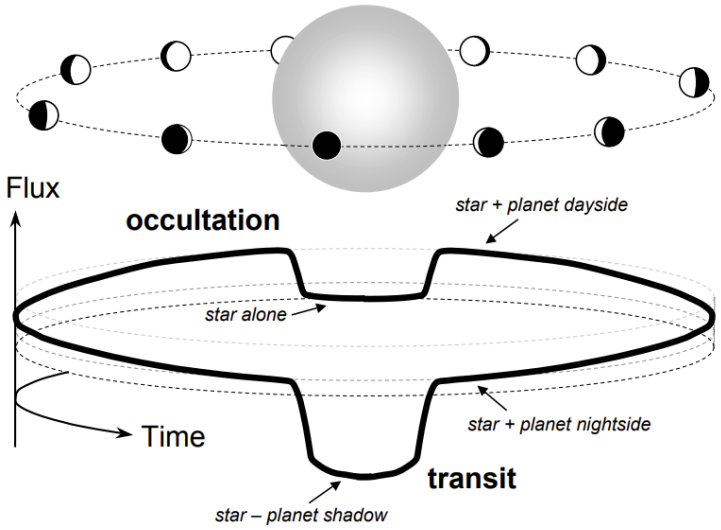

Fig. 14: illustration of transit and occultation phenomena. Credit: Winn 2010 [20]

The depth and duration of a transit depend on the planet's orbital period as well as its radius. A relatively large planet orbiting a smaller star will block more of its light, leading to a deeper transit, easier to detect. In this report, I work with hot subdwarfs, these stars are relatively small, but the planets I expect may also be small since they may be remnants of massive planets that were engulfed in their host star during the RGB phase.

Note also that very precise geometric conditions have to be met in order to observe such events since the observer needs to be nearly perfectly aligned with the planet's orbital plane. Planets orbiting a distant star will project a shadow in the celestial sphere. Only the observers fortunate enough to be located in this shadow band can hope to see a transit. This geometric configuration is illustrated in Fig. 15.

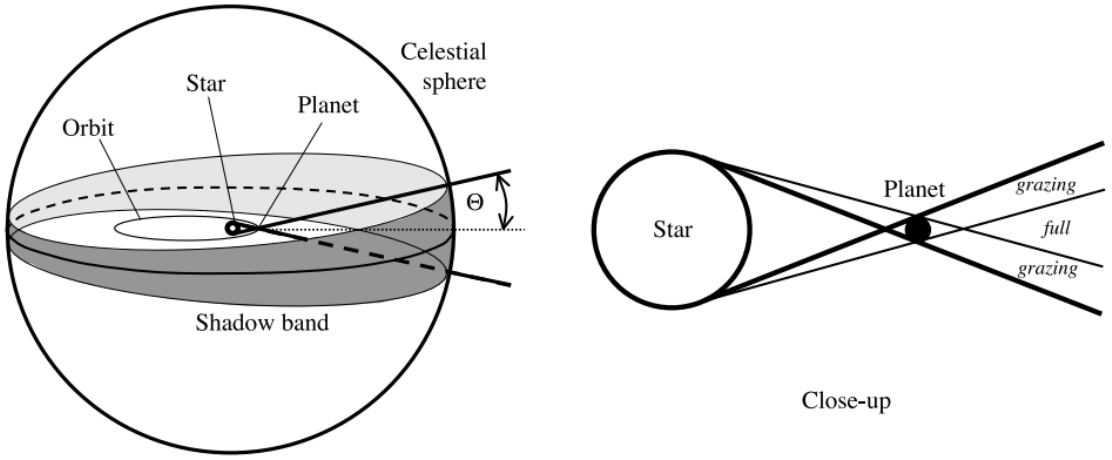

Fig. 15: Illustration of the shadow band. In the left panel, a representation of the shadow band and its associated cone with an opening angle Θ. The right panel described the penumbra (grazing) and the antumbra, where the transits are full. Credit: Winn 2010 [20]

Winn et al. [20] describe the probability of meeting this configuration as follows:

$$p_{tra} = p_{occ} = \frac{R_\star}{a} \approx 0.005 \frac{R_\star}{R_\odot} \left(\frac{a}{1AU}\right)^{-1}$$

where p_{tra} and p_{occ} are the probability for transit and occultation respectively, $R_\star$ is the star's radius, $R_\odot$ the sun's radius and a the planet's semi-major axis.

Let us calculate transit probabilities for a typical case of a hot subdwarf. We assume a star of $0.15 R_\odot$ with a mass of $0.5 M_\odot$. We also represent the period of a planet orbiting such stars to better link these probabilities with our results.

Transit probabilities for various planetary scenarios							
T [days]	0.1	2	10	50	200	514	1600
a [AU]	0.0035	0.025	0.072	0.21	0.53	1	2.1
P_{tra} [%]	~ 21	~ 3	~ 1	0.36	0.14	0.075	0.036

These relatively low probabilities are the main disadvantage of the transit method. Another disadvantage is the relatively high number of false positives, especially for weak signals we expect to find. Any variation in the light curve could be falsely interpreted as a potential transit, and more observations are often necessary to confirm a candidate.

Note also that since the probability of transit decreases with distance (see above), we have higher chances of detecting objects that are now close to their star and would correspond to planets that have been engulfed. For the solar system, for example, the limit to escape engulfment during the RGB phase is close to 1AU, where transit probability is extremely low.

3.2 Strategy and choice of data

I aim to find relatively small planets orbiting close to their stars for this work. Planets with Earth-like radii or even smaller, with periods of only a few days, would not be surprising at all around hot subdwarfs since we investigate remnants of massive planets that were engulfed. The vast majority of targets I investigated in this work had only a few quarters in SC data, reducing the required computation time, even with this higher time resolution. The worst-case scenario is stars for which only one subquarter (30 days) is available. Even with such a short observation time, any planet with a period of only a few days would be detectable, with the upper limit being placed at P=15d, beyond which two occurrences of transit are no longer guaranteed.

The strategy applied in this work is the following: I will focus on the SC data to search for transiting planetary candidates. For the promising signals detected, I will try to confirm them using other data sets when possible. This could be using LC data from Kepler when the duration is long enough, light curves from TESS if the target has been observed, or ground-based follow-ups if the target is bright enough and the transit deep enough to be observed by telescopes such as TRAPPIST.

I used the injection-and-recovery results from Van Grootel et al. 2021 [21] to know what planets I can expect to detect around our hot subdwarf stars. This work performed injection-and-recovery tests for a series of representative Kepler targets for one subquarter (30 days) to one full quarter (90 days). In this work, we see that for the relatively bright KIC8054179 (G=14.34), using an entire quarter (90 days of data), planets as small as $0.3R\oplus$ for an orbital period of one day could be detected. This value increases with the period, but Earth-like planets can still be detected for periods of 25 days. On the other end of the spectrum, fainter targets such as KIC5342213 (G=17.7) provide poorer results, as expected. These results are shown in Table 1.

Table 1: Minimum size of planets in units of $R_\oplus$ detectable in typical light curves with a $\gtrsim$ 90% recovery rate. All stars have $0.175 \pm 0.025\ R_\odot$ and $0.47 \pm 0.03\ M_\odot$.

Object ID	G Mag	Data length (d)	1 d	5 d	15 d	25 d	35 d
Kepler							
8054179	14.3	90	0.3	0.5	0.8	1.0	1.2
		30	0.5	0.6	1.0	–	–
3353239	15.2	30	0.6	0.8	1.1	–	–
5938349	16.1	30	0.7	1.1	2.0	–	–
8889318	17.2	30	0.9	1.2	2.4	–	–
5342213	17.7	30	1.2	1.7	3.2	–	–

These injection and recovery tests let us know what planets we can expect to find around hot subdwarfs in Kepler data. Most of our targets have a magnitude higher than 15 (see section 3.3), and we expect to be able to detect objects as small as $0.6R\oplus$ for the lower periods.

3.3 Dataset

The full list of investigated targets and their magnitude, class, and quarters of available data from Kepler can be seen in Table 4 in the annex. The magnitude is given in Kepler's bandpass (400-850nm), hence the "Kp" notation. Most of our targets were relatively faint (Kp>15.0), which impacts the minimum planet size we can expect to detect (see Table 1). About a third of investigated hot subdwarfs had Kp>17.0. These targets correspond to non-pulsator hot subdwarfs. These are relatively calm stars, ideal for our search.

In this report, I searched 54 stars in total. 47 of these are sdB/sdOB, and the remaining 7 are post-sdB sdO stars.

All targets are available in at least one subquarters in SC, which is what I will focus on.

4 The SHERLOCK pipeline

SHERLOCK (Searching for Hints of Exoplanets fRom Light curves Of spaCe-Based seeKers) is a pipeline designed to search for exoplanetary candidates using data from space-based missions, such as TESS or, as investigated in this work, Kepler [22]. In this section, I will detail the inner working of SHERLOCK, as this pipeline was the main tool I used for exoplanetary detection; hence understanding SHERLOCK is crucial to interpret our results correctly.

To perform a search, SHERLOCK has six modules, used to (1) acquire and prepare light curves from the MAST, (2) search for exoplanetary candidates, (3) vet the most promising candidates, (4) perform a statistical validation, (5) model the signals to refine their ephemerides and (6) compute observational windows for ground-based follow-up when it is possible. My humble contribution to SHERLOCK was mainly in bug fixing and optimizing the pipeline specifically for Kepler data, whereas TESS data had mainly been used prior.

SHERLOCK uses the LIGHTKURVE package [23] to download the Kepler light curves from the MAST, giving us access to both long and short cadence data for each target (see more in section 2). These light curves are then detrended using the Wōtan package [24], and exoplanetary detection is performed via the TLS (Transit Least Square) package [25].

Before I began my work on subdwarfs, I analyzed three main sequence stars for which exoplanets had already been confirmed. This first phase was crucial to learn how to use SHERLOCK in a controlled environment since I knew what results were expected in advance. In the following sections, I will use these test targets as examples to showcase how SHERLOCK typically works.

The test targets are the following:

Test targets			
	Kepler-21	Kepler-445	Kepler-1649
Spectral type	F6IV	M4V	M5V
Exoplanets	1	3	2
Cadence	LC/SC	LC/SC	LC
ID	KIC3632418	KIC9730163	KIC6444896

With the following confirmed exoplanets:

Test targets confirmed exoplanets			
	Orbital Period (d)	Planetary radius ($R_\oplus$)	semi-major axis (AU)
Kepler-21b	2.79	1.639	0.0434
Kepler-445b	2.98	1.58	/
Kepler-445c	4.87	2.51	/
Kepler-445d	8.15	1.25	/
Kepler-1649b	8.70	1.017	0.0514
Kepler-1649c	19.53	1.06	/

Note that these candidates come from a confirmed exoplanetary detection around a main sequence star. This is therefore an ideal case, for practicing and learning how SHERLOCK works.

Let us take Kepler-445 as our main example here, as we have multiple confirmed planets and both LC and SC data to analyze. To execute all of SHERLOCK's modules, I fill a YAML file containing all the target's information. This file contains the star's ID, exposure time to analyze LC and SC data separately, the maximum number of runs SHERLOCK can perform, etc...

```yaml
# Run with:
# nice -15 python3 -m sherlockpipe --properties input.yaml

TARGETS:

  'KIC 9730163': # Star's identifier (TIC/KIC/... number)
    SECTORS: [6, 8, 9, 12, 13, 14, 16, 17] # 'all'
    EXPTIME: 1800
    INITIAL_SMOOTH_ENABLED: True
    INITIAL_HIGH_RMS_MASK: False
    INITIAL_HIGH_RMS_THRESHOLD: 1.5
    DETREND_METHOD: 'biweight'
    DETRENDS_NUMBER: 12
    #DETREND_CORES: 80
    MAX_RUNS: 4 # 4
    SNR_MIN: 6 #<0xa0>6
    SDE_MIN: 7 # 7
    #CPU_CORES: 80
    OVERSAMPLING: 3

    #FILE: 'TIC1234567890_light_curve.csv' # name of a .csv file containing a light curve to use instead of the one from the MAST
    #INITIAL_MASK: [[1901, 1903],<0xa0>[1912, 1918]] # [[1550, 1551], [1560, 1561]] | [[1656, 1657]]
```

Fig. 16: Example of a typical .yaml file used in this work. Here for Kepler-445 (KIC9730163), in long cadence (exptime=1800s) for many quarters.

Let us detail the parameters used in this file:

• **SECTORS**: For Kepler, this line corresponds to the quarters we want to use. We can manually choose which ones we want to analyze.

• **EXPTIME**: Simply the exposure time. For Kepler, this line allows us to choose between long cadence data (1800s) and short cadence data (60s).

• **INITIAL_SMOOTH_ENABLED**: When set to true, this will apply a Savitzky-Golay (Sav-Gol) filter to smooth our data and allow for better values of SNR. More detail below.

• **INITIAL_HIGH_RMS_MASK**: When set to true, automatically masks the noisy regions where the RMS (Root Mean Square) is too high.

• **INITIAL_HIGH_RMS_THRESHOLD**: Define the threshold for applying the high RMS filter.

• **DETREND_METHOD**: Specifies the method used to detrend the light curves. We used the biweight method by default throughout this work.

• **DETRENDS_NUMBER**: Number of detrends per run.

• **DETREND_CORES**: The number of CPU cores allocated to perform the initial detrend. Useful when sharing a machine with others.

• **MAX_RUNS**: The maximum amount of runs SHERLOCK is allowed to do before stopping. Useful to reduce calculation time.

• **SNR_MIN**: The minimum value of SNR that SHERLOCK considers as promising. If the last candidate has a lower SNR value, the search stops, as we have "seen everything worth seeing."

• **SDE_MIN**: Exact same idea as before, for the SDE

• **CPU_CORE**: The number of CPU cores allocated to perform the entire calculations after the detrending.

• **OVERSAMPLING**: A factor to be multiplied by our period grid to make it denser and hence conduct a more sensitive search for planetary signals

• **FILE**: Used to analyze a light curve directly from a file, not downloading it from the MAST. Mainly used when we cleaned some targets using Felix instead of the built-in SHERLOCK tools.

• **INITIAL_MASK**: Used to manually mask a region of data, providing an array of days we want to get rid of. Useful when clear issues are seen in the light curve, such as stellar flares or systematics from Kepler (issues at quarter boundaries, anomalies, ...)

The Sav-Gol filter was used for all of our runs, as it allows us to lower the noise and therefore enhances the SNR while the SDE remains the same. In the example below, it is

found that the SNR without Sav-Gol is ≈ 13, while the SNR using this filter is ≈ 27. Example found in the SHERLOCK tutorials[4].

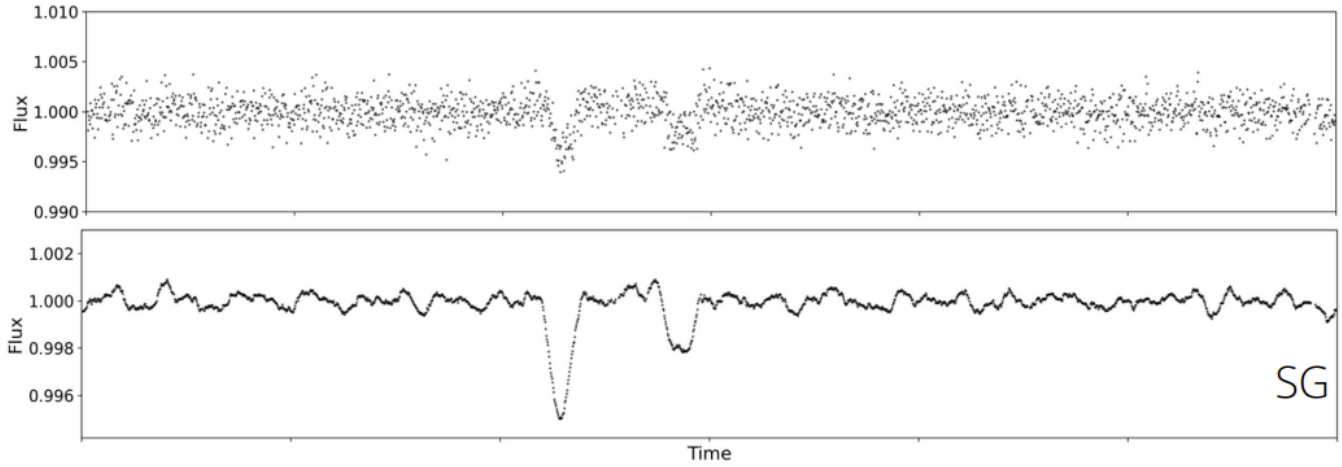

Fig. 17: Example of the Sav-Gol filter applied to a typical light curve. Above with no filter, below with Sav-Gol applied.

The high RMS mask was particularly useful for masking noisy regions in our data. When enabled, we are able to check what points have been masked to see if the selected threshold is right. In the test target I used so far, the high RMS mask was not necessary; hence I use KIC6188286, one of our hot subdwarfs as an example instead in Fig. 18.

[4]https://github.com/iaa-so-training/sherlock-tutorial/blob/main/Jupyter_Notebooks/sherlock_algorithm.ipynb

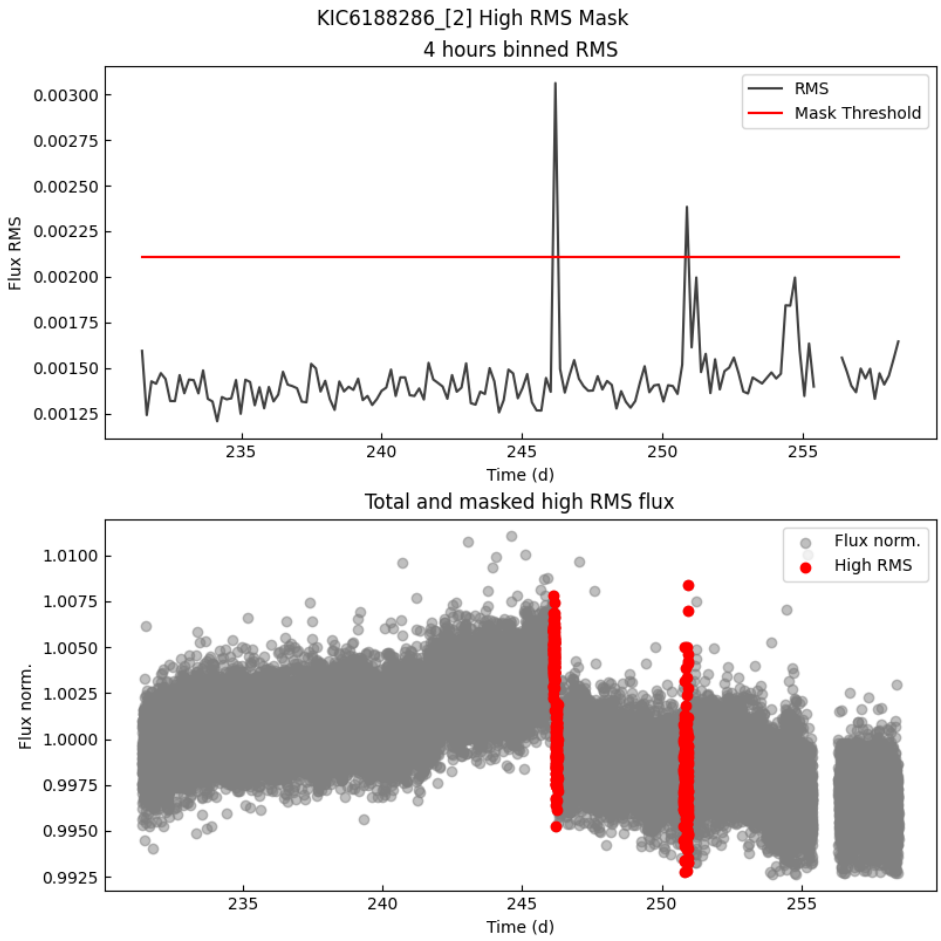

Fig. 18: Example of high RMS mask applied to KIC6188286. Noisy regions related to data gaps are clearly visible. These plots are particularly useful for manually checking if our threshold value is appropriate.

Short cadence data were typically clean, with little to no use of the RMS filter most of the time, as Kepler has high photometric precision in such cadence. Long cadence data, however, often needed more attention in this regard.

Before actual calculations, one would often run SHERLOCK in explore mode. This is a useful tool allowing us to perform only the detrending. In explore mode, SHERLOCK stops right before the detection phase begins, allowing us to check if the detrending was satisfactory, the RMS mask and threshold were appropriate, or if any strong variability (binary system, etc.) was properly removed without having to wait for the whole run to finish. Since some targets can take days of computation time, this extra step is crucial to ensure the conditions are met to detect any potential transit beforehand.

Using the parameters seen in Fig. 16, SHERLOCK will download our target's light curves, detrend them and try to find possible candidates. For every run, the most promising candidate is selected and masked to search for other possible signals, allowing for the detection of multiple planets. The computations will stop once one of these two conditions are met: (1)

the maximum amount of runs have been performed (4 runs in the example above, as stated in line 15), (2) the last candidate had SNR and SDE values below the minimum (line 16 and 17 in the example above). From this workflow, we expect the candidate found in run 1 to be the most promising and the signals found in the next runs to be weaker.

To perform the detrending, the Wōtan package uses a rectangular window as a kernel smoother. The window length is an important parameter, as it should be as short as possible to remove stellar variability but also long enough to preserve the transits. Note also that the same window length will remove or preserve transit of different periods.

To account for this behavior, SHERLOCK uses a multi-detrend approach. Each run performs a given amount of detrend with increasing window sizes. The user chooses this amount, and I use 12 detrends by run as the default value. See Fig. 113 for multi-detrend performed by SHERLOCK. Due to the multi-detrend approach we just described, many of our candidates will be spotted in multiple detrends, i.e., for multiple window lengths throughout a run or even spread across many runs. The number of detrends in which a signal appears is a good indicator of the signal strength; hence I will put more credit on signals detected in many detrends.

4.1 Initial test results

Let us now see the results from the SHERLOCK's search on our test target. We will first look at two things: (1) the candidate log, which summarizes the selected candidates from each run, and (2) the SHERLOCK output from each of these candidates.

Listing most promising candidates for ID KIC9730163_[6, 8, 9, 12, 13, 14, 16, 17]:

Detrend no.	Period	Per_err	Duration	T0	Depth	SNR	SDE	FAP	Border_score	Matching OI	Harmonic	Planet radius (R_Earth)	Rp/Rs	Semi-major axis	Habitability Zone
0	4.8712	0.00046	68.17	542.83	5.671	30.76	189.91	0.000080	0.97	nan	-	2.47185	0.07014	0.03674	I
1	2.9842	0.00017	55.34	541.95	1.803	17.87	206.35	0.000080	0.99	nan	-	1.39366	0.03954	0.02650	I
2	8.1526	0.00018	76.35	541.84	0.989	6.80	470.96	0.000080	0.99	nan	-	1.03245	0.02843	0.05179	I
0	0.5516	0.00001	3.52	539.80	1.946	7.04	12.54	0.000080	1.00	nan	-	1.44798	0.01990	0.00860	I

Fig. 19: Candidate log for Kepler-445, in which we directly see the three expected planets have indeed been detected.

Fig. 19 directly shows the retrieved candidates for each run. The three planets we expected to detect are indeed present in the three first runs. This candidate log is extremely useful to give a quick idea of the detection made as well as their quality since we can directly see important information, such as each candidate's SNR, SDE, and transit depth, among others. To go further, we must examine each signal separately to determine if they are promising candidates fit for further analysis.

Two values mainly determine the interest of a candidate at first; the SNR (Signal to Noise Ratio) and the SDE (Signal Detection Efficiency) computed by the TLS package. The SDE is obtained as per Kovács et al. 2002 [26]. When investigating hot subdwarfs, I consider a signal to be strong and, therefore, possibly promising when SNR>5 and SDE>7. I chose relatively low values for the SNR and SDE since the expected signals for such targets may be weak. We are looking for planets remnants that have been engulfed in their star during the RGB phase; hence the planets orbiting such stars may be small and fairly hard to detect.

The greater these two values are, the better. The border score (BS) is also important to consider since it gives us information about whether or not our transits are located at the border of a data gap, which can lead to false detection. A perfect value would be BS=1.

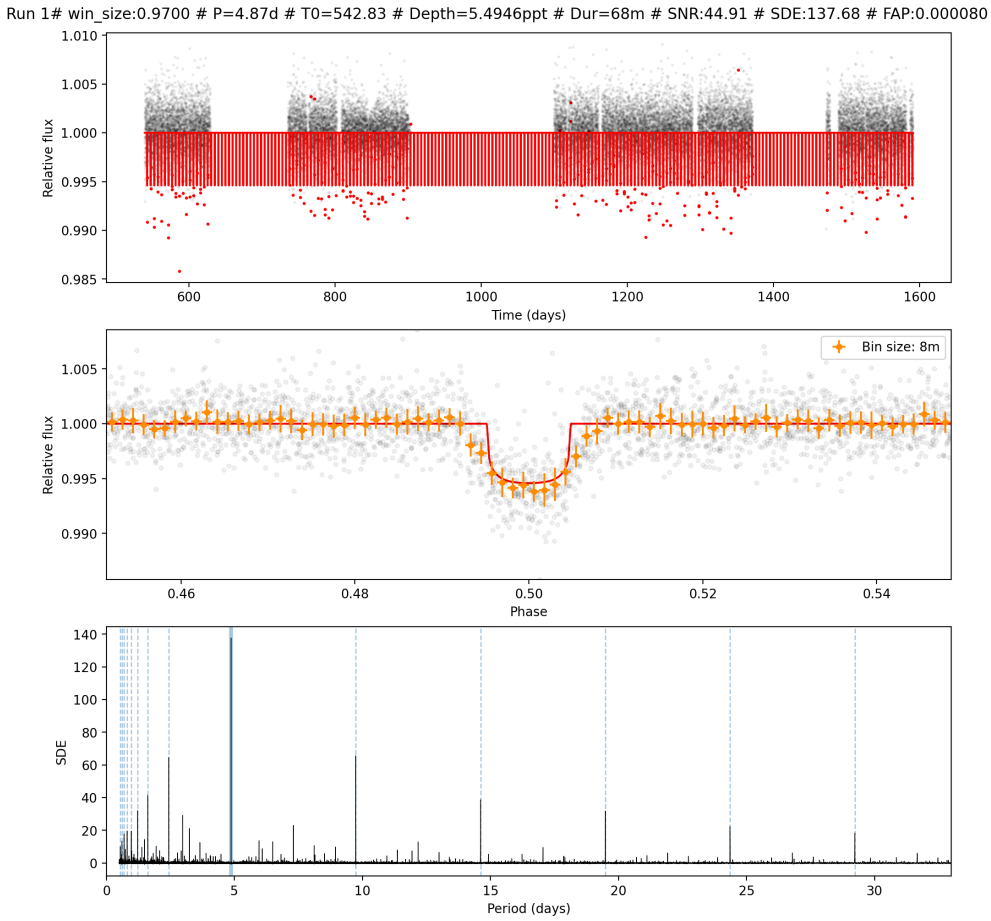

Fig. 20: Output for the first run of our test target.

Figure 20 is composed of three distinct parts:

(1) The upper-most graphic shows the detrended light curves. The red lines correspond to expected transits, which are numerous in this case since we have years of data and an orbital period of only a few days. This first panel is especially useful to investigate gaps in the data, light curves not correctly detrended, possible stellar flare still visible in our light curve, etc...

(2) The middle panel represents the folded light curves centered around the presumed transit at phase 0.50. In this case, the transit shape is clearly visible, with no alarming behavior, except a bit of a V shape, which could be the sign of an eclipsing binary instead. This scenario will be ruled our later though.

(3) The bottom panel displays the SDE as a function of the period. The semi-transparent

blue line represents the detected period, while the dotted lines represent the associated harmonics and sub-harmonics. A good signal is expected to show harmonics, as is clearly the case in the example, where very clear harmonics are spotted at around 10, 15, 20, and 25 days.

This plot is the first thing I investigate and is used to determine if the candidate is promising enough for further investigations. I am typically looking for nicely detrended light curves in the first panel, with transits that don't align with a gap in the data or any other peculiar phenomenon; a nice transit shape, not associated with a wavy light curve or any gap in the data; and finally, some harmonics are expected to be seen in the bottom panel.

4.2 Vetting

Once these first results have been discussed, we might perform the vetting to investigate the most promising candidates further. To do so, I use the WATSON (Visual Vetting and Analysis of Transit for Space ObservatioNs) sub-module. This extra step is crucial since our signals are typically rather weak and could be caused by instrumental artifacts or other astrophysical phenomena. The vetting is, therefore, necessary to rule out these scenarios. For this purpose, a series of tests are performed and compiled into a validation report. Let us take once again Kepler-445 as an example and go through all of these. Here is a typical validation report summary:

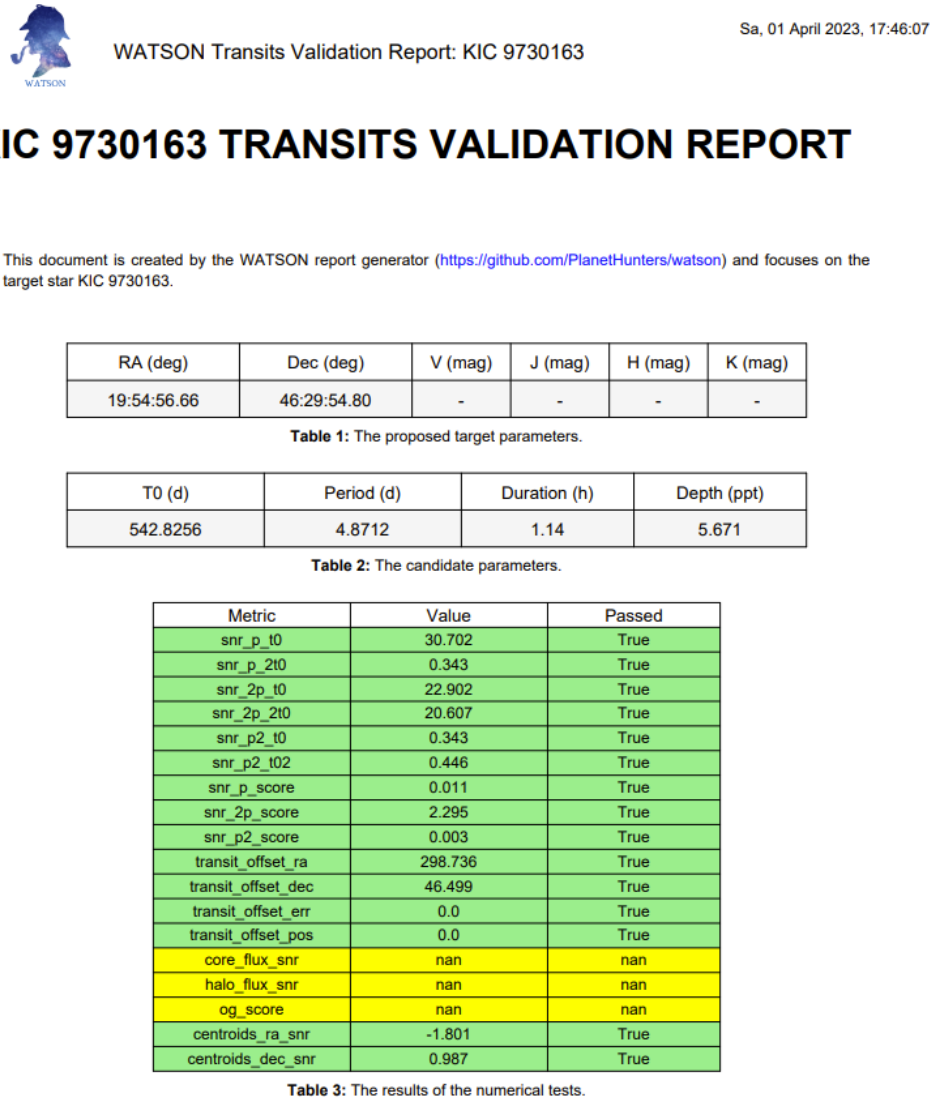

WATSON Transits Validation Report: KIC 9730163

Sa, 01 April 2023, 17:46:07

KIC 9730163 TRANSITS VALIDATION REPORT

This document is created by the WATSON report generator (https://github.com/PlanetHunters/watson) and focuses on the target star KIC 9730163.

RA (deg)	Dec (deg)	V (mag)	J (mag)	H (mag)	K (mag)
19:54:56.66	46:29:54.80	-	-	-	-

Table 1: The proposed target parameters.

T0 (d)	Period (d)	Duration (h)	Depth (ppt)
542.8256	4.8712	1.14	5.671

Table 2: The candidate parameters.

Metric	Value	Passed
snr_p_t0	30.702	True
snr_p_2t0	0.343	True
snr_2p_t0	22.902	True
snr_2p_2t0	20.607	True
snr_p2_t0	0.343	True
snr_p2_t02	0.446	True
snr_p_score	0.011	True
snr_2p_score	2.295	True
snr_p2_score	0.003	True
transit_offset_ra	298.736	True
transit_offset_dec	46.499	True
transit_offset_err	0.0	True
transit_offset_pos	0.0	True
core_flux_snr	nan	nan
halo_flux_snr	nan	nan
og_score	nan	nan
centroids_ra_snr	-1.801	True
centroids_dec_snr	0.987	True

Table 3: The results of the numerical tests.

Fig. 21: Validation report summary for the vetting of Kepler-445's first signal.

This first panel displays the candidate's parameters and the results from all numerical tests.

• **snr_p_t0**: SNR of the transit model in the period selected by SHERLOCK, this is the main transit events. Passed if >3

• **snr_p_2t0**: SNR of the transit model in the period selected by SHERLOCK centered on T0 + P/2. This value is expected to be low, and the test is passed if <3

• **snr_2p_t0**: SNR of the transit model at twice the period selected by SHERLOCK at T0. Expected to be high since it represents the odd transits. Passed if >3

• **snr_2p_2t0**: Similar to the previous test but T0+Period. Expected to be high since

it represents even transits. Passed if >3

• **snr_p2_t0**: SNR of the transit model with P/2, centered on T0 and with the original masked. Passed if <3

• **snr_p2_t02**: SNR of the transit model with P/2, centered on TO+P/2 with the original signal being masked. Passed if <3

• **transit_offset_ra**: Distance being the computed transit source and the target star in Right Ascension, in degrees. Passed if <3.98" (Kepler pixel size)

• **transit_offset_dec**: Same than the previous test but in Declination

• **transit_offset_err**: The error on the computed transit offset, in degrees. Passed if <12" (3*4")

• **transit_offset_pos**: Absolute distance between the computed transit source and the target's position, in degrees. Passed if <offset_err

• **core_flux_snr**: Computed aperture flux SNR with the transit model. Passed if >3

halo_flux_snr: The computed aperture flux with a ring aperture over the core with the transit model. Passed if >3

• **og_score**: The ratio halo_flux_snr/core_flux_snr. Passed if <1

• **centroids_ra_snr**: The SNR of the transit model Right Ascension curve. Passed if <3

• **centroids_dec_snr**: Same as previous test with the Declination

All of these information are available in the SHERLOCK documentation[5]

This summary gives us all the information we need at first glance. As expected, the candidate we took as an example passed every test. Cases in which some numerical tests are not passed, and the implications of these failures, will be discussed in section 5.

Now that we discussed the summary let us take a look at the report itself. The first interesting series of plots correspond to the first six numerical tests we have discussed.

[5] `https://sherlock-ph.readthedocs.io/en/latest/index.html`

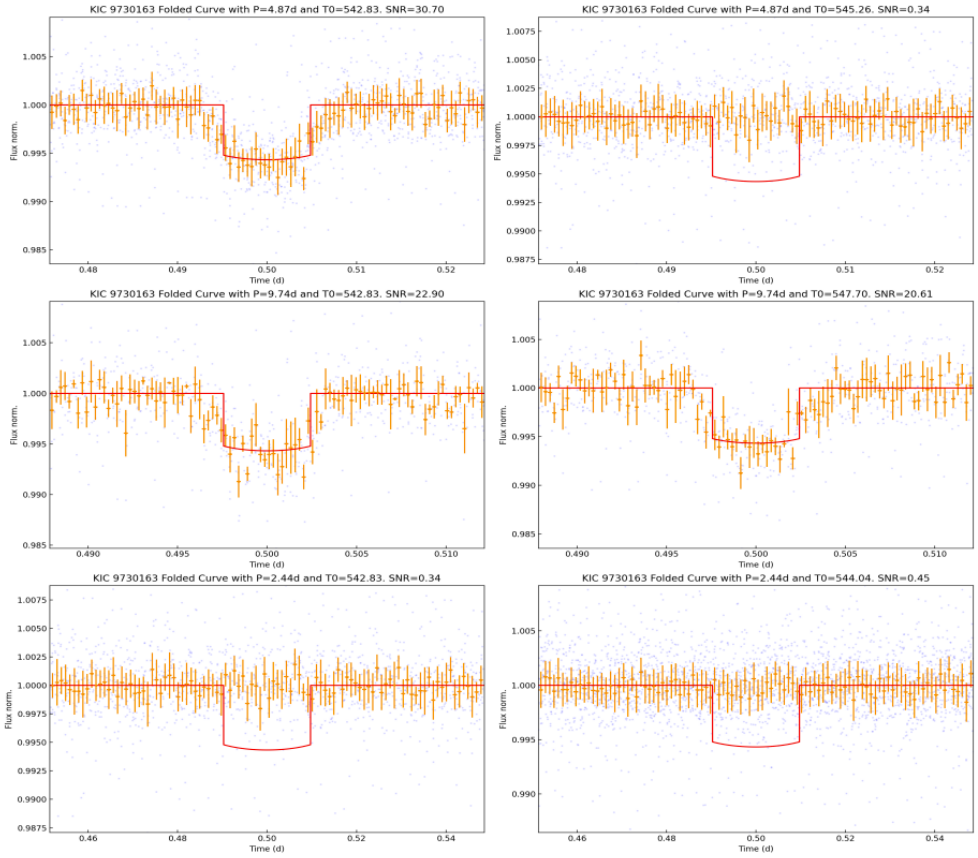

Fig. 22: Results of the first six numerical tests for Kepler-445's first signal.

Above, we see the first two tests; the candidate folded at its found period for the found epoch (T0) and at T0+P/2. We obviously expect a nice transit shape in the first plot and nothing in the second.

The middle row represents the next two tests, accounting for odd and even transits. Here we see the candidate folded at its first harmonic for the found epoch T0 and T0+P. Again, we expect to see nice transit shapes here, associated with a relatively high SNR.

The bottom raw represents the candidate folded at its first subharmonic for the found epoch T0 and T0+P/2, where the initial candidate has been masked. Any detection in these tests could mean two things; (1) the selected period is wrong, and the actual object has an orbital period half of what was initially believed, (2) the light curve has not been properly detrended and exhibits some artifacts and wavy patterns that are deep enough to be interpreted as transits. In this last case, the initial candidate might be linked to these patterns instead of an actual substellar object.

Again, the candidate passes all the tests successfully, and Fig. 22 is a perfect example of what we hope to find in our actual data.

Let us now focus on the transit offset. This section of the validation report aims to determine if our signal comes from the investigated target and not a nearby star which might have contaminated our light curves.

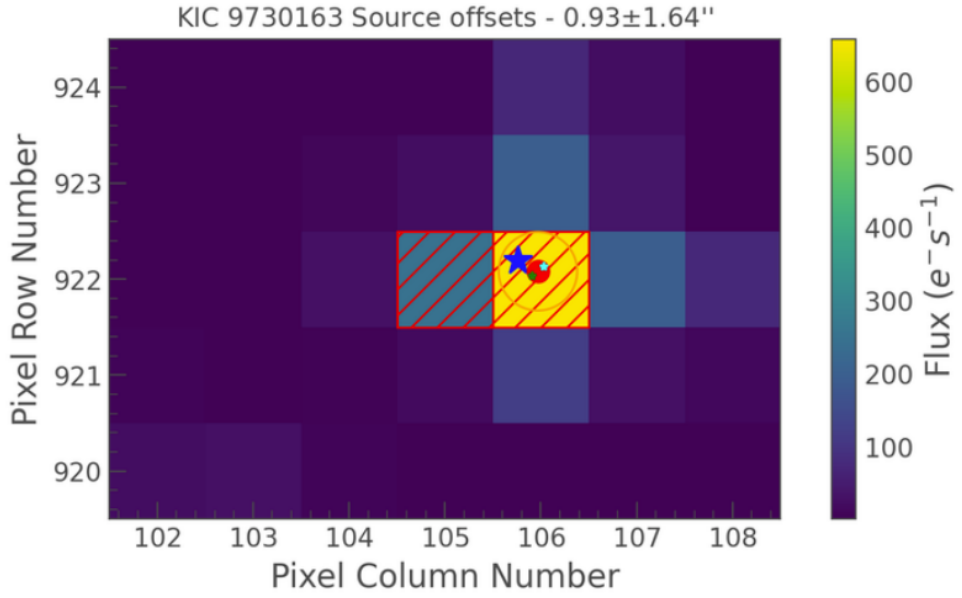

Fig. 23: Source offset for Kepler-445's first signal.

In Fig. 23, we see the known position of our target star in dark blue and the computed position of the transit's source in red. The cyan dot is the differential image offset, the green dot is the per-pixel BLS SNR offset, and the red dot is simply the average of these two methods. The thin circle around this offset shows the corresponding error. Once again, this plot showcases what we hope to see: the target's position is indeed within the error of the computed offset, and both are located in the same pixel.

Additionally, the absolute distance between these two is $0.93 \pm 1.64''$, which is below Kepler's pixel size of 3.98". Note that in some instances, it is sensible to check Kepler's FOV to make sure that no contaminating star is located within the same pixel. This check can be performed via the statistical validation module within SHERLOCK, which will be discussed later in this report, or directly on the MAST.

Note that for our actual hot subdwarf targets, the error around the offset position was not calculated correctly. Hence I had to manually check the source offset plots, as the corresponding numerical test would almost return "FALSE" (transit_offset_pos in fig21).

The last important piece of information I want to showcase is the light curves of adjacent pixels from Kepler. These plots allow us to manually check for contamination, thus ensuring the detected signal comes from the target.

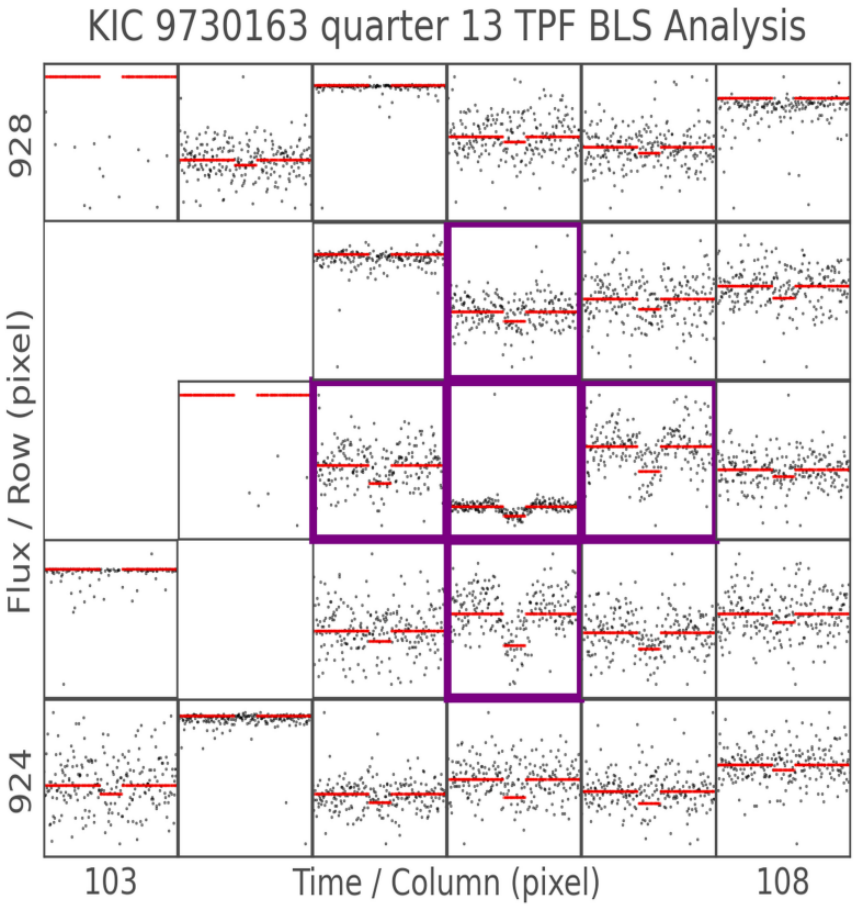

Fig. 24: Light curves for Kepler-445's first signal, in Quarter 13.

In fig.24, we clearly see a transit shape in the center, where our target lies, and nothing of interest in other pixels. This is the ideal case, where no obvious contamination from nearby stars can be observed. Such a plot is produced for every quarter of data. This, combined with fig. 23, allow us to make sure the detected signal comes indeed from the investigated target. Similar plots are also available for every single transit.

4.3 Statistical Validation

When the vetting has not ruled out a candidate, we can investigate further by performing a statistical validation. To do so, SHERLOCK makes use of the TRICERATOPS package [27], which investigates all stars within a radius of 10 pixels around the target to check for false positives. The procedure is as follows: (1) TRICERATOPS calculates the proportions of flux given by each nearby star. Given the transit depth of the investigated candidate, a series of nearby stars bright enough to produce this kind of result is assembled. (2) Based on the candidate's light curve and model for eclipsing binary, etc., TRICERATOPS computes the marginal likelihood of each scenario. (3) The probability of each scenario is then calculated. (4) All these probabilities are then taken into account to determine if the candidate is likely a planet or likely a false positive. Here are all the scenarios tested during the statistical

validation:

Scenario	Configuration
TP	No unresolved companion; transiting planet with P_{orb} around target star
EB	No unresolved companion; eclipsing binary with P_{orb} around target star
EBx2P	No unresolved companion; eclipsing binary with $2 \times P_{orb}$ around target star
PTP	Unresolved bound companion; transiting planet with P_{orb} around primary star
PEB	Unresolved bound companion; eclipsing binary with P_{orb} around primary star
PEBx2P	Unresolved bound companion; eclipsing binary with $2 \times P_{orb}$ around primary star
STP	Unresolved bound companion; transiting planet with P_{orb} around secondary star
SEB	Unresolved bound companion; eclipsing binary with P_{orb} around secondary star
SEBx2P	Unresolved bound companion; eclipsing binary with $2 \times P_{orb}$ around secondary star
DTP	Unresolved background star; transiting planet with P_{orb} around target star
DEB	Unresolved background star; eclipsing binary with P_{orb} around target star
DEBx2P	Unresolved background star; eclipsing binary with $2 \times P_{orb}$ around target star
BTP	Unresolved background star; transiting planet with P_{orb} around background star
BEB	Unresolved background star; eclipsing binary with P_{orb} around background star
BEBx2P	Unresolved background star; eclipsing binary with $2 \times P_{orb}$ around background star
NTP	No unresolved companion; transiting planet with P_{orb} around nearby star
NEB	No unresolved companion; eclipsing binary with P_{orb} around nearby star
NEBx2P	No unresolved companion; eclipsing binary with $2 \times P_{orb}$ around nearby star

Fig. 25: Exhaustive list of all the scenarios tested by TRICERATOPS during the statistical validation. The orbital period is given by the candidate we investigate. Source: Giacalone et al. 2021[27]

Our example, Kepler-445 was not in the catalog used by TRICERATOPS to perform the validation, let us take one of our hot-subdwarf as an example instead. We will use KIC12021724 for this.

As mentioned above, TRICERATOPS can give us stars that are bright enough to potentially contaminate our light curves. Said stars located within 10 pixels of our target are shown in Fig. 27. This is particularly useful to check for contamination, especially when compared to the source offset given by the vetting.

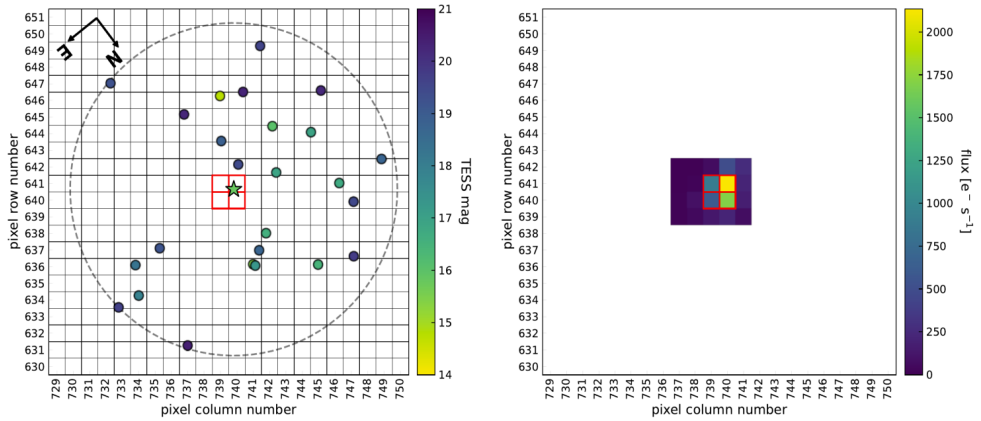

Fig. 26: Bright nearby stars for the target and its aperture

The results of the actual statistical validation can then be investigated. For each of the scenarios described in Fig. 25, as seen in the upper table in Fig. 27, or the whole results in the lower table, where FPP stands for False Positive Probability and NFPP for Nearby FPP.

ID	scenario	M_s	R_s	P_orb	inc	b	ecc	w	R_p	M_EB	R_EB	prob
27766711	TP	0.47	0.18	3.5	88.62	0.51	0.71	150.76	0.8	0.0	0.0	0.461755
27766711	EB	0.47	0.18	3.5	87.84	1.95	0.0	222.67	0.0	0.42	0.18	0.027899
27766711	EBx2P	0.47	0.18	7.0	88.81	1.93	0.21	224.89	0.0	0.46	0.18	0.083668
27766711	PTP	0.47	0.18	3.5	88.24	0.63	0.72	79.2	0.86	0.0	0.0	0.141566
27766711	PEB	0.47	0.18	3.5	87.66	1.93	0.01	168.88	0.0	0.2	0.18	0.020596
27766711	PEBx2P	0.47	0.18	7.0	88.68	1.92	0.01	244.83	0.0	0.46	0.18	0.031418
27766711	STP	0.3	0.18	3.5	88.21	0.44	0.8	208.68	1.73	0.0	0.0	0.122597
27766711	SEB	0.35	0.18	3.5	87.48	1.92	0.0	168.75	0.0	0.19	0.18	0.049009
27766711	SEBx2P	0.46	0.18	7.0	88.67	1.91	0.0	193.55	0.0	0.44	0.18	0.006517
27766711	DTP	0.47	0.18	3.5	88.47	0.55	0.66	156.46	0.86	0.0	0.0	0.035633
27766711	DEB	0.47	0.18	3.5	87.74	1.91	0.0	185.93	0.0	0.26	0.18	0.003013
27766711	DEBx2P	0.47	0.18	7.0	88.72	1.88	0.04	202.34	0.0	0.46	0.18	0.005769
27766711	BTP	0.21	0.22	3.5	84.3	0.71	0.83	151.39	3.4	0.0	0.0	0.001229
27766711	BEB	0.27	0.26	3.5	83.88	0.43	0.92	220.48	0.0	0.08	0.11	0.008935
27766711	BEBx2P	0.14	0.16	7.0	82.21	1.81	0.8	27.14	0.0	0.14	0.16	0.00038
1883115794	NTP	1.0	1.0	3.5	88.94	0.11	0.51	86.74	19.96	0.0	0.0	2e-06
1883115794	NEB	1.0	1.0	3.5	58.42	1.31	0.87	76.83	0.0	0.37	0.37	1.2e-05
1883115794	NEBx2P	1.0	1.0	7.0	59.62	1.92	0.85	23.39	0.0	0.99	1.0	2e-06

Table 3: Scenarios attributes and probabilities.

Scenario	FPP	NFPP	FPP2	FPP3+
0	0.362564	1.5e-05	0.022245	0.011248
1	0.349423	1.5e-05	0.021032	0.010628
2	0.363097	1.6e-05	0.022295	0.011273
3	0.379516	1.6e-05	0.023882	0.012085
4	0.350628	1.5e-05	0.021141	0.010684
MEAN	0.361046	1.5e-05	0.022119	0.011184

Table 4: Validation results.

Fig. 27: Results of the statistical validation for KIC12021724

Finally, we can inspect the best fit for each scenarios on our candidate's folded light curve, as seen in Fig. 28.

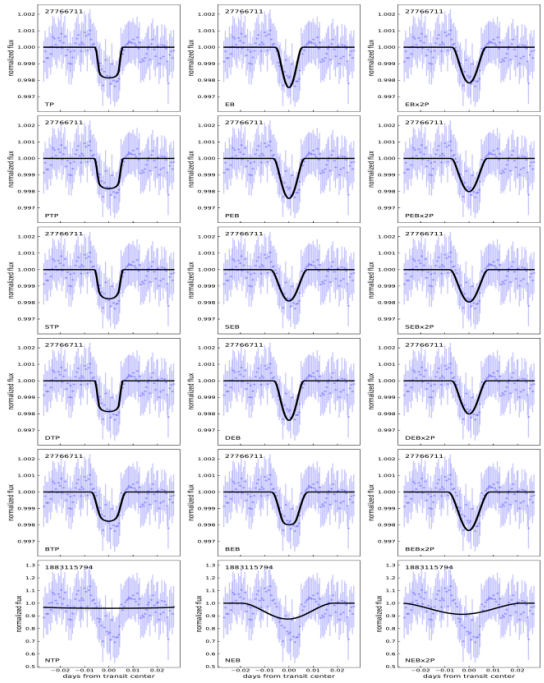

Fig. 28: Best fit for each scenario for KIC12021724

Statistical validation is also particularly useful to check Kepler's FOV, in which we can see nearby stars. This FOV, combined with the source offset computed in the vetting (fig 23) allows us to check for possible contamination from nearby stars with great precision.

4.4 Fitting

If a candidate passes both the vetting and statistical validation, the last step is to perform follow-up observations from a ground-based instrument. To do so, we need to obtain accurate planetary parameters and refine its ephemerides. For that, SHERLOCK makes use of the Allesfitter package [28] to perform the fitting. Allesfitter uses photometric data from our candidate to run various transit/eclipse models and provide the best fit.

The fitting makes use of Bayesian statistics to compare transit models with the provided photometric data. In our case, the main approach was the usage of Nested Sampling (NS) algorithms. A deep dive into Bayesian statistics is beyond the scope of this work, however, so let us focus on the SHERLOCK's output for our test target, Kepler-445.

We start with an initial guess, which roughly fits our data. It is often important to check if the initial guess looks satisfactory before initiating the nested sampling. This guess can also be investigated for each individual transit if necessary.

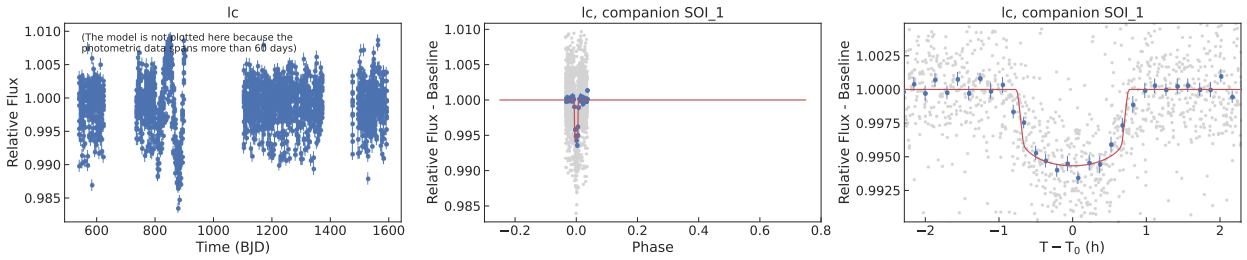

Fig. 29: Initial guess for Kepler-445c. All light curves, separated in several quarters, are plotted at the far left. The middle and right plots show the transit compared with the initial fit, showcased as a red line. In this example, the initial guess is satisfactory, and we can go further.

Once the nested sampling is complete, we obtain a final plot, similar to fig29 but with the best fit.

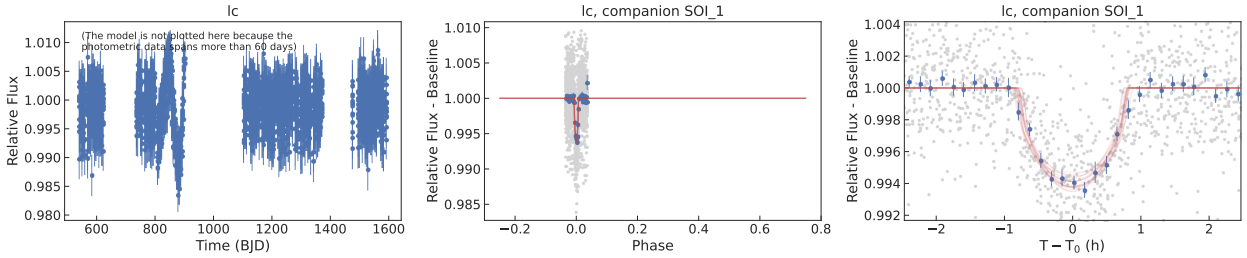

Fig. 30: Final plot for the same test target after the nested sampling has been completed. The selected models fit our data much better than in the initial guess, as expected.

These last two figures are only visual plots. We are mainly interested in the star and planet parameters associated with the models used to fit these light curves. These parameters are compiled into a text file, directly in latex format, that can, therefore, directly be imported into a report such as this one. The first of these files is a table compiling all parameters, showcasing what was fixed and what was derived from the fitting itself.

Parameter	Value	Source
Derived parameters		
Host radius over semi-major axis SOI_1;$R_\star/a_{SOI_1}$	$0.0419^{+0.0017}_{-0.0016}$	derived
Semi-major axis SOI_1 over host radius; $a_{SOI_1}/R_\star$	23.88 ± 0.97	derived
Companion radius SOI_1 over semi-major axis SOI_1;R_{SOI_1}/a_{SOI_1}	$0.002682^{+0.00011}_{-0.000098}$	derived
Companion radius SOI_1;R_{SOI_1} ($R_\oplus$)	2.106 ± 0.10	derived
Companion radius SOI_1;R_{SOI_1} (R_{jup})	0.1879 ± 0.0091	derived
Semi-major axis SOI_1;a_{SOI_1} ($R_\odot$)	7.18 ± 0.37	derived
Semi-major axis SOI_1;a_{SOI_1} (AU)	0.0334 ± 0.0017	derived
Inclination SOI_1;i_{SOI_1} (deg)	$89.68^{+0.20}_{-0.29}$	derived
Impact parameter SOI_1;$b_{tra;SOI_1}$	$0.132^{+0.12}_{-0.083}$	derived
Total transit duration SOI_1;$T_{tot;SOI_1}$ (h)	1.637 ± 0.062	derived
Full-transit duration SOI_1;$T_{full;SOI_1}$ (h)	1.433 ± 0.061	derived
Host density from orbit SOI_1;$\rho_{\star;SOI_1}$ (cgs)	$10.9^{+1.4}_{-1.2}$	derived
Equilibrium temperature SOI_1;$T_{eq;SOI_1}$ (K)	416 ± 28	derived
Transit depth SOI_1;$\delta_{tr;dil;SOI_1;lc}$ (ppt)	$6.03^{+0.30}_{-0.28}$	derived
Limb darkening; $u_{1;lc}$	$1.18^{+0.24}_{-0.29}$	derived
Limb darkening; $u_{2;lc}$	$-0.40^{+0.32}_{-0.21}$	derived
Combined host density from all orbits; $\rho_{\star;combined}$ (cgs)	$10.9^{+1.4}_{-1.2}$	derived

Table 3: Parameters derived from the fitting

parameter	value	unit	fit/fixed
Fitted parameters			
$R_b/R_\star$	0.0642 ± 0.0023		fit
$(R_\star + R_b)/a_b$	0.0446 ± 0.0018		fit
$\cos i_b$	$0.0055^{+0.0050}_{-0.0035}$		fit
$T_{0;b}$	$1068.91624^{+0.00093}_{-0.00087}$	BJD	fit
P_b	4.871230 ± 0.000014	d	fit
$\sqrt{e_b}\cos\omega_b$	0.0		fixed
$\sqrt{e_b}\sin\omega_b$	0.0		fixed
$q_{1;lc}$	$0.67^{+0.18}_{-0.19}$		fit
$q_{2;lc}$	$0.75^{+0.15}_{-0.20}$		fit
$\log\sigma_{lc}$	-5.672 ± 0.016	log rel.flux.	fit

Table 2: Fitted parameters

The second latex file is a combination of all parameters that can be derived from our results. These are interesting in our case, as we can directly compare them with the literature. Here we investigated Kepler-445c; the values are not perfect but remain close to expected.

Since none of our candidates could be observed using ground-based instruments, the fitting package was never used. Hence we will end the discussion here.

4.5 Variable stars

Some stars exhibit high variability in their light curves; in this work, this was often the consequence of binary systems, as discussed in section 1.

Most binaries in this work had short orbital periods, with only a few days or even a few hours in some cases. These close binaries have been already discussed in section 1, with the case of eclipsing and reflection binaries. Non-eclipsing binaries typically have that sinus shape in their lightcurve, which can be removed using the autodetrend. For the case of eclipsing binaries, the best way to proceed is often to mask the actual transit events. However, short period planets around such system are unexpected, as stable orbits are unlikely.

Another case of binary is the fast rotators, for which the rotation of the companion can dominate the lightcurve. Stellar spots in a companion can explain this phenomenon for example. In this case, we used the simple oscillation reduction to clean the light curves, as migrating spots at different latitudes introduce many periods, something the sequential substration used with this flag is particularly suited to deal with.

Long binaries, with orbital periods of hundreds or thousands of days, could harbor a close planet (with period of only a few days) around the hot subdwarfs, as such orbits are more likely to be dynamically stable.

To investigate the detrending we used with SHERLOCK for such cases, let us use the example mentioned in section 1: KIC1868650, aka KBS13.

As we already know from the literature, KBS13 is a reflection binary with a period of 0.29 days. To remove this period, we used the autodetrend function from SHERLOCK. The autodetrend will identify the strongest and most obvious period and remove it from the light curve. The .yaml file used for such a case is shown in Fig. 31.

```
TARGETS:

  'KIC 1868650': # Star's identifier (TIC/KIC/... number)
    SECTORS: [1] # 'all'
    EXPTIME: 60
    INITIAL_SMOOTH_ENABLED: True
    INITIAL_HIGH_RMS_MASK: True
    INITIAL_HIGH_RMS_THRESHOLD: 1.5
    DETREND_METHOD: 'biweight'
    DETRENDS_NUMBER: 12
    MAX_RUNS: 4 # 4
    SNR_MIN: 6 #<0xa0>6
    SDE_MIN: 7 # 7
    OVERSAMPLING: 3


    SIMPLE_OSCILLATIONS_REDUCTION: True # Pre-whitening (FELIX-like cleaning) | abrev "pw"
    AUTO_DETREND_ENABLED: True # Sav-Gol filter | abrev "sg"
    #AUTO_DETREND_PERIOD: 0.5 # Force the autodetrend period in days (useful for eclipsing, among others)
    PERIOD_MIN: 0.1
    PERIOD_MAX: 15
```

Fig. 31: SHERLOCK input file for KIC1868650.

Let us discuss the new parameters we use in such cases:

• **SIMPLE_OSCILLATION_REDUCTION**: Cleaning of the light curve by the prewhitening technique, consisting in substracting sequentially from the light curve each periodic variation spotted above a pre-defined threshold. Often used for fast rotators and stars exhibiting pulsations.

• **AUTO_DETREND_ENABLED**: Enables the autodetrend module to clean single periodicity, useful to clean fast rotators. See more in section 4.5.

• **AUTO_DETREND_PERIOD**: Used to force the removal of the given period. Useful for binary systems of which the period is known

• **PERIOD_MIN**: The minimum period the autodetrend is allowed to remove

• **PERIOD_MAX**: The maximum period the autodetrend is allowed to remove

If the period is known in advance, we can force SHERLOCK to remove it. I never truly used this function however, as I opted to compare the period independently found by SHERLOCK to the values in the literature instead.

As we said, SHERLOCK identifies and removes the main period from the binary, and this is especially obvious when looking at the periodograms as in Fig. 32.

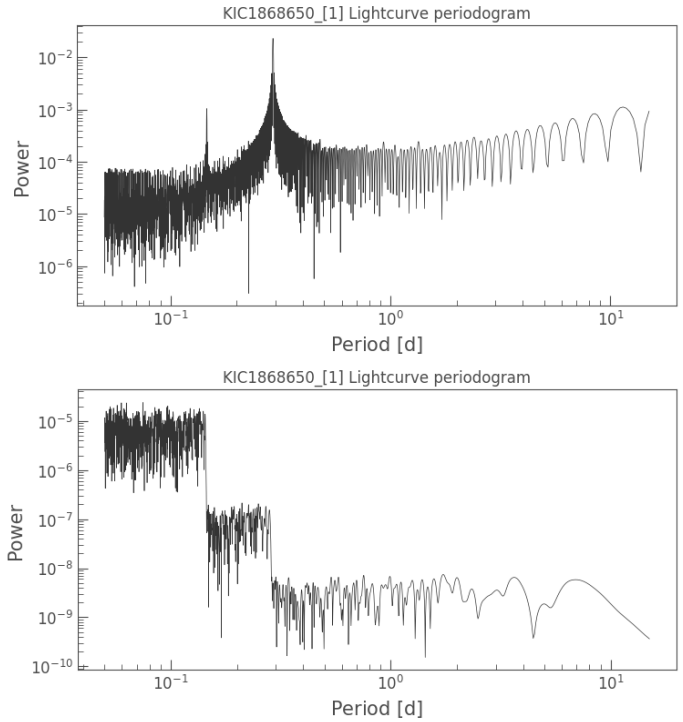

Fig. 32: Periodograms from KIC1868650. Above is the initial plot before the autodetrend, where the orbital period of the binary is clearly visible. Below is the final periodogram after the autodetrend.

We can also check the phase-folded period removed during this process, which is especially useful to compare these values with the literature. In our example, the period of 0.29d with the characteristic sinusoidal shape has indeed been removed, as seen in Fig. 33.

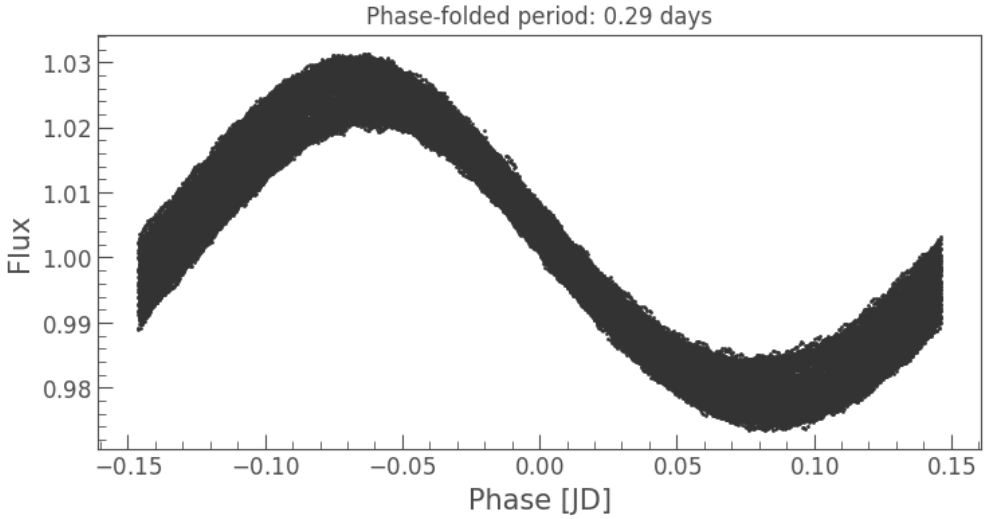

Fig. 33: Phase-folded period removed by SHERLOCK using the autodetrend for KIC1868650.

Finally, the effects of the autodetrend are especially obvious in the Autocorrelation plots as well, seen in Fig. 34. The autocorrelation is close to zero in the final plot, with the expected exception of this maximum value at time lags 0, where we have the maximum value of 1 (the light curve is of course perfectly correlated with itself).

These are the tool I used to detrend fast rotating binaries. Note however that signals spotted close to the system's orbital period or its harmonics are to be taken with extreme caution. In this work, the period removed using SHERLOCK would systematically be compared with values in the literature to confirm the ablated signal corresponds to the binary period. Note also that in some cases, such as a binary system with a white dwarf, planetary detection is not expected due to the short orbital period of such systems, resulting in a common envelope between the two stars. No close planet is expected to survive in such conditions, and the same goes for sdB+dM binaries. Such cases remain interesting, nonetheless as they are good candidates to test SHERLOCK's limit in removing strong periodicities.

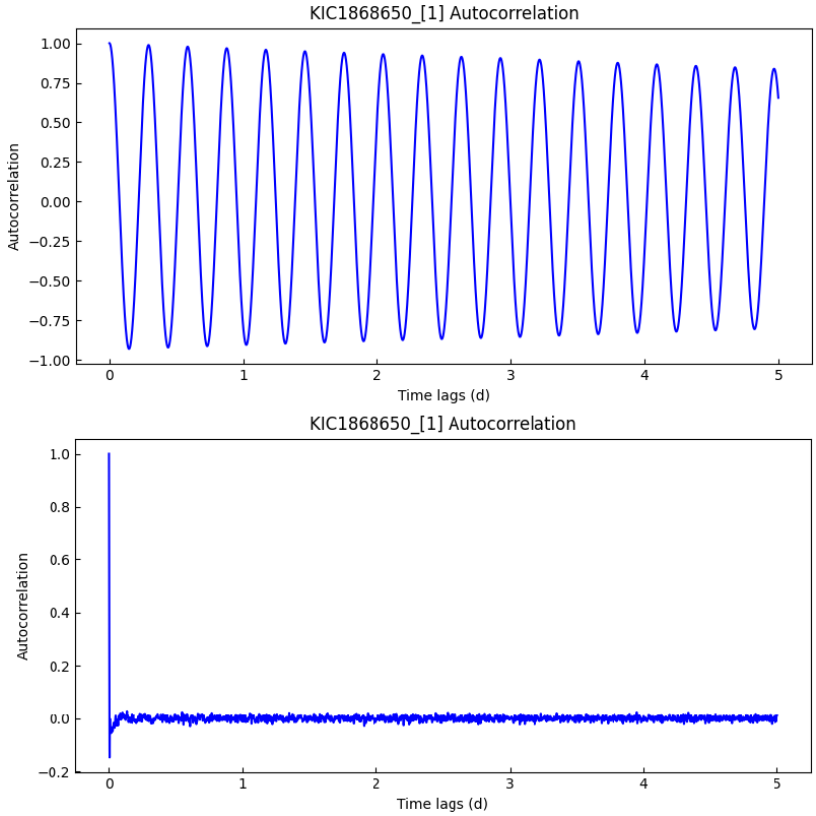

Fig. 34: Autocorrelation plots for KIC1868650. Above the initial plot, before the autodetrend was applied, below the final plot, after the autodetrend.

5 Results

Now that we have discussed the tools and methods used for this search, let us see the results of our work. In this section, I will mainly discuss the most promising candidates found in our list of targets, as well as stars exhibiting peculiar behavior worthy of discussion. Stars investigated in this section are shown in order of appearance in Table 4 and 5, i.e. in order of increasing values of Kp.

5.1 KIC6188286 (sdOB)

KIC6188286 is a relatively bright (Kp=14.2) sdOB star observed in Q2.3 in short cadence. SHERLOCK retrieved four signals, but only the first and last ones were considered for further investigations.

KIC6188286_[2]_candidates - Bloc-notes

Fichier Edition Format Affichage Aide

Listing most promising candidates for ID KIC6188286_[2]:

Detrend no.	Period	Per_err	Duration	T0	Depth	SNR	SDE	FAP	Border_score	Matching OI	Harmonic	Planet radius (R_Earth)	Rp/Rs	Semi-major axis
6	6.4446	0.01026	57.35	233.11	0.792	17.47	6.18	0.040896	1.00	nan	-	0.43935	0.02845	0.05280
0	16.9864	0.05227	151.75	239.55	1.499	20.24	12.30	0.000080	1.00	nan	-	0.60463	0.06412	0.10074
0	15.7500	0.08752	166.20	239.55	3.616	22.61	14.78	0.000080	1.00	nan	-	0.93897	0.05822	0.09579
8	9.5826	0.01045	42.30	232.31	1.050	17.27	6.89	0.011525	1.00	nan	-	0.50593	0.03308	0.06878

Fig. 35: List of candidates retrieved by SHERLOCK for KIC6188286

Let us first rapidly showcase why signal two and three were discarded immediately. In Fig. 36, it is clear that the signals correspond to the undetrended PDCSAP fluxes. Even though the values of SNR and SDE are high, these variations clearly don't come from any substellar objects orbiting the target but rather from instrumental artifacts in the light curves.

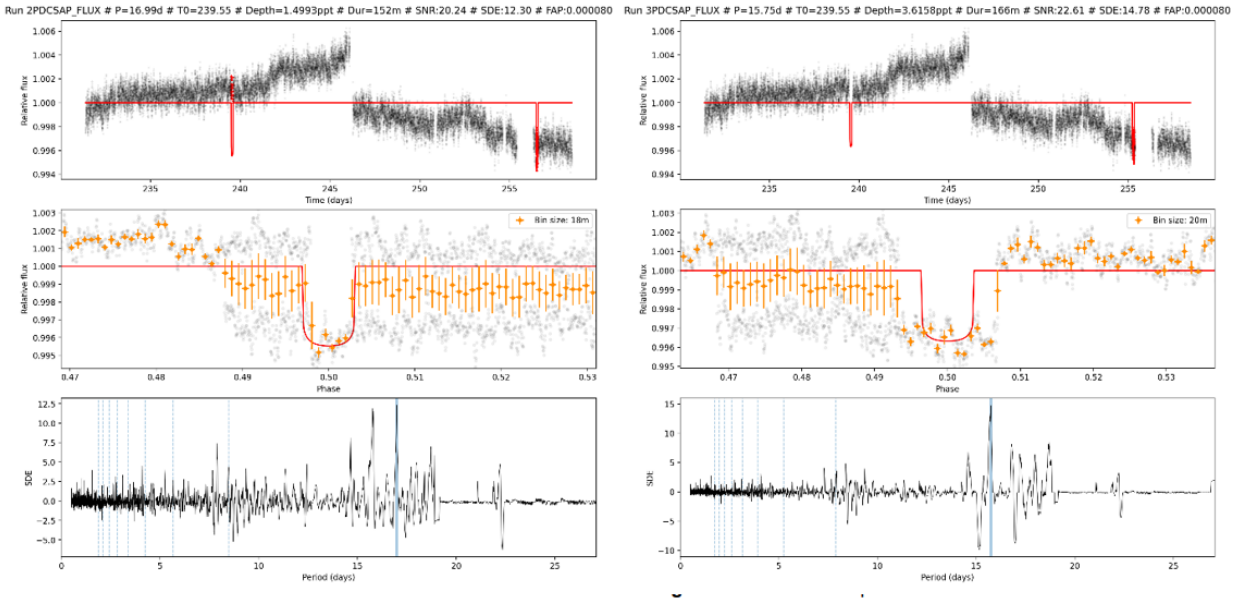

Fig. 36: KIC618286, discarded candidates

The first detected signal, with a period of 6.44 days, was spotted in 5 detrends, as shown in Fig. 37. The low SDE and lack of clear harmonics are a concern, but the high SNR and relatively obvious transit shape in the light curve are encouraging. The fourth signal, with a period of 9.58 days was spotted in a total of 27 detrends, spread across all four runs. This signal was, therefore, strong enough to be spotted at least once in every run, even though it was selected as a candidate only in the last one. The first harmonic can clearly be seen in Fig. 37. Similarly to the first signal, the SNR is high, but the relatively low SDE might be of concern. Neither of these candidates exhibits a transit long enough to be retrieved in long cadence data.

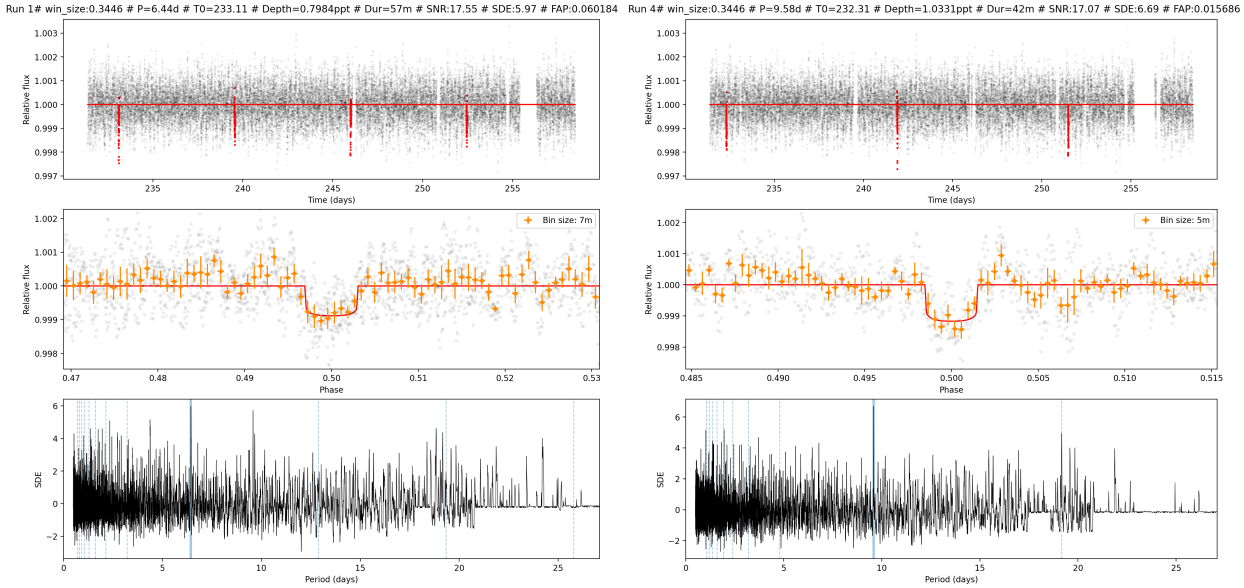

Fig. 37: KIC6188286, first signal (left) and fourth signal (right).

These results seem promising at first and deserve to go to the vetting step. To this end, let us look at the vetting of these two candidates.

T0 (d)	Period (d)	Duration (h)	Depth (ppt)
233.1064	6.4446	0.96	0.792

Table 2: The candidate parameters.

T0 (d)	Period (d)	Duration (h)	Depth (ppt)
232.3124	9.5826	0.7	1.05

Table 2: The candidate parameters.

Metric	Value	Passed
snr_p_t0	17.902	True
snr_p_2t0	0.001	True
snr_2p_t0	11.786	True
snr_2p_2t0	12.763	True
snr_p2_t0	0.001	True
snr_p2_t02	0.001	True
snr_p_score	0.0	True
snr_2p_score	0.977	True
snr_p2_score	0.0	True
transit_offset_ra	285.708	True
transit_offset_dec	41.582	True
transit_offset_err	0.0	True
transit_offset_pos	0.0	False
core_flux_snr	1.81	nan
halo_flux_snr	-0.281	nan
og_score	-0.155	nan
centroids_ra_snr	3.467	False
centroids_dec_snr	2.189	True

Table 3: The results of the numerical tests.

Metric	Value	Passed
snr_p_t0	17.075	True
snr_p_2t0	0.001	True
snr_2p_t0	16.712	True
snr_2p_2t0	5.986	True
snr_p2_t0	0.001	True
snr_p2_t02	0.001	True
snr_p_score	0.0	True
snr_2p_score	10.726	True
snr_p2_score	0.0	True
transit_offset_ra	285.709	True
transit_offset_dec	41.584	True
transit_offset_err	0.0	True
transit_offset_pos	0.001	False
core_flux_snr	0.422	nan
halo_flux_snr	0.335	nan
og_score	0.793	nan
centroids_ra_snr	3.356	False
centroids_dec_snr	4.229	False

Table 3: The results of the numerical tests.

Fig. 38: KIC6188286, vetting of first signal (left) and fourth signal (right).

In Fig. 38, we can see the summary of the vetting's numerical tests. The red flag for the target offset position is expected (see section 3), but the red flags for centroids have to be more closely investigated.

In section 4, when describing the vetting, we mentioned that the centroid SNRs metric is passed if SNR < 3. In this specific case, we see that even if the test is not passed, the values

of SNR are relatively close to three; hence a manual inspection is necessary to see if these failed tests could disqualify our candidates. Let us investigate the corresponding plots in the vetting report, focusing only on the failed tests.

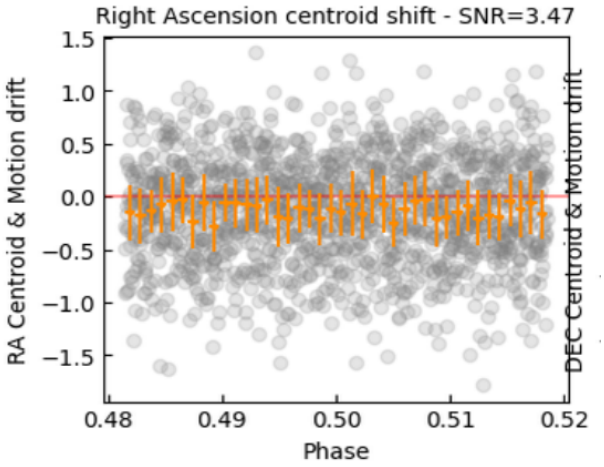

Fig. 39: KIC6188286, centroids RA plot for the first signal

In Fig. 39, we see the plot corresponding to the failed test for the first signal. The SNR is indeed > 3, but not by a huge margin. There is no obvious transit shape in this plot, which is what we would expect in case of contamination. Overall, and after discussion with the rest of the team, we concluded that this red flag in the vetting is not conclusive enough to discard the first candidate. However, this issue has to be kept in mind.

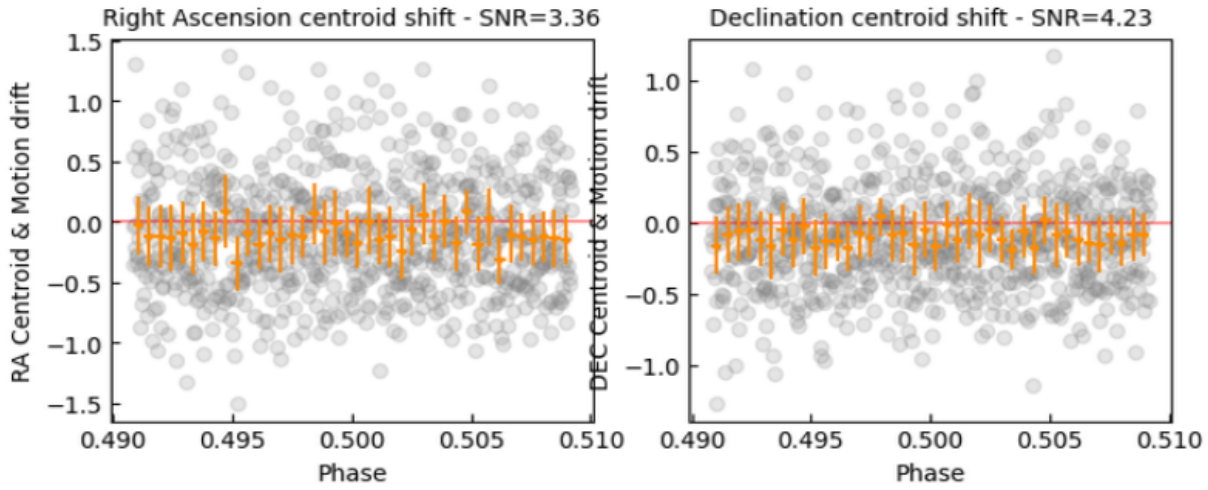

Fig. 40: KIC6188286, centroids RA and DEC plots for the fourth signal.

In Fig. 40, we see the centroids plots for the fourth signal. As for the first signal, there is

no obvious transit shape, and the SNRs remain relatively low. Hence the signal is also not discarded.

Let us finally take a look at the source offset for both candidates in Fig. 41.

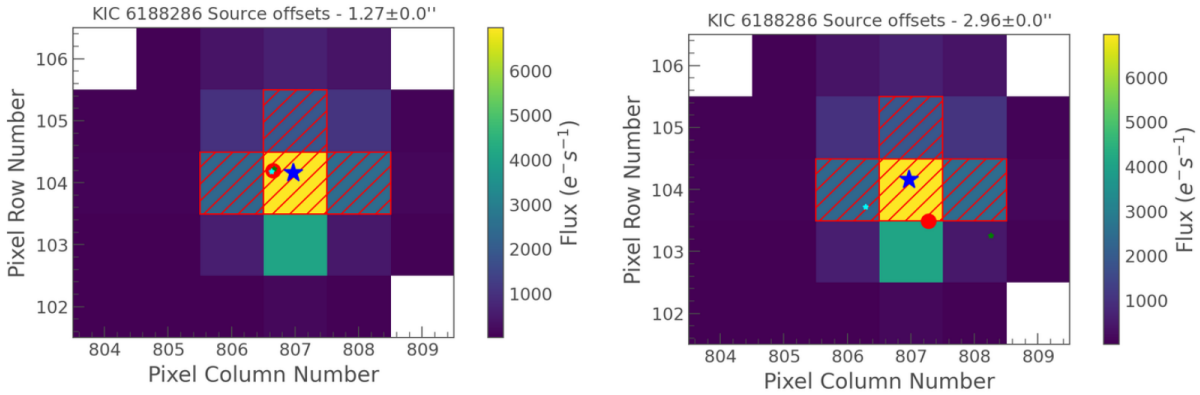

Fig. 41: KIC6188286, source offset for the first signal (left) and the fourth one (right).

The source offset is satisfactory for the first signal, with a high agreement between the two methods yielding a source on the same pixel as our target star. The fourth signal is less ideal, and the two methods are not in agreement, creating high uncertainty. The source offset for this signal might be inconclusive.

Let us go even further and perform the statistical validation for these candidates. Firstly, the validation allows us to check Kepler's FOV around our target and see which stars are bright enough to contaminate our results. Comparing this with Fig. 41 will help better interpret the results from the vetting.

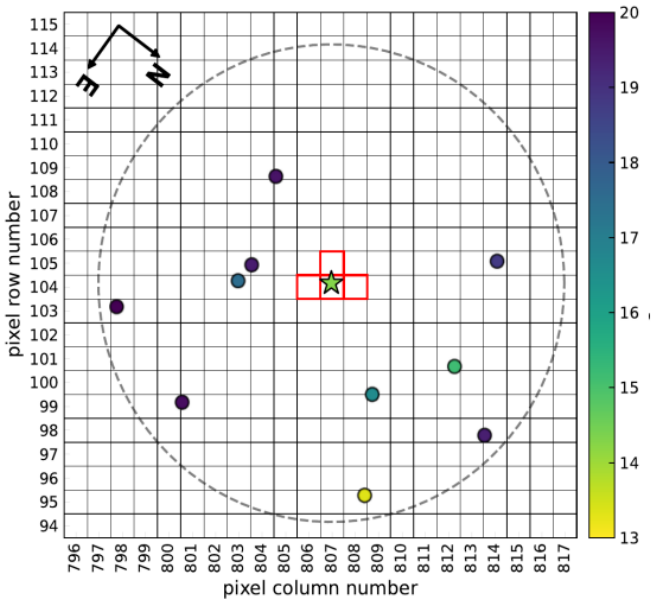

Fig. 42: KIC6188286, Kepler FOV and nearby stars bright enough to contaminate.

In Fig. 42, we clearly see that no bright star is too close to our target, which is a good sign. The results from the vetting concerning the source offset might no be too worrying.

Let us now check the actual statistical validation as performed by TRICERATOPS, starting by the first candidate.

ID	scenario	M_s	R_s	P_orb	inc	b	ecc	w	R_p	M_EB	R_EB	prob
120577802	TP	0.47	0.14	6.44	89.83	0.19	0.45	186.33	0.51	0.0	0.0	0.002459
120577802	EB	0.47	0.14	6.44	88.83	1.97	0.0	247.41	0.0	0.36	0.14	0.0
120577802	EBx2P	0.47	0.14	12.89	89.44	0.67	0.77	184.97	0.0	0.45	0.14	1e-06
120577802	PTP	0.47	0.14	6.44	89.85	0.15	0.47	184.4	0.58	0.0	0.0	0.005664
120577802	PEB	0.47	0.14	6.44	88.76	1.95	0.0	213.35	0.0	0.23	0.14	0.0
120577802	PEBx2P	0.47	0.14	12.89	89.35	0.81	0.6	177.16	0.0	0.46	0.14	0.0
120577802	STP	0.21	0.14	6.44	89.71	0.2	0.37	147.98	1.22	0.0	0.0	0.458053
120577802	SEB	0.1	0.13	6.44	88.6	1.45	0.05	210.48	0.0	0.03	0.1	6.5e-05
120577802	SEBx2P	0.18	0.14	12.89	89.28	0.99	0.62	198.61	0.0	0.18	0.14	0.001664
120577802	DTP	0.47	0.14	6.44	89.85	0.18	0.45	180.01	0.52	0.0	0.0	0.00122
120577802	DEB	0.47	0.14	6.44	88.81	1.96	0.01	153.56	0.0	0.34	0.14	0.0
120577802	DEBx2P	0.47	0.14	12.89	89.46	1.2	0.42	204.33	0.0	0.46	0.14	0.0
120577802	BTP	0.72	0.67	6.44	84.85	0.64	0.64	41.28	10.31	0.0	0.0	0.080412
120577802	BEB	0.54	0.5	6.44	86.54	0.67	0.62	155.81	0.0	0.29	0.3	0.385294
120577802	BEBx2P	0.47	0.43	12.89	84.09	0.92	0.7	77.43	0.0	0.46	0.43	0.065168

Table 3: Scenarios attributes and probabilities.

Scenario	FPP	NFPP	FPP2	FPP3+
0	0.989724	0.0	0.793922	0.658268
1	0.990663	0.0	0.8093	0.679684
2	0.992723	0.0	0.845118	0.731779
3	0.989173	0.0	0.785151	0.646295
4	0.990998	0.0	0.814929	0.687663
MEAN	0.990656	0.0	0.809684	0.680738

Table 4: Validation results.

Fig. 43: KIC6188286, statistical validation results for the first signal.

In Fig. 43, we see the results from the statistical validation of the first signal. The mean FPP (False Positive Probability) is extremely high. It looks like the most probable scenario is BEB (Background Eclipsing Binary) which might explain our signal.

Let us check the validation report for the fourth signal (Fig. 44)

ID	scenario	M_s	R_s	P_orb	inc	b	ecc	w	R_p	M_EB	R_EB	prob
120577802	TP	0.47	0.14	9.58	89.78	0.35	0.12	109.28	0.52	0.0	0.0	0.311226
120577802	EB	0.47	0.14	9.58	89.09	1.95	0.01	144.2	0.0	0.35	0.14	0.0
120577802	EBx2P	0.47	0.14	19.17	89.53	1.31	0.39	178.81	0.0	0.46	0.14	0.0
120577802	PTP	0.47	0.14	9.58	89.76	0.43	0.15	156.21	0.6	0.0	0.0	0.112872
120577802	PEB	0.47	0.14	9.58	89.03	1.95	0.0	159.14	0.0	0.18	0.14	0.0
120577802	PEBx2P	0.47	0.14	19.17	89.58	1.08	0.52	176.71	0.0	0.45	0.14	0.0
120577802	STP	0.14	0.14	9.58	89.23	0.58	0.38	155.22	2.44	0.0	0.0	0.436564
120577802	SEB	0.12	0.14	9.58	88.84	1.44	0.0	163.71	0.0	0.03	0.1	0.008337
120577802	SEBx2P	0.15	0.14	19.17	89.27	1.62	0.12	156.7	0.0	0.14	0.14	0.009668
120577802	DTP	0.47	0.14	9.58	89.78	0.36	0.26	182.79	0.57	0.0	0.0	0.083648
120577802	DEB	0.47	0.14	9.58	89.06	1.96	0.0	225.77	0.0	0.25	0.14	0.0
120577802	DEBx2P	0.47	0.14	19.17	89.61	0.79	0.58	165.91	0.0	0.46	0.14	0.0
120577802	BTP	0.38	0.36	9.58	88.75	0.34	0.71	155.53	8.62	0.0	0.0	0.002929
120577802	BEB	0.4	0.37	9.58	88.61	0.33	0.74	214.8	0.0	0.12	0.16	0.029454
120577802	BEBx2P	0.37	0.34	19.17	85.47	1.37	0.8	31.29	0.0	0.36	0.34	0.005302

Table 3: Scenarios attributes and probabilities.

Scenario	FPP	NFPP	FPP2	FPP3+
0	0.469431	0.0	0.034181	0.017388
1	0.494163	0.0	0.037607	0.019164
2	0.514489	0.0	0.040664	0.020754
3	0.489433	0.0	0.036928	0.018811
4	0.493757	0.0	0.037548	0.019133
MEAN	0.492255	0.0	0.037386	0.01905

Table 4: Validation results.

Fig. 44: KIC6188286, statistical validation results for the fourth signal.

In this case, the mean FPP is much lower. Our signal might not be a false positive! A mean FPP below 0.5 corresponds to an object that is likely a planet, which is excellent news for this candidate. We must remain cautious, however, as the probability we get remains extremely close to this limit value of 0.5. Figure 45 compares the validation results for both candidates.

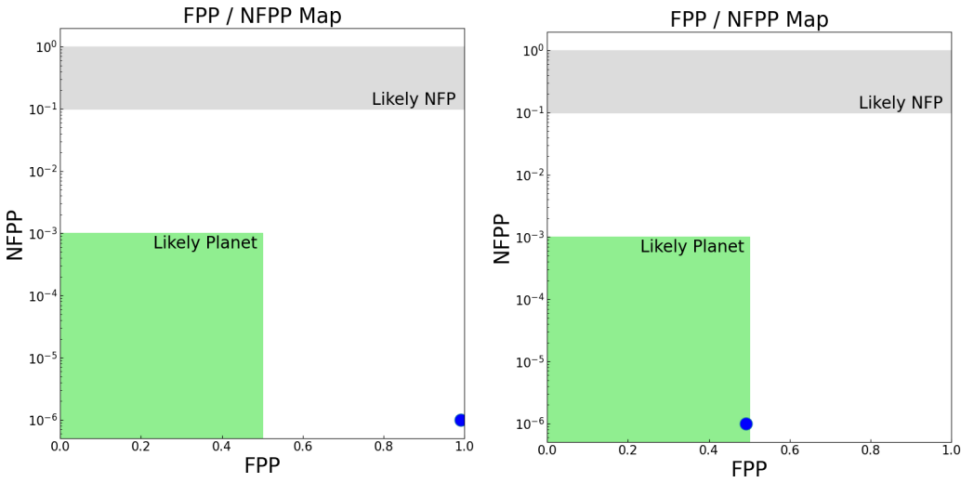

Figure 3: Validation map for the mean scenario.

Figure 3: Validation map for the mean scenario.

Fig. 45: KIC6188286, comparison between the first signal (left) and fourth signal (right) for the mean scenario. NFPP stands for Nearby False Positive Probability.

For this specific target, the fourth signal seems to be the most promising. It was spotted in 27 detrends, passed the vetting successfully, and the statistical validation yielded satisfactory results.

The high likelihood of a false positive for the first candidate proves to be worrying; hence, we must remain skeptical of this signal.

5.2 KIC7975824 (sdB+WD)

This binary system has been briefly discussed in section 1. Although there is no promising signal, the unique nature of this target was a perfect testing ground to see the limits of SHERLOCK in terms of detrending. Note that due to the short orbital period, these two stars have a common envelope in which we don't expect to detect a close planet. A surviving planet in such an environment would likely be circumbinary, which much longer orbital period and therefore a much lower transit probability.

As mentioned in section 1, KIC7975824 is an eclipsing binary with an orbital period of 0.4 days, and with the sdB being deformed by the gravitational influence of its white dwarf companion, leading to clear variations in the light curves. Additionally, a Doppler beaming effect creates asymmetries in the minima and maxima of the light curve.

Unsurprisingly with such variability, SHERLOCK was not able to detrend the light curves completely, even while using the autodetrend. The removed period was 0.2 days, half the actual orbital period of the system. We suspect this is due to the different depths from the white dwarf eclipsing the sdB and the sdB eclipsing the white dwarf. It is entirely possible that SHERLOCK removed only one of these scenarios.

Every selected candidate was due to the eclipses from this binary system. In fact, we systematically detected something with a period of 0.81 days, twice the system's orbital period. This is especially clear when looking at the SDE plots since we skip every other harmonic (see Fig. 48). Let us take a look at the periodograms and auto-correlation plots to investigate a bit further.

In Fig. 46, the effects of the autodetrend are clearly visible, yet the peaks corresponding to the variability can still be seen even on the final plot. From this figure alone, it is clear that SHERLOCK didn't completely remove the trends.

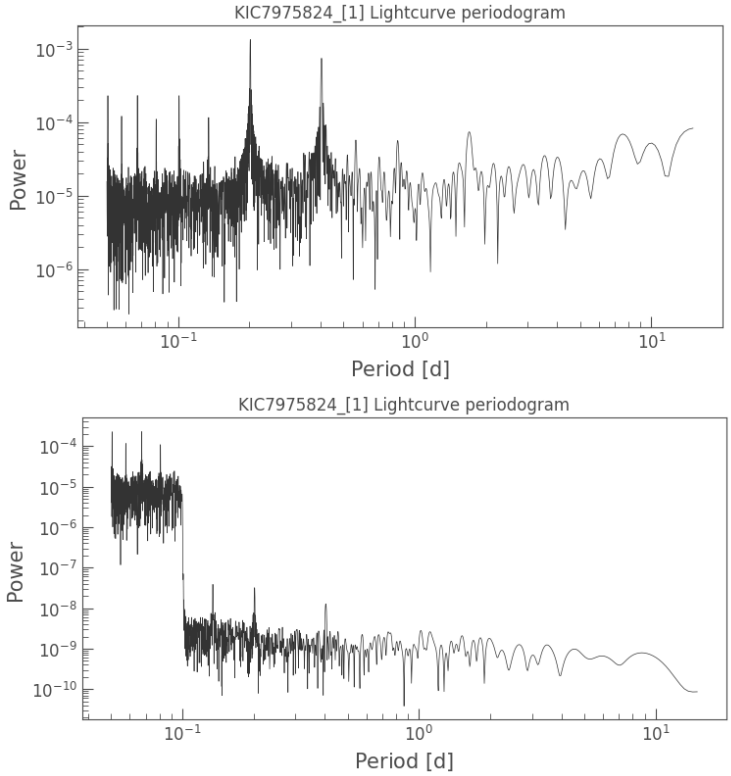

Fig. 46: Initial (above) and final (below) periodograms for KIC7975824.

The auto-correlation plots show a similar behavior. In Fig. 47, we can clearly see that even if the variability is reduced, it is far from completely gone.

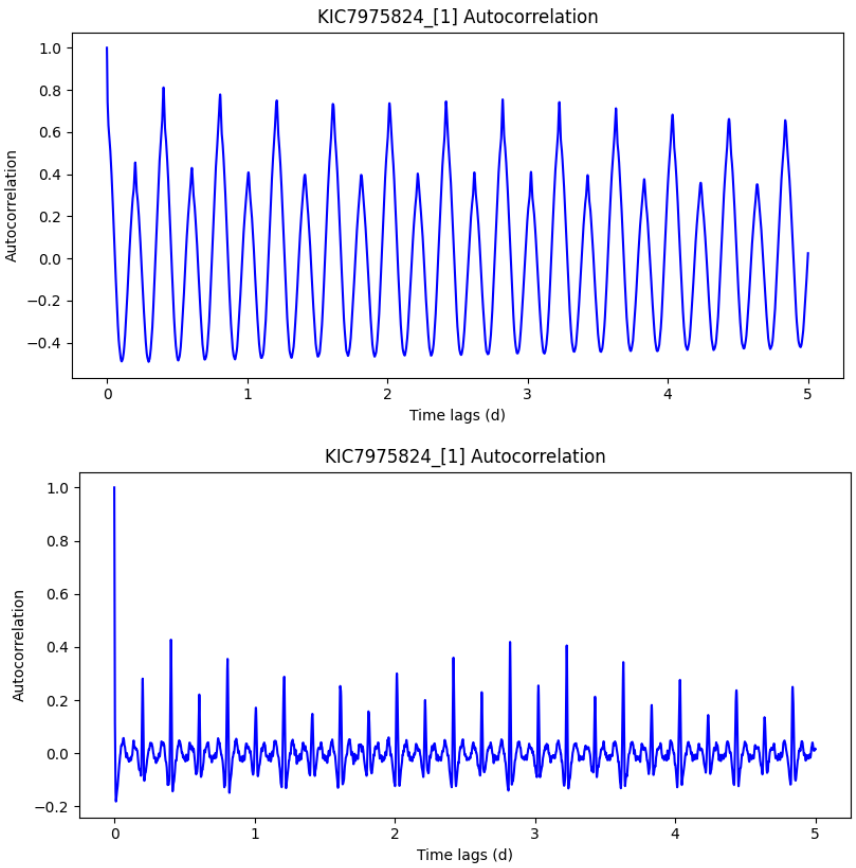

Fig. 47: Initial (above) and final (below) autocorrelation plots for KIC7975824?

The variability unsurprisingly highly contaminates the output from SHERLOCK. The detrended light curves look exactly like what we discussed in section 1 (see Fig. 7).

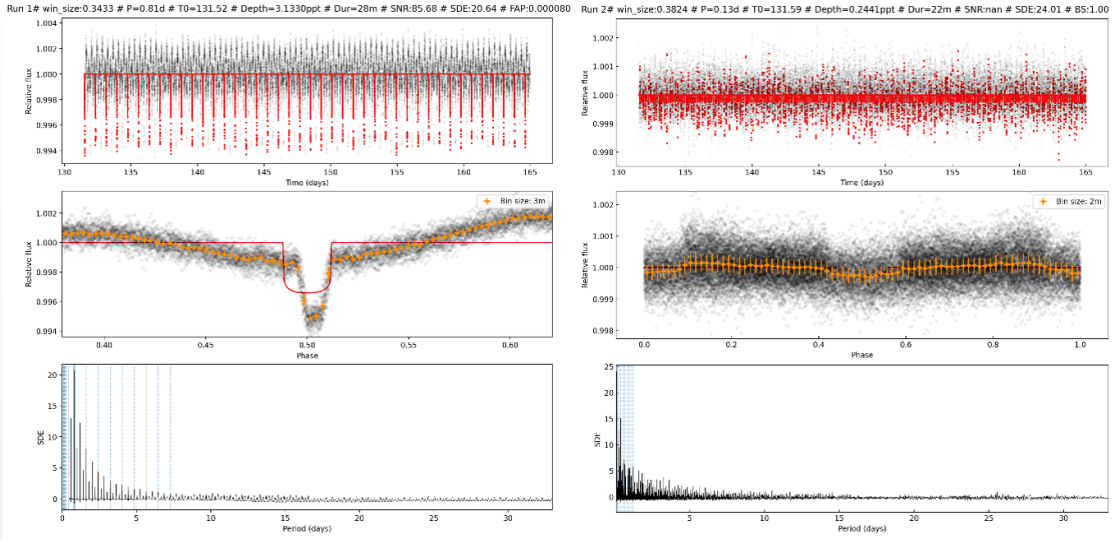

Fig. 48: SHERLOCK output for KIC7975824. The variability is clearly still present in the left plot, while the right plot is unusable (SNR:nan)

At this point, we stopped our work on this target. Since no transiting planets are expected to be detected in such an environment, and seeing the tremendous effort it would take to detrend such variability properly, we chose to move on. This example is interesting, nonetheless, as it clearly highlights the limits of SHERLOCK for such highly variable targets.

5.3 KIC10449976 (He-sdOB)

KIC10449976 is a He-sdOB star observed in Q3.2 in short cadence. The signal we deemed interesting in this case is the second one selected by SHERLOCK.

This candidate has a period of 2.55 days and was spotted in five detrends (SNR=11, SDE=7.14). Values of SDE are on the lower side but not a red flag. Some harmonics can be seen, especially the first and second, but since their SDE values are even lower, these harmonics do not appear very clearly. The transit is relatively shallow, with a depth of only 547 ppm. The error bars are almost the depth of the transit, which might be worrying. All of these comments can be seen looking at Fig. 49.

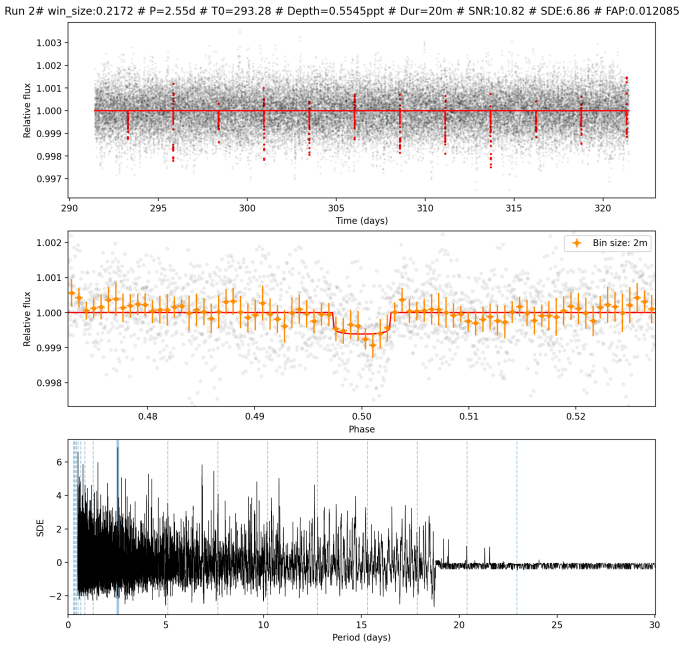

Fig. 49: SHERLOCK output for KIC10449976.

This target is a typical case of detection that is not overly promising and exciting at first glance, but it is still worth further investigation.

To investigate further, let us take a look at the vetting. In Fig. 50, we can see the vetting is promising, with all numerical tests passed, with the expected exception of the transit offset. Let us see the source offset plot to confirm this red flag is not a worrying sight.

T0 (d)	Period (d)	Duration (h)	Depth (ppt)
293.2792	2.5495	0.34	0.564

Table 2: The candidate parameters.

Metric	Value	Passed
snr_p_t0	11.029	True
snr_p_2t0	0.806	True
snr_2p_t0	9.585	True
snr_2p_2t0	5.817	True
snr_p2_t0	0.806	True
snr_p2_t02	0.492	True
snr_p_score	0.073	True
snr_2p_score	3.768	True
snr_p2_score	0.028	True
transit_offset_ra	281.809	True
transit_offset_dec	47.696	True
transit_offset_err	0.0	True
transit_offset_pos	0.0	False
core_flux_snr	0.441	nan
halo_flux_snr	-0.742	nan
og_score	-1.681	nan
centroids_ra_snr	-1.201	True
centroids_dec_snr	-1.661	True

Table 3: The results of the numerical tests.

Fig. 50: Summary of the numerical tests for KIC10449976's second candidate's vetting.

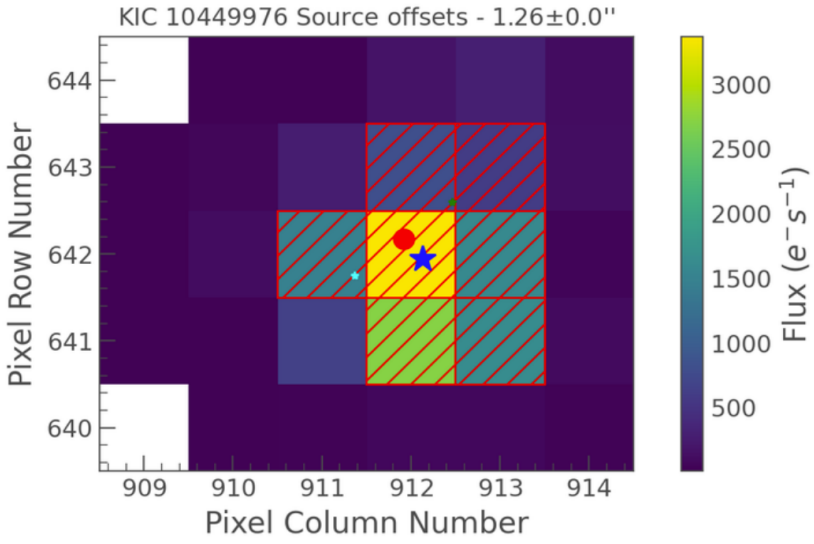

Fig. 51: Source offset for KIC10449976 second candidate.

As we can see in Fig. 51, the source offset is satisfactory. It appears to be on the same pixel, with an offset of only 1.26", less than Kepler's pixel size of 3.98". The relatively high discrepancy between the two methods used during the vetting might lead to higher uncertainty, though, and that has to be taken into account.

With the vetting from this candidate passed, we now need to perform the statistical validation. Firstly, we see in Fig. 52 that the stellar neighborhood is sparsely populated, an encouraging sign of a lack of nearby contamination.

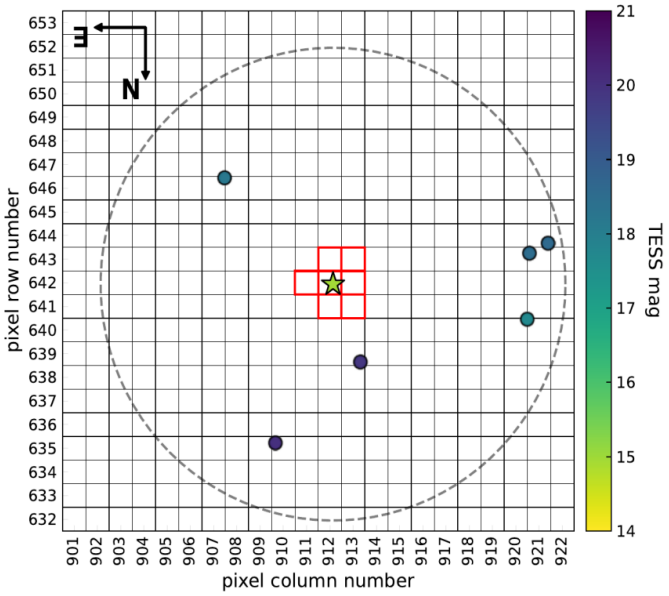

Fig. 52: Stellar neighborhood around KIC10449976, as provided by TRICERATOPS.

Fig. 53 shows the results from the statistical validation. As we can see, the mean result yields a high probability of false positives, with the most likely scenarios being a background eclipsing binary (BEB) or a background transiting planet (BTP). These results are worrying and might be enough to discard this candidate.

ID	scenario	M_s	R_s	P_orb	inc	b	ecc	w	R_p	M_EB	R_EB	prob
123414355	TP	0.47	0.14	2.55	89.05	0.48	0.59	183.2	1.4	0.0	0.0	0.035233
123414355	EB	0.47	0.14	2.55	87.86	1.97	0.0	231.58	0.0	0.41	0.14	0.018598
123414355	EBx2P	0.47	0.14	5.1	89.07	0.95	0.59	184.3	0.0	0.46	0.14	0.016739
123414355	PTP	0.47	0.14	2.55	89.21	0.57	0.15	105.74	0.53	0.0	0.0	0.036947
123414355	PEB	0.47	0.14	2.55	87.65	1.91	0.02	223.01	0.0	0.16	0.14	0.006883
123414355	PEBx2P	0.47	0.14	5.1	88.64	1.0	0.76	197.01	0.0	0.46	0.14	0.005789
123414355	STP	0.28	0.14	2.55	89.36	0.35	0.35	162.75	0.95	0.0	0.0	0.474921
123414355	SEB	0.12	0.14	2.55	87.11	1.6	0.04	204.38	0.0	0.04	0.1	0.077114
123414355	SEBx2P	0.17	0.14	5.1	88.32	1.72	0.12	172.85	0.0	0.17	0.14	0.056894
123414355	DTP	0.47	0.14	2.55	89.13	0.64	0.09	167.13	0.51	0.0	0.0	0.004782
123414355	DEB	0.47	0.14	2.55	87.67	1.97	0.0	136.55	0.0	0.23	0.14	0.001821
123414355	DEBx2P	0.47	0.14	5.1	88.84	1.29	0.49	208.32	0.0	0.46	0.14	0.001591
123414355	BTP	0.29	0.28	2.55	84.79	0.54	0.77	101.67	3.4	0.0	0.0	0.098582
123414355	BEB	0.37	0.33	2.55	86.27	0.55	0.86	260.44	0.0	0.09	0.11	0.133729
123414355	BEBx2P	0.2	0.2	5.1	86.68	1.49	0.36	154.88	0.0	0.19	0.2	0.030376

Table 3: Scenarios attributes and probabilities.

Scenario	FPP	NFPP	FPP2	FPP3+
0	0.92096	0.0	0.317905	0.188993
1	0.924785	0.0	0.329672	0.19737
2	0.924312	0.0	0.328176	0.196298
3	0.922415	0.0	0.322292	0.192102
4	0.92272	0.0	0.323225	0.192766
MEAN	0.923038	0.0	0.324254	0.193506

Table 4: Validation results.

Fig. 53: Results of the statistical validation performed by TRICERATOPS on KIC10449976's second signal.

5.4 KIC2569583 (sdB)

This star is relatively faint (Kp=15.4, see section 3.3) and was observed in Q11.2 in short cadence. In this case, only the first candidate was considered promising and will be investigated further. The other three signals had low SDEs and often coincided with light curve patterns.

This first signal was spotted in six detrends, with a period of 2.00 days. Values of SNR and SDE are satisfactory (SNR=11.5, SDE=7.3). Although the transit is quite shallow in the folded curve, harmonics are relatively easy to spot in the power spectrum, as seen in Fig. 54.

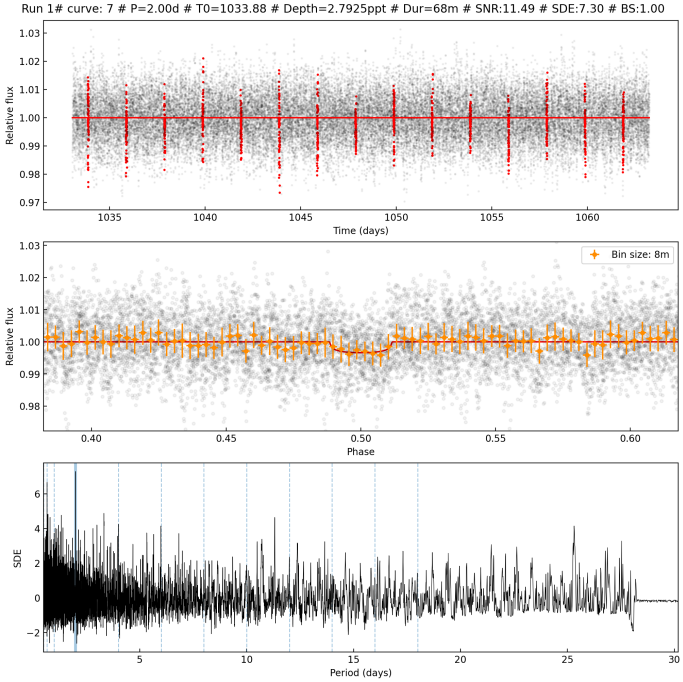

Fig. 54: KIC2569583, results for the first selected candidate.

These first results don't raise any red flags, and a closer inspection is in order. As usual, the next step in such cases is to perform the vetting.

T0 (d)	Period (d)	Duration (h)	Depth (ppt)
1033.8754	1.9994	1.13	2.792

Table 2: The candidate parameters.

Metric	Value	Passed
snr_p_t0	11.219	True
snr_p_2t0	2.067	True
snr_2p_t0	6.701	True
snr_2p_2t0	8.381	True
snr_p2_t0	2.067	True
snr_p2_t02	0.902	True
snr_p_score	0.184	True
snr_2p_score	1.68	True
snr_p2_score	0.104	True
transit_offset_ra	290.188	False
transit_offset_dec	37.806	True
transit_offset_err	0.0	True
transit_offset_pos	0.001	False
core_flux_snr	2.281	nan
halo_flux_snr	0.92	nan
og_score	0.403	nan
centroids_ra_snr	0.13	True
centroids_dec_snr	-1.733	True

Table 3: The results of the numerical tests.

Fig. 55: KIC2569583, results of vetting the numerical tests

As seen in Fig. 55, every metric is passed except for the transit offset RA. Let us take a closer look at the source offset.

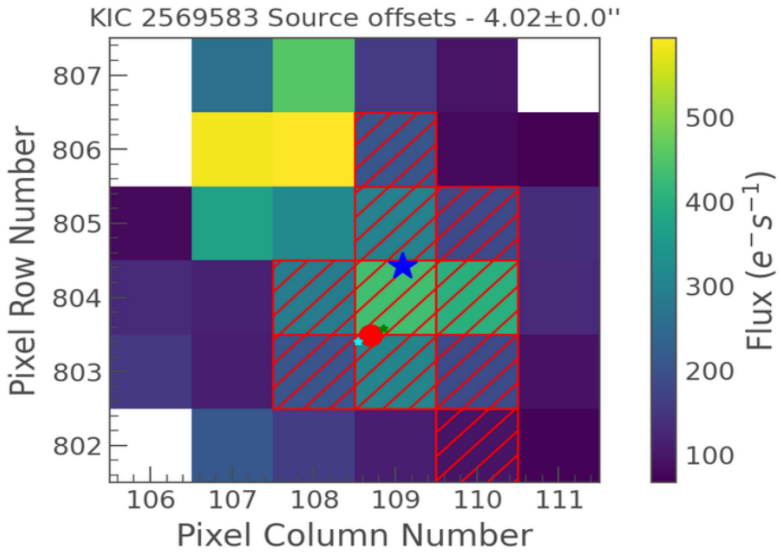

Fig. 56: KIC2569583, source offset as computed during the vetting.

A few things can be inferred from Fig. 56. First, the source offset is only 4.02". This is bigger than Kepler's pixel size of 3.98", hence the red flag, but the margin is so small

we decided not to consider this disqualifying, especially since our target and the computed source are on the same pixel.

The high flux in the top left corner is a more worrying sight, only a few pixels away from our target. This indicates the presence of a bright source nearby that could contaminate our results, even though the source offset doesn't seem to align with this higher flux.

Looking at the statistical validation would be particularly useful in this case, especially to see what nearby stars are bright enough to cause possible contamination. Unfortunately, this specific target is unavailable in TRICERATOPS catalog, and we can't proceed further.

5.5 KIC7104168 (sdB)

This target was observed in Q3.1 in short cadence. The first signal, with a period of 1.15 days, is the one we focus on. This candidate was spotted in eleven detrends, with satisfactory values of SNR and SDE (SNR=11.91, SDE=9.64). Figure 57 shows the result from SHERLOCK for this candidate, where we can see the transit is relatively shallow, and harmonics are not easily spotted. However, the values of SNR and SDE, as well as the high number of detrends the signal was spotted on, make it fit to be investigated further. As always, we perform the vetting.

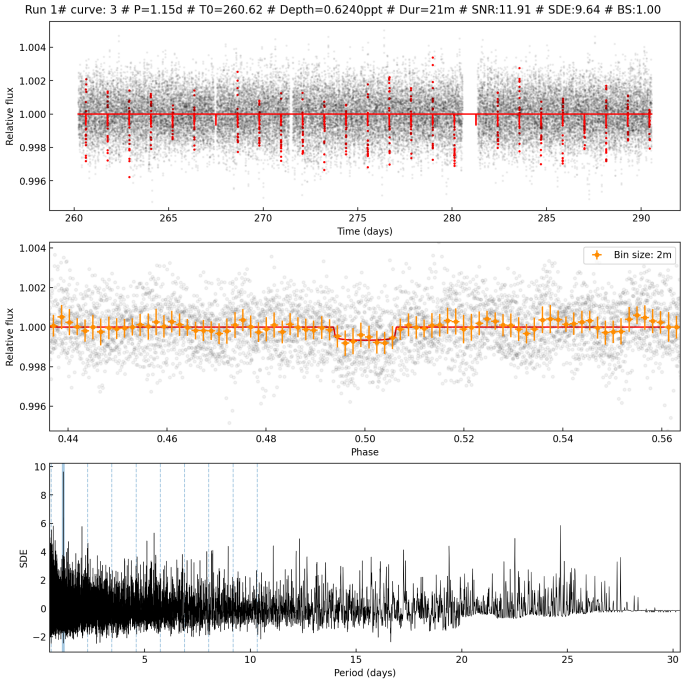

Fig. 57: KIC7104168, SHERLOCK results for the first candidate.

Figure 58 shows no obvious red flag in the numerical tests, except for the transit offset position, of which the error is not calculated. Let us look at the source offset to investigate.

T0 (d)	Period (d)	Duration (h)	Depth (ppt)
260.6188	1.1469	0.35	0.624

Table 2: The candidate parameters.

Metric	Value	Passed
snr_p_t0	12.404	True
snr_p_2t0	0.001	True
snr_2p_t0	7.882	True
snr_2p_2t0	9.741	True
snr_p2_t0	0.001	True
snr_p2_t02	0.001	True
snr_p_score	0.0	True
snr_2p_score	1.859	True
snr_p2_score	0.0	True
transit_offset_ra	287.191	True
transit_offset_dec	42.642	True
transit_offset_err	0.0	True
transit_offset_pos	0.0	False
core_flux_snr	4.122	True
halo_flux_snr	-0.674	nan
og_score	-0.163	True
centroids_ra_snr	0.904	True
centroids_dec_snr	-0.07	True

Table 3: The results of the numerical tests.

Fig. 58: KIC7104168, vetting numerical test results.

Figure 59 shows the source offset, where the source is only 0.8" away from our target, with relatively high agreement from both methods. This alone is a good sign, but the high flux in the adjacent pixels might indicate a brighter star nearby. It is necessary to perform statistical validation to rule out this possibility.

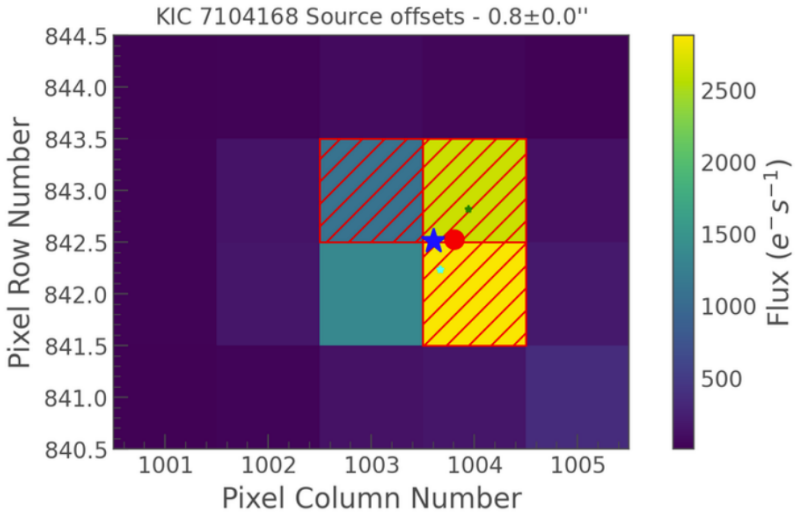

Fig. 59: KIC7104168, source offset plot from the vetting.

We first check nearby stars bright enough to cause contamination since this is the main

concern that arose from our vetting. Our suspicions seem to be confirmed, as seen in Fig. 60. We have a bright star only one pixel away from our target, the position of which likely explains the high flux seen in Fig. 59. Let us see the false positive probabilities obtained by TRICERATOPS.

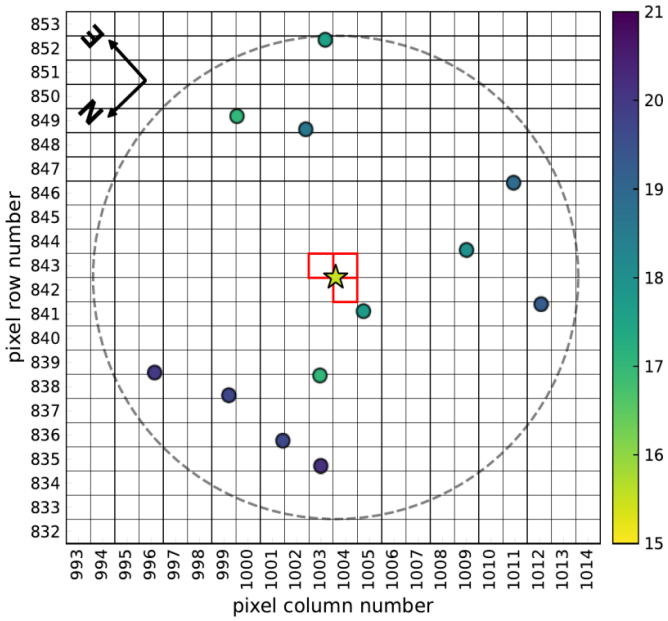

Fig. 60: KIC7104168, stellar neighborhood from the statistical validation.

Figure 61 confirms our fears. The probabilities of false positives are high, and the probabilities of nearby false positives (NFPP) as well, which points toward contamination. From these results, the culprit seems to be TIC158425873, as seen from the three nearby scenarios (NTP, NEB, and NEBx2P). Unfortunately, I could not obtain more information about this star and any possible variability that may cause contamination.

ID	scenario	M_s	R_s	P_orb	inc	b	ecc	w	R_p	M_EB	R_EB	prob
158425875	TP	0.47	0.18	1.15	88.31	0.64	0.13	235.36	0.5	0.0	0.0	0.115662
158425875	EB	0.47	0.18	1.15	58.86	1.79	0.86	61.02	0.0	0.29	0.18	0.043853
158425875	EBx2P	0.47	0.18	2.29	87.7	0.49	0.75	165.57	0.0	0.46	0.18	0.040781
158425875	PTP	0.47	0.18	1.15	89.18	0.28	0.36	274.67	0.6	0.0	0.0	0.045876
158425875	PEB	0.47	0.18	1.15	63.98	1.79	0.69	54.07	0.0	0.26	0.18	0.01495
158425875	PEBx2P	0.47	0.18	2.29	87.92	1.06	0.59	189.75	0.0	0.46	0.18	0.013192
158425875	STP	0.14	0.16	1.15	89.2	0.18	0.47	272.07	1.9	0.0	0.0	0.190597
158425875	SEB	0.11	0.14	1.15	86.05	1.08	0.33	174.83	0.0	0.03	0.1	0.038144
158425875	SEBx2P	0.13	0.15	2.29	87.1	1.45	0.31	182.18	0.0	0.12	0.15	0.03567
158425875	DTP	0.47	0.18	1.15	88.57	0.42	0.35	127.6	0.54	0.0	0.0	0.018269
158425875	DEB	0.47	0.18	1.15	62.67	1.92	0.69	93.76	0.0	0.26	0.18	0.005977
158425875	DEBx2P	0.47	0.18	2.29	87.56	0.46	0.81	162.87	0.0	0.45	0.18	0.005655
158425875	BTP	0.22	0.23	1.15	86.58	0.52	0.52	85.52	2.68	0.0	0.0	0.126224
158425875	BEB	0.45	0.41	1.15	81.57	0.82	0.72	202.16	0.0	0.1	0.12	0.163117
158425875	BEBx2P	0.22	0.23	2.29	85.61	1.75	0.03	153.85	0.0	0.21	0.23	0.055967
158425873	NTP	0.74	0.57	1.15	74.31	0.76	0.71	19.64	9.96	0.0	0.0	0.017379
158425873	NEB	0.74	0.57	1.15	77.15	1.18	0.44	23.13	0.0	0.14	0.16	0.057888
158425873	NEBx2P	0.74	0.57	2.29	72.57	1.93	0.63	34.07	0.0	0.72	0.57	0.0108

Table 3: Scenarios attributes and probabilities.

Scenario	FPP	NFPP	FPP2	FPP3+
0	0.818789	0.085985	0.153072	0.082879
1	0.821176	0.085991	0.15518	0.084117
2	0.819958	0.08701	0.154099	0.083481
3	0.817521	0.085492	0.151969	0.082233
4	0.823523	0.085855	0.157297	0.085362
MEAN	0.820193	0.086066	0.154323	0.083615

Table 4: Validation results.

Fig. 61: KIC7104168, results from the statistical validation.

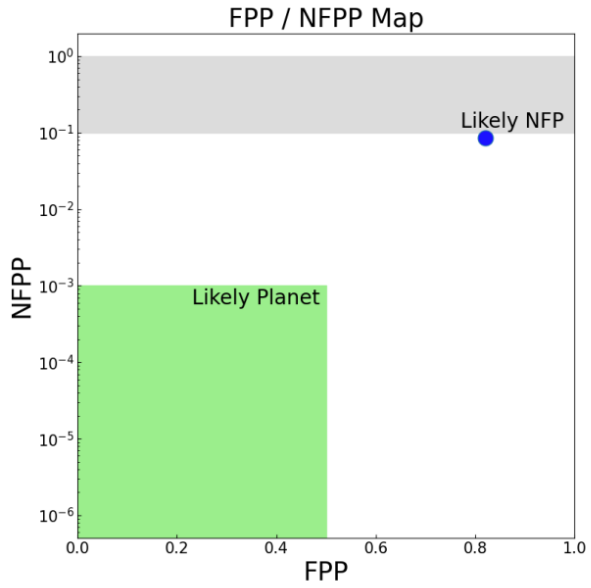

Fig. 62: KIC7104168, FPP (False Positive Probability)/NFPP (Nearby FPP) map from the statistical validation.

The visual FPP/NFPP map shown in Fig. 62 is clear. This candidate is likely the result of contamination from a nearby star instead of an actual substellar object orbiting our hot subdwarf. With this in mind, we discarded this signal.

5.6 KIC10149211 (sdB+?)

This target is interesting, as it shows variations with a period of roughly 0.6 days, the origins of which are unclear. It is proposed in Østensen et al. 2011 [29] that these variations come from a contaminating object instead of the sdB itself. A contaminating star with many stellar spots could account for the behavior seen in KIC10149211's light curve.

Given this variability, I used the autodetrend in SHERLOCK. As expected, it removed a period of 0.6 days, leaving us with clean light curves.

I searched this target for Q4.2 in short cadence. Of the four detected candidates, I will focus on the first one, which I consider the most promising. This first signal, with a period of 5.54d, was spotted in 10 detrends. Values of SDE and SNR are satisfactory (SNR=10.44, SDE=7.35). In Fig. 63, we can see the results, where a nice transit shape can be seen in the folded light curve, and the first and second harmonics are easy to spot in the power spectrum. This promising candidate deserves to move to the next step, the vetting.

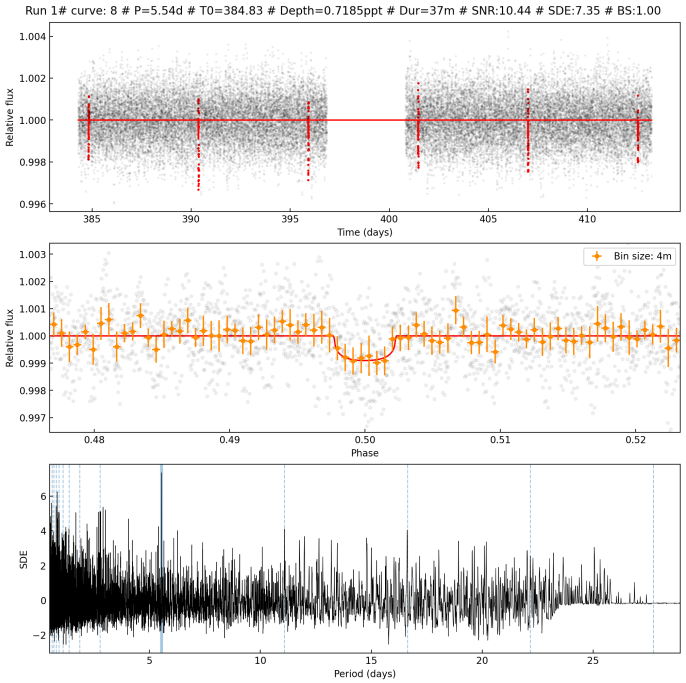

Fig. 63: KIC10149211, results for the first candidate.

Figure 64 reveals no red flags from the vetting. Every test is passed except, of course, the transit offset. Let us check the source offset plot to see if there is something to worry about.

T0 (d)	Period (d)	Duration (h)	Depth (ppt)
384.8256	5.5431	0.62	0.719

Table 2: The candidate parameters.

Metric	Value	Passed
snr_p_t0	10.222	True
snr_p_2t0	1.184	True
snr_2p_t0	7.347	True
snr_2p_2t0	7.205	True
snr_p2_t0	1.184	True
snr_p2_t02	1.051	True
snr_p_score	0.116	True
snr_2p_score	0.142	True
snr_p2_score	0.013	True
transit_offset_ra	294.826	True
transit_offset_dec	47.149	True
transit_offset_err	0.0	True
transit_offset_pos	0.0	False
core_flux_snr	-0.168	nan
halo_flux_snr	-0.143	nan
og_score	0.851	nan
centroids_ra_snr	-0.83	True
centroids_dec_snr	-0.455	True

Table 3: The results of the numerical tests.

Fig. 64: KIC10149211, results of the vetting's numerical tests.

Figure 65 reveals a source only 1.3" away from our target, less than Kepler's pixel size of 3.98". The source also seems to be in the same pixel as our target, a good sign. From this plot, I infer that the source offset is satisfactory. We can now move to the next step: statistical validation. This is especially important in this case since we already know that our target might be contaminated, and the source offset does show a high flux right next to our target. Hence checking stellar neighborhoods is essential to investigate potential contamination.

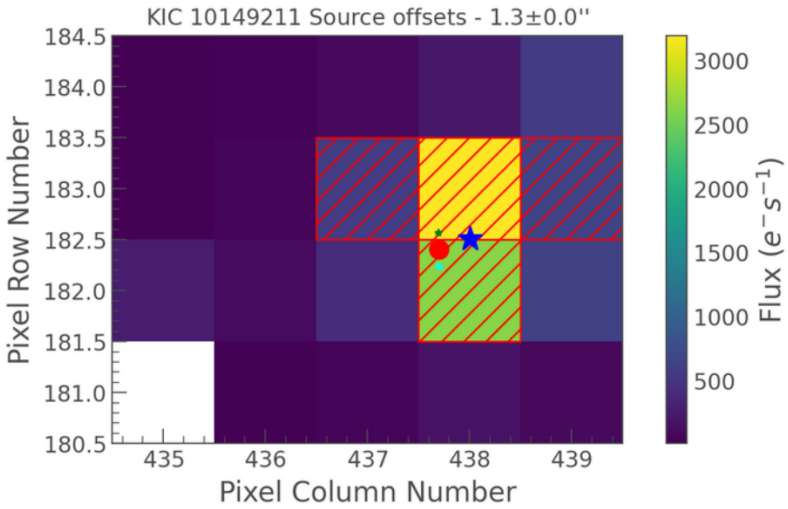

Fig. 65: KIC10149211, source offset plot.

Figure 66 reveals a relatively busy neighborhood. Many stars bright enough to contribute to our light curve are within a few pixels. The higher flux seen in Fig. 65 doesn't seem to correspond to one of these neighbors, which is a good sign. Sadly, the statistical validation itself could not be computed since TRICERATOPS could not retrieve enough information about our target. Follow-up observations were considered for this candidate, but the sdB is not bright enough (Kp=15.5) for TRAPPIST, the ground-based telescope we usually use for such purposes.

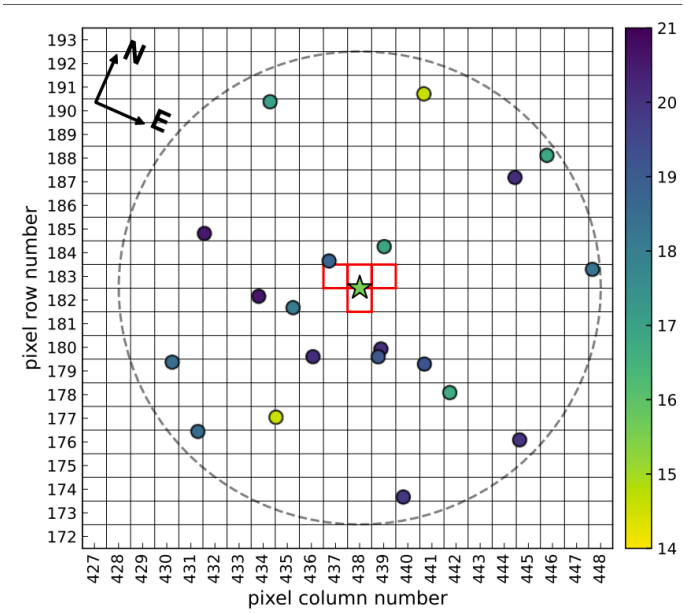

Fig. 66: KIC10149211, stellar neighborhood from the statistical validation.

This candidate remains promising, but the lack of follow-up observations and the inability to fully perform the statistical validation restrains me from drawing more solid conclusions. Contamination from nearby stars is not out of the picture at all.

5.7 KIC2020175 (sdB)

KIC2020175 is an sdB star observed in Q3.1 in short cadence. In this work, I selected the second candidate spotted by SHERLOCK as the most promising and worthy of further investigation.

With a period of 2.70d, this first signal was spotted in 11 detrends. SNR and SDE are satisfactory (SNR=12.07, SDE=8.80). Figure 67 displays the first results from SHERLOCK, where we see a relatively nice transit shape and some discreet but present harmonics in the power spectrum. This, combined with the good values of SNR & SDE and the high number of detrends this signal was spotted on, justifies moving to the next step.

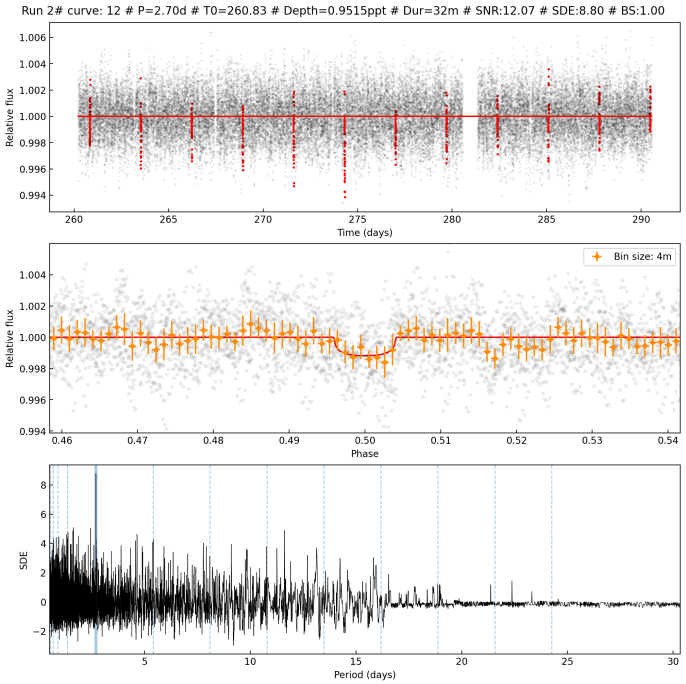

Fig. 67: KIC2020175, result for the second signal

Figure 68 shows a promising vetting, where every numerical test has been passed. Let us check the source offset to see if the target position is worrying.

T0 (d)	Period (d)	Duration (h)	Depth (ppt)
260.8315	2.6956	0.54	0.951

Table 2: The candidate parameters.

Metric	Value	Passed
snr_p_t0	12.034	True
snr_p_2t0	0.001	True
snr_2p_t0	9.108	True
snr_2p_2t0	7.983	True
snr_p2_t0	0.001	True
snr_p2_t02	0.427	True
snr_p_score	0.0	True
snr_2p_score	1.125	True
snr_p2_score	0.035	True
transit_offset_ra	292.703	True
transit_offset_dec	37.472	True
transit_offset_err	0.0	True
transit_offset_pos	0.001	False
core_flux_snr	1.129	nan
halo_flux_snr	0.057	nan
og_score	0.051	nan
centroids_ra_snr	-0.406	True
centroids_dec_snr	-0.639	True

Table 3: The results of the numerical tests.

Fig. 68: KIC2020175, numerical tests results from the vetting

Figure 69 is reassuring. The source is 1.7" away from our target, less than Kepler's pixel size of 3.98", and in the same pixel. However, the two methods used to calculate this source

offset are not in good agreement, raising uncertainty. Even if this offset is not an obvious red flag, this increased uncertainty has to be kept in mind. To investigate this target further, I perform the statistical validation.

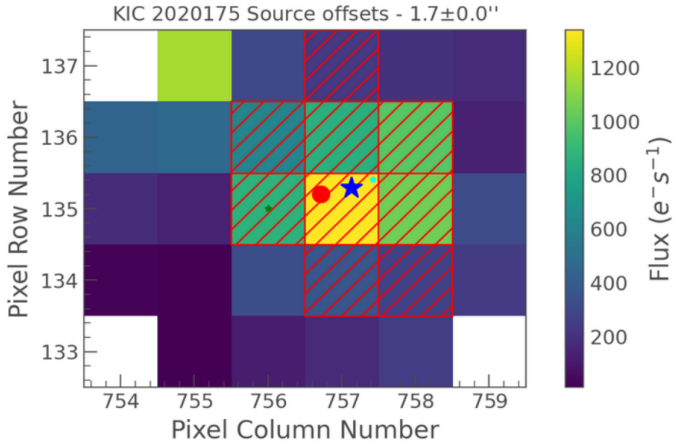

Fig. 69: KIC2020175, source offset plot from the vetting

Figure 70 shows a relatively busy stellar neighborhood, with many stars bright enough to contribute to our target's light curves. One such star is almost on the same pixel as KIC2020175. Sadly, TRICERATOPS could not perform the full validation for the same reason as for KIC10149211. Hence we don't have the probability of nearby false positives.

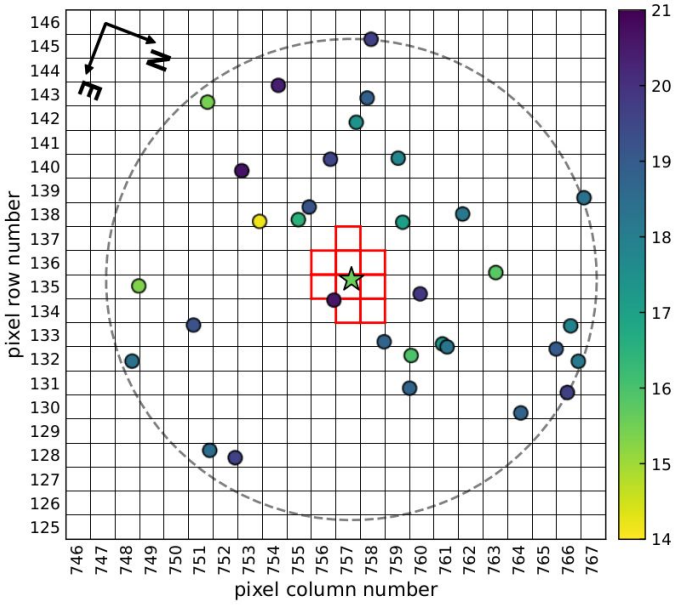

Fig. 70: KIC2020175, stellar neighborhood from the statistical validation.

This signal remains promising, but I could not completely remove the possibility of con-

tamination from a nearby star.

5.8 KIC1202174 (sdB+WD?)

KIC1202174 is believed to be an sdB+WD binary system with an orbital period of 0.67490d. A WD companion is a possible interpretation proposed by Østensen et al. 2011 [29], although we have no certainty.

The target was observed for Q4.2 in short cadence. As for all variable stars, the autodetrend was used. In this case, a period of 0.68d was removed, as expected from the literature values. I selected the second signal as the most promising.

With a period of 3.50d, the signal was spotted in 10 detrends. Values of SNR and SDE are satisfactory (SNR=11.43, SDE=7.41). Figure 71 displays the first results, in which we see a nice deep (depth=1.4918ppt) transit in the folded light curve. However, harmonics are not easily seen in the power spectrum. Despite the lack of obvious harmonics, this candidate deserves further investigation, as every else seems to be a green flag.

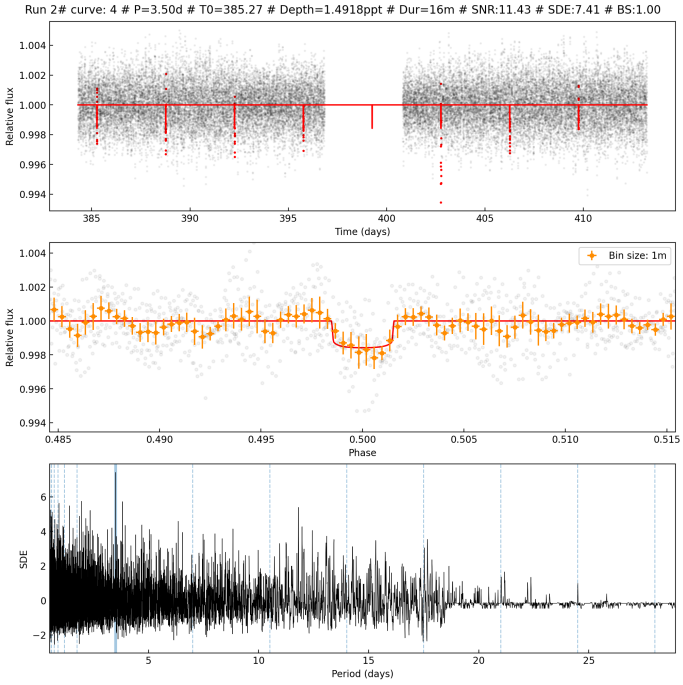

Fig. 71: KIC12021724, results for the second candidate.

Figure 72 shows a promising vetting, where our candidate passed all numerical tests. We must inspect the source offset to check this last potential red flag.

T0 (d)	Period (d)	Duration (h)	Depth (ppt)
385.2697	3.4985	0.26	1.492

Table 2: The candidate parameters.

Metric	Value	Passed
snr_p_t0	10.938	True
snr_p_2t0	0.001	True
snr_2p_t0	7.149	True
snr_2p_2t0	8.5	True
snr_p2_t0	0.001	True
snr_p2_t02	0.011	True
snr_p_score	0.0	True
snr_2p_score	1.351	True
snr_p2_score	0.001	True
transit_offset_ra	296.054	True
transit_offset_dec	50.494	True
transit_offset_err	0.0	True
transit_offset_pos	0.0	False
core_flux_snr	1.918	nan
halo_flux_snr	0.064	nan
og_score	0.033	nan
centroids_ra_snr	0.468	True
centroids_dec_snr	0.15	True

Table 3: The results of the numerical tests.

Fig. 72: KIC12021724, numerical test results from the vetting

The source offset seen in Fig. 73 doesn't raise any alarm. The two methods to compute source position seem in relative agreement, and the distance between the source and our target is smaller than Kepler's pixel size.

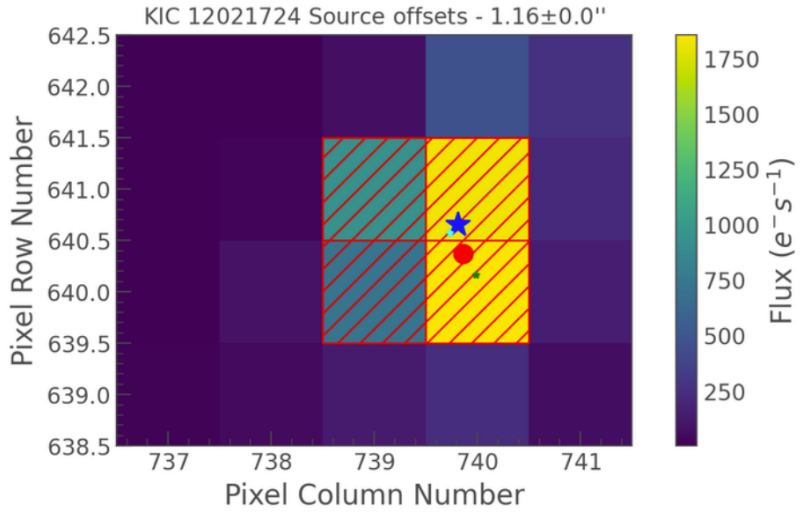

Fig. 73: KIC12021724, source offset plot from the vetting.

The vetting hasn't shown any obvious red flags, and the candidate deserves to be investigated even further. As always, I now perform the statistical validation. I first look at the stellar neighborhood, as seen in Fig. 74. Many stars bright enough to potentially contribute to our light curve are present within 10 pixels of our target, which calls for caution. Let us

look at the results from the statistical validation itself to investigate potential false positive scenarios.

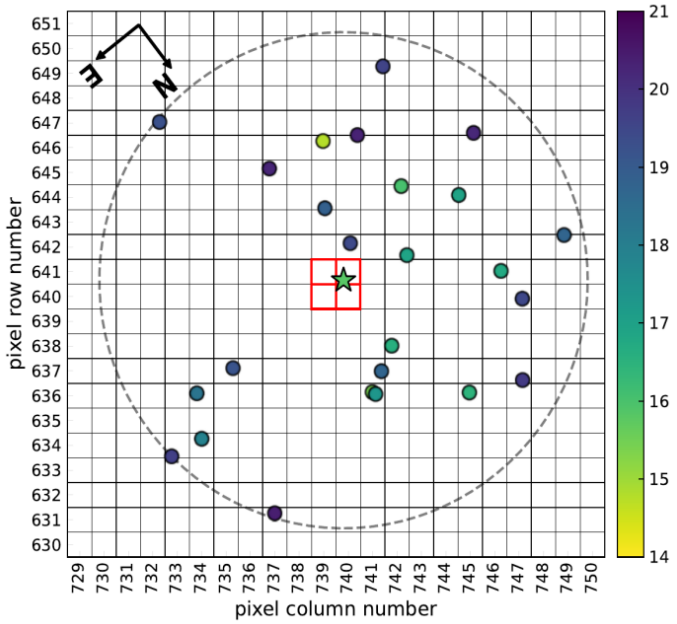

Fig. 74: KIC12021724, stellar neighborhood as given by TRICERATOPS during the statistical validation.

Figure 75 displays the results of the statistical validation itself. These are particularly good, with a mean FPP of only 0.36. We consider a candidate is likely a planet if this value of false positive probability is lower than 0.5. Additionally, the probabilities of nearby false positives, accounting for possible contamination, are extremely low. These are the best results from this validation we got so far.

ID	scenario	M_s	R_s	P_orb	inc	b	ecc	w	R_p	M_EB	R_EB	prob
27766711	TP	0.47	0.18	3.5	88.62	0.51	0.71	150.76	0.8	0.0	0.0	0.461755
27766711	EB	0.47	0.18	3.5	87.84	1.95	0.0	222.67	0.0	0.42	0.18	0.027899
27766711	EBx2P	0.47	0.18	7.0	88.81	1.93	0.21	224.89	0.0	0.46	0.18	0.083668
27766711	PTP	0.47	0.18	3.5	88.24	0.63	0.72	79.2	0.86	0.0	0.0	0.141566
27766711	PEB	0.47	0.18	3.5	87.66	1.93	0.01	168.88	0.0	0.2	0.18	0.020596
27766711	PEBx2P	0.47	0.18	7.0	88.68	1.92	0.01	244.83	0.0	0.46	0.18	0.031418
27766711	STP	0.3	0.18	3.5	88.21	0.44	0.8	208.68	1.73	0.0	0.0	0.122597
27766711	SEB	0.35	0.18	3.5	87.48	1.92	0.0	168.75	0.0	0.19	0.18	0.049009
27766711	SEBx2P	0.46	0.18	7.0	88.67	1.91	0.0	193.55	0.0	0.44	0.18	0.006517
27766711	DTP	0.47	0.18	3.5	88.47	0.55	0.66	156.46	0.86	0.0	0.0	0.035633
27766711	DEB	0.47	0.18	3.5	87.74	1.91	0.0	185.93	0.0	0.26	0.18	0.003013
27766711	DEBx2P	0.47	0.18	7.0	88.72	1.88	0.04	202.34	0.0	0.46	0.18	0.005769
27766711	BTP	0.21	0.22	3.5	84.3	0.71	0.83	151.39	3.4	0.0	0.0	0.001229
27766711	BEB	0.27	0.26	3.5	83.88	0.43	0.92	220.48	0.0	0.08	0.11	0.008935
27766711	BEBx2P	0.14	0.16	7.0	82.21	1.81	0.8	27.14	0.0	0.14	0.16	0.00038
1883115794	NTP	1.0	1.0	3.5	88.94	0.11	0.51	86.74	19.96	0.0	0.0	2e-06
1883115794	NEB	1.0	1.0	3.5	58.42	1.31	0.87	76.83	0.0	0.37	0.37	1.2e-05
1883115794	NEBx2P	1.0	1.0	7.0	59.62	1.92	0.85	23.39	0.0	0.99	1.0	2e-06

Table 3: Scenarios attributes and probabilities.

Scenario	FPP	NFPP	FPP2	FPP3+
0	0.362564	1.5e-05	0.022245	0.011248
1	0.349423	1.5e-05	0.021032	0.010628
2	0.363097	1.6e-05	0.022295	0.011273
3	0.379516	1.6e-05	0.023882	0.012085
4	0.350628	1.5e-05	0.021141	0.010684
MEAN	0.361046	1.5e-05	0.022119	0.011184

Table 4: Validation results.

Fig. 75: KIC12021724, results from the statistical validation performed by TRICERATOPS.

The investigated signal seems promising, as it passed every test successfully. From good values of SNR and SDE, a visually nice and deep transit to good results for both the vetting and statistical validation, this candidate is our most promising so far. Moreover, this candidate's period is not a multiple of the binary orbital period, i.e. it doesn't appear to be linked to this binarity, which seems to have been removed properly during the detrending phase. However, planets with short orbital periods are not expected in such binary systems. These close binaries typically share a common envelope, making the survival of any close substellar object unlikely. Moreover, a planet with a period of 3.50d around a binary with a period of only 0.68d is unlikely from a dynamical point of view, as such an orbit would typically be unstable. Note, however, that this binarity is not confirmed even if this target shows a likely binary period. Østensen mentioned a white dwarf as a valid interpretation of KIC12021724 behavior, but there is no certainty.

Additional observations would be interesting to perform. Alas, this target is not bright enough for follow-up observation from ground-based telescopes such as TRAPPIST (Kp=15.6).

5.9 KIC9211123 (sdB)

KIC9211123 is an sdB observed in Q3.3 in short cadence. The fourth candidate selected by SHERLOCK proved promising at first and deserved to be investigated further.

With a period of 5.62d, this signal was spotted in 8 detrends. Values of SNR and SDE are satisfactory (SNR=11.34, SDE=7.69). Figure 76 displays the first results for this candidate. The suspected transit is relatively clear. However, the harmonics are not obvious in the power spectrum. This is typically not the most promising signal we have seen, but it deserves

investigation.

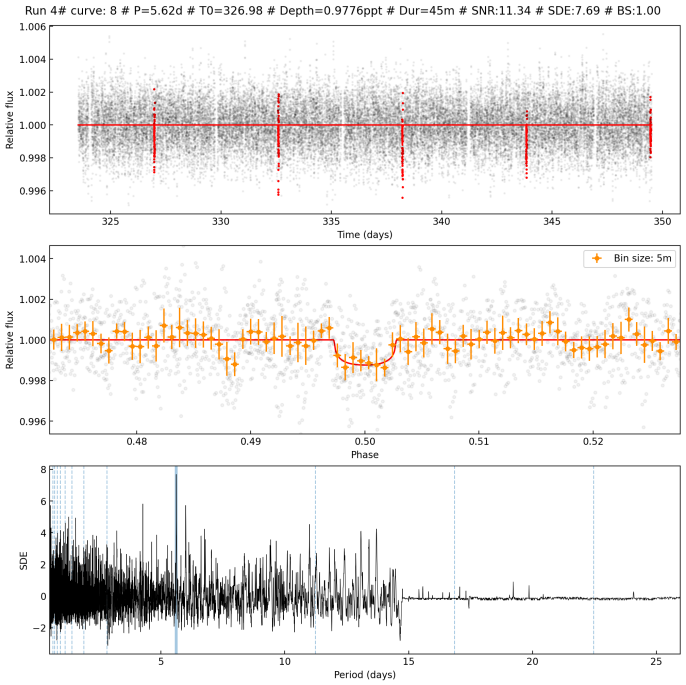

Fig. 76: KIC9211123, results for the fourth signal selected by SHERLOCK.

Most tests in the vetting are passed successfully, as seen in Fig. 77, with the notable exception of the centroids RA. We will check this red flag further to see if it could disqualify this signal.

T0 (d)	Period (d)	Duration (h)	Depth (ppt)
326.9823	5.6175	0.75	0.978

Table 2: The candidate parameters.

Metric	Value	Passed
snr_p_t0	11.904	True
snr_p_2t0	1.011	True
snr_2p_t0	7.862	True
snr_2p_2t0	8.179	True
snr_p2_t0	1.011	True
snr_p2_t02	0.001	True
snr_p_score	0.085	True
snr_2p_score	0.317	True
snr_p2_score	0.085	True
transit_offset_ra	288.614	True
transit_offset_dec	45.652	True
transit_offset_err	0.0	True
transit_offset_pos	0.001	False
core_flux_snr	0.815	nan
halo_flux_snr	0.146	nan
og_score	0.18	nan
centroids_ra_snr	-3.681	False
centroids_dec_snr	-2.27	True

Table 3: The results of the numerical tests.

Fig. 77: KIC9211123, results of the numerical tests from the vetting.

Figure 78 shows the RA centroid shift. At first glance, this plot has no obvious structure, and the SNR is close to the limit value of 3, below which this test would have passed. I decided not to give up on this candidate just yet. However, this red flag is to be kept in mind.

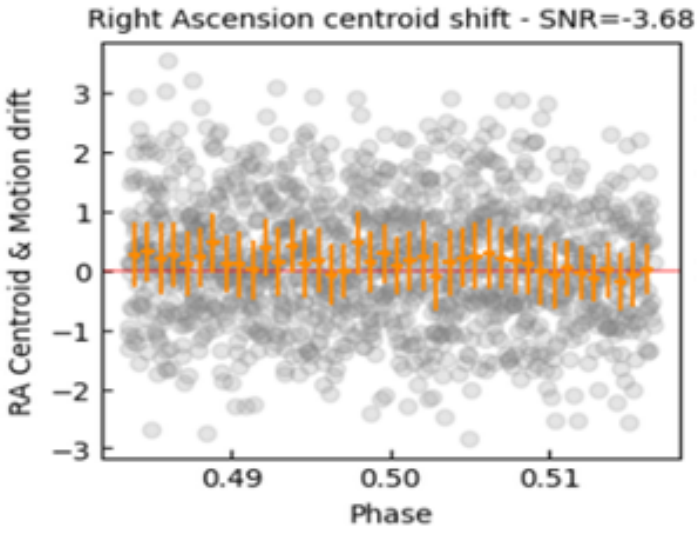

Fig. 78: KIC9211123, Right Ascension centroid shift for the fourth candidate.

The source see in Fig. 79 offset seems alright at first glance, with a source only 2.54" away from our target. However, this source is consistently on another pixel, which begs for caution, especially after the sub-optimal results from the centroid shift tests. Checking stellar neighborhoods using TRICERATOPS becomes essential to see if these issues are due to a contaminating star nearby.

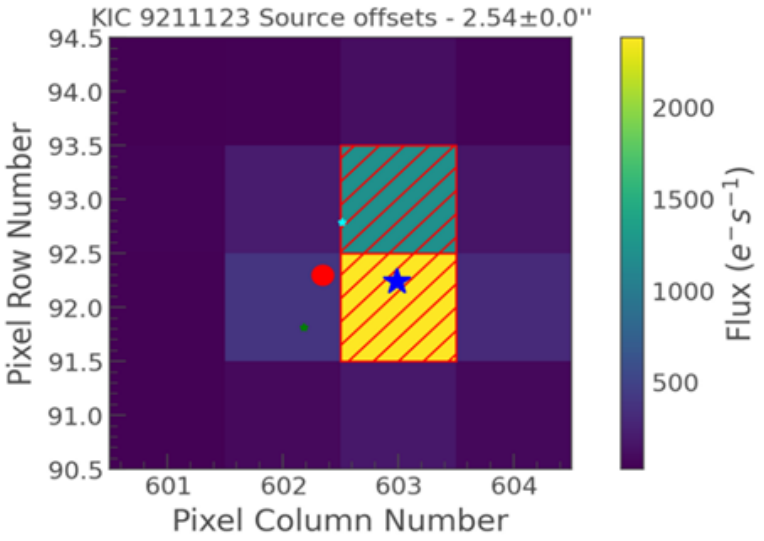

Fig. 79: KIC9211123, Source offset plot for the fourth candidate.

Figure 80 shows a busy neighborhood with stars extremely close to our target. One, in particular, is on the very next pixel, almost at the exact position given for the source offset in Fig. 79. Sadly TRICERATOPS could not perform the full statistical validation for this candidate, but the results we have seen so far seem to point toward contamination from this nearby star.

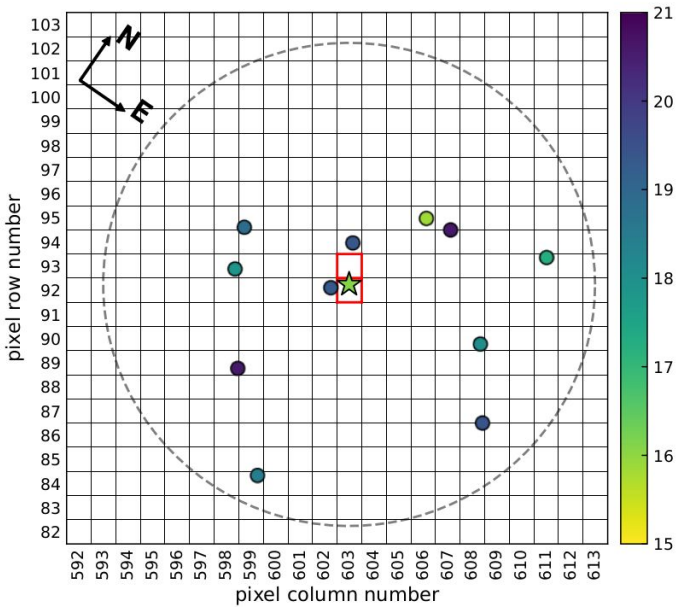

Fig. 80: Stellar neighborhood around KIC9211123 as given by TRICERATOPS.

This signal around KIC9211123 seemed promising initially, but all evidence points toward a contaminated signal from nearby stars. Therefore, I chose to discard it.

5.10 KIC8022110 (sdB)

KIC8022110 is an sdB star observed in Q2.3 in short cadence. The second signal selected by SHERLOCK is the one I investigated further, as it was initially promising.

With a period of 14.51d, this candidate was spotted in 6 detrends. SNR and SDE values are satisfactory (SNR=16.50, SDE=8.70). In Fig. 81, we see a relatively deep (depth=2.3114ppt) transit. Because of the long period, we cannot check for harmonics in the power spectrum. The top plot also shows that the second transit seems close to a small data gap. Further investigation revealed this gap does not impact this transit. These first results are promising, we have one of the deepest transit so far, with good values of SNR and SDE. Hence I chose to investigate this candidate further. The main issue with this signal is that we have only two transits.

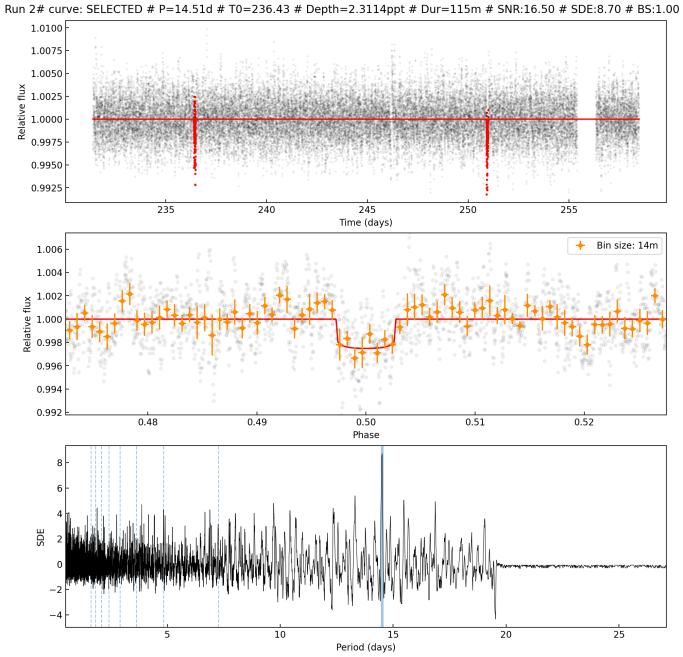

Fig. 81: KIC8022110, results for the second signal selected by SHERLOCK.

Results from the vetting are encouraging, with all numerical tests passed, as seen in Fig. 82. Only the source offset is left to be checked.

T0 (d)	Period (d)	Duration (h)	Depth (ppt)
236.4349	14.5114	1.92	2.311

Table 2: The candidate parameters.

Metric	Value	Passed
snr_p_t0	16.338	True
snr_p_2t0	0.001	True
snr_2p_t0	9.969	True
snr_2p_2t0	13.333	True
snr_p2_t0	0.001	True
snr_p2_t02	0.001	True
snr_p_score	0.0	True
snr_2p_score	3.364	True
snr_p2_score	0.0	True
transit_offset_ra	289.495	True
transit_offset_dec	43.839	True
transit_offset_err	0.0	True
transit_offset_pos	0.0	False
core_flux_snr	-0.212	nan
halo_flux_snr	-0.211	nan
og_score	0.994	nan
centroids_ra_snr	-1.019	True
centroids_dec_snr	-1.456	True

Table 3: The results of the numerical tests.

Fig. 82: KIC8022110, results of the numerical tests for the vetting.

Figure 83 reveals good signs. The computed position of our source is close to the target, at a distance of only 0.61". Both the source and target are located on the same pixel, something both methods agree on. This is another green flag, and this candidate deserves to be investigated even further.

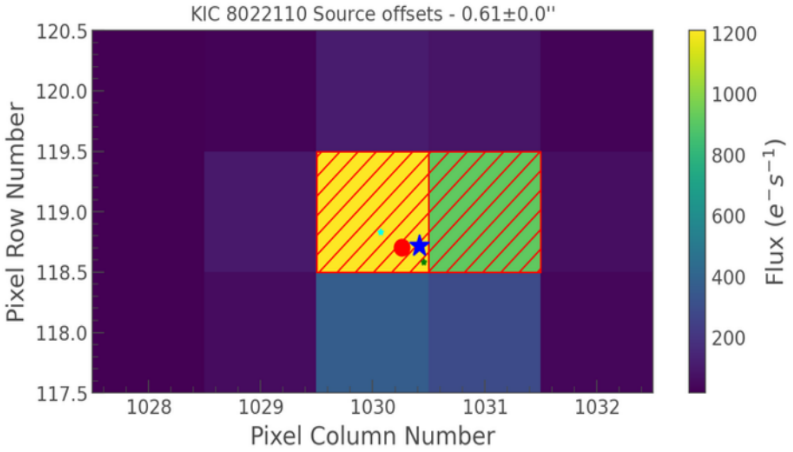

Fig. 83: KIC8022110, plot of the source offset from the vetting.

The stellar neighborhood around KIC8022110 seem sparsely populated, with no bright star directly adjacent to our target, as seen in Fig. 84. Combined with the source offset computed during the vetting, this is a good sign that contamination from nearby stars seems unlikely.

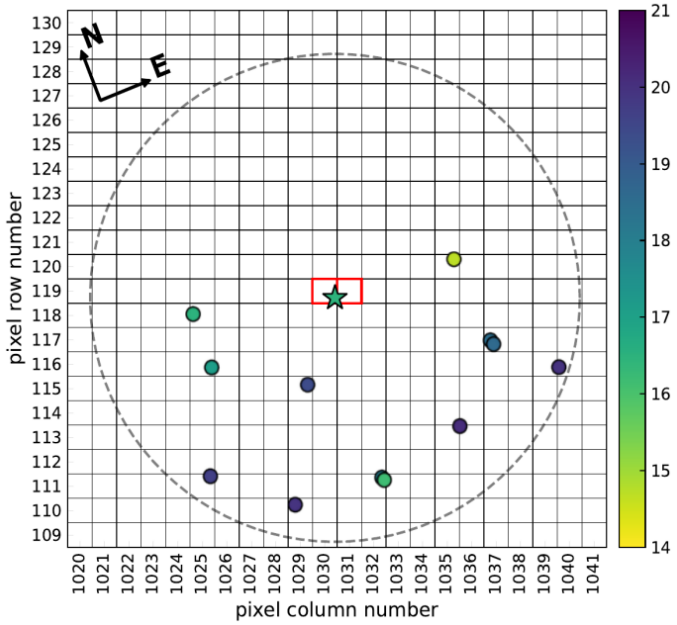

Fig. 84: KIC8022110, stellar neighborhood as given by TRICERATOPS.

The results from the actual statistical validation are more worrying. As detailed in Fig. 85, the False Positive Probability (FPP) is high. Upon closer inspection of the probabilities for each scenario, we see that the most probable source for this candidate is a Background Transiting Planet (BTP) or a Secondary Transiting Planet (STP), i.e., a planet transiting an unresolved companion. I am aware that some of our targets might be unidentified binary systems, which might explain this relatively high STP probability.

ID	scenario	M_s	R_s	P_orb	inc	b	ecc	w	R_p	M_EB	R_EB	prob
159099173	TP	0.47	0.18	14.51	89.9	0.13	0.64	195.55	0.97	0.0	0.0	0.087643
159099173	EB	0.47	0.18	14.51	59.82	1.74	0.79	89.18	0.0	0.26	0.18	0.0
159099173	EBx2P	0.47	0.18	29.02	89.65	0.25	0.88	173.49	0.0	0.46	0.18	0.001246
159099173	PTP	0.47	0.18	14.51	89.93	0.08	0.62	179.28	1.07	0.0	0.0	0.028809
159099173	PEB	0.47	0.18	14.51	61.95	1.64	0.8	83.99	0.0	0.25	0.18	0.0
159099173	PEBx2P	0.47	0.18	29.02	89.42	0.28	0.89	169.21	0.0	0.46	0.18	1.1e-05
159099173	STP	0.18	0.18	14.51	89.88	0.13	0.4	162.55	2.84	0.0	0.0	0.270565
159099173	SEB	0.12	0.15	14.51	89.34	0.5	0.69	172.06	0.0	0.03	0.1	0.000333
159099173	SEBx2P	0.13	0.16	29.02	89.59	0.68	0.59	167.4	0.0	0.13	0.16	0.006584
159099173	DTP	0.47	0.18	14.51	89.89	0.12	0.64	175.8	0.95	0.0	0.0	0.010249
159099173	DEB	0.47	0.18	14.51	66.69	1.79	0.6	78.36	0.0	0.24	0.17	0.0
159099173	DEBx2P	0.47	0.18	29.02	89.5	0.23	0.92	173.49	0.0	0.46	0.18	6.2e-05
159099173	BTP	0.37	0.34	14.51	89.68	0.32	0.15	232.85	3.14	0.0	0.0	0.461257
159099173	BEB	0.44	0.4	14.51	89.68	0.27	0.06	110.95	0.0	0.11	0.13	0.087112
159099173	BEBx2P	0.6	0.55	29.02	88.75	1.76	0.1	171.82	0.0	0.58	0.55	0.04613

Table 3: Scenarios attributes and probabilities.

Scenario	FPP	NFPP	FPP2	FPP3+
0	0.914651	0.0	0.300046	0.176503
1	0.857113	0.0	0.193511	0.10712
2	0.883788	0.0	0.233245	0.132019
3	0.886455	0.0	0.237969	0.135054
4	0.824487	0.0	0.158181	0.085883
MEAN	0.873299	0.0	0.22459	0.127316

Table 4: Validation results.

Fig. 85: KIC8022110, results of the statistical validation.

This candidate remained promising until the very end. From the statistical validation, this might be a transit, possibly in an unresolved background star or orbiting an unidentified companion rather than our sdB target.

5.11 KIC6878288 (He-sdOB+?)

KIC6878288 is a He-sdOB believed to be in a binary system with a period of 3.04d and was observed in Q3.1 in short cadence. In Østensen et al. 2011 [29], it is observed that this star has a high contamination factor, with about half the light coming from other sources nearby. Therefore, the nature of the observed variability in KIC6878288's light curve is unknown. This high contamination factor must be kept in mind for our interpretations of any potential transit candidate.

As for all binary systems, the autodetrend was used. SHERLOCK removed a period of 3.03d, coherent with the above values. In this work, I focused on the first and third signals selected by SHERLOCK. These two candidates are shown in Fig. 86.

With a period of 1.75d, the first signal was spotted in 7 detrends. Values of SNR and SDE are satisfactory (SNR=10.44, SDE=7.88). Harmonics are not obvious in the power

spectrum. This candidate is typically not the most promising, but there is no obvious red flag that would provide a good reason not to investigate a bit deeper.

The third signal, with a period of 4.78d, was spotted in 8 detrends. SNR and SDE values are also satisfactory, although lower than the first candidate for the SDE (SNR=10.78, SDE=6.82). The transit shape and depth are roughly the same as for the first candidate, but harmonics are easier to spot especially the second and fourth ones. Again, nothing prevents me from investigating further.

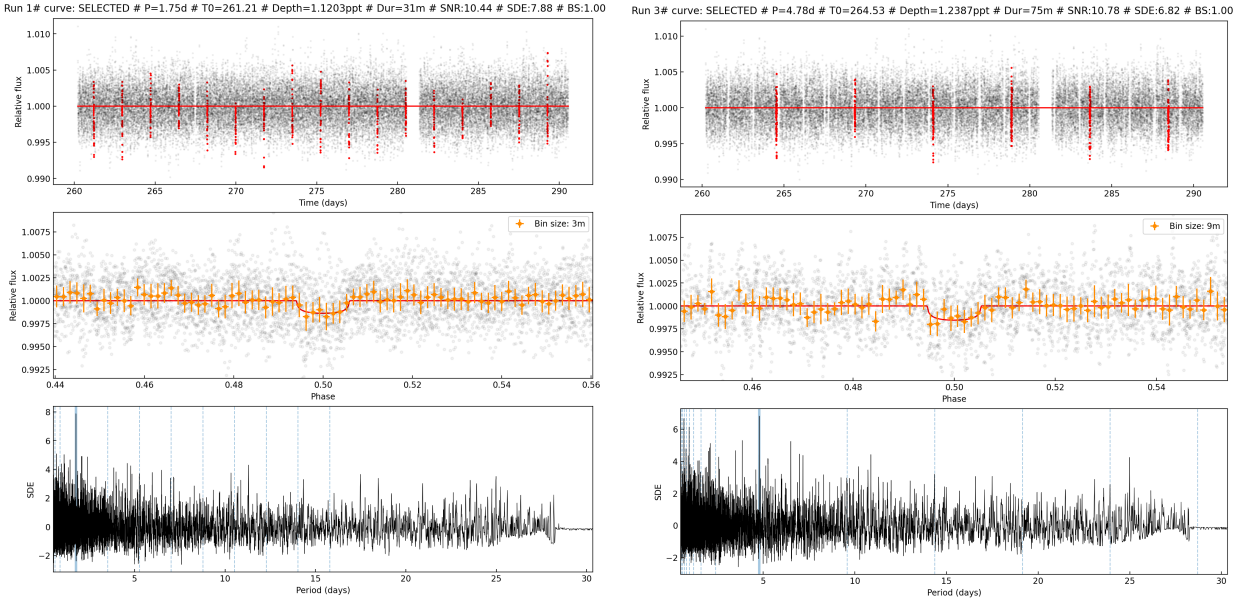

Fig. 86: KIC6878288, results for the first candidate (left) and the third (right) candidate.

The vetting seems to be passed successfully for both candidates, with only the transit offset to be checked, as seen in Fig. 87.

T0 (d)	Period (d)	Duration (h)	Depth (ppt)
261.2053	1.7539	0.51	1.12

Table 2: The candidate parameters.

Metric	Value	Passed
snr_p_t0	10.518	True
snr_p_2t0	0.001	True
snr_2p_t0	7.656	True
snr_2p_2t0	7.156	True
snr_p2_t0	0.001	True
snr_p2_t02	1.492	True
snr_p_score	0.0	True
snr_2p_score	0.501	True
snr_p2_score	0.142	True
transit_offset_ra	295.905	True
transit_offset_dec	42.349	True
transit_offset_err	0.0	True
transit_offset_pos	0.001	False
core_flux_snr	2.969	nan
halo_flux_snr	0.078	nan
og_score	0.026	nan
centroids_ra_snr	-0.834	True
centroids_dec_snr	-0.221	True

Table 3: The results of the numerical tests.

T0 (d)	Period (d)	Duration (h)	Depth (ppt)
264.5305	4.7834	1.24	1.239

Table 2: The candidate parameters.

Metric	Value	Passed
snr_p_t0	10.099	True
snr_p_2t0	0.001	True
snr_2p_t0	6.477	True
snr_2p_2t0	7.817	True
snr_p2_t0	0.001	True
snr_p2_t02	1.543	True
snr_p_score	0.0	True
snr_2p_score	1.341	True
snr_p2_score	0.153	True
transit_offset_ra	295.904	True
transit_offset_dec	42.349	True
transit_offset_err	0.0	True
transit_offset_pos	0.0	False
core_flux_snr	1.711	nan
halo_flux_snr	-0.884	nan
og_score	-0.516	nan
centroids_ra_snr	-0.226	True
centroids_dec_snr	1.585	True

Table 3: The results of the numerical tests.

Fig. 87: KIC6878288, results of the vetting's numerical tests for the first candidate (left) and the third (right) candidate.

Source offsets are satisfactory for both candidates, as seen in Fig 88. The computed source for the first candidate is a bit further away, and the two methods don't agree as much, but all is within the acceptable range. For the third candidate, the two methods are almost in perfect agreement, giving a source extremely close to the target. This is good news, especially knowing we are dealing with a potentially highly contaminated target. Since no obvious red flag arose from the vetting, I investigated these candidates further.

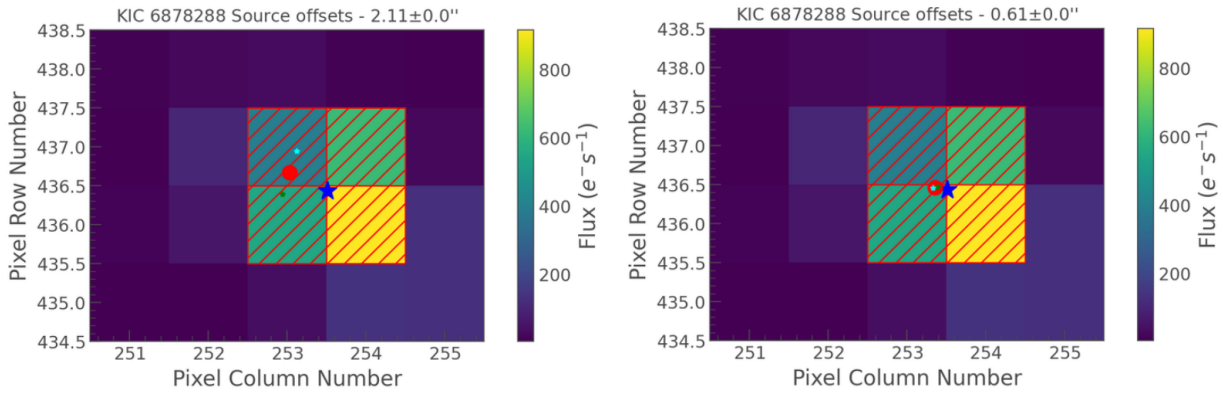

Fig. 88: KIC6878288, plots of the vetting's source offset for the first candidate (left) and the third (right) candidate.

Sadly, as is the case for some of our hot subdwarf targets, TRICERATOPS could not perform statistical validation here. We do, however, have access to the stellar neighborhood around KIC6878288. This will prove especially useful since we have a suspicion of contami-

nation. Comparing the source offsets with stars bright enough to contribute to KIC6878288's light curve is an essential step.

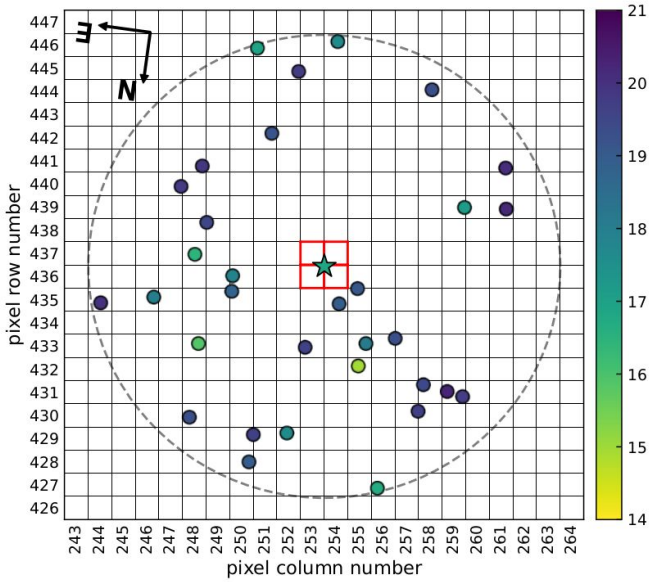

Fig. 89: KIC6878288, stellar neighborhood as given by TRICERATOPS.

Figure 89 shows the nearby stars that are bright enough to contaminate our results potentially. The higher flux in the bottom right of our target, seen in Fig. 88 may be due to the two stars nearby, which could highly contribute to our light curve. It is possible that the signals we see come from these two stars, but the source position computed in the vetting and also seen in that figure does not seem to point in that direction.

These two signals remain promising, although contamination from nearby stars could not be completely ruled out.

5.12 KIC6522967 (sdB)

KIC6522967 is an sdB star observed in Q3.2 in short cadence by Kepler. I selected signals 1 and 4 as the most promising in this work.

With a period of 3.12d, the first signal was spotted in 9 detrends and the original light curve (PDCSAP flux). When the data are clean enough, or a signal is strong, it can be spotted there directly, even before detrending, so this behavior is not unexpected. In this case, the PDCSAP Flux is particularly clean. The SNR and SDE values are satisfactory (SNR=11.97, SDE=8.76). In Fig. 90, we can see a relatively nice transit shape in the folded light curve. The first and second harmonics can be seen in the power spectrum, although not obvious. Note that there might also be a sub-harmonic, something we will have to investigate further during the vetting phase.

The fourth signal, with a period of 5.86d, was spotted in 6 detrends and the PDCSAP

flux. Values of SNR and SDE are again satisfactory (SNR=10.59, SDE=9.03). In Fig. 90, we see an even deeper transit, although there seem to be variations in the folded curve just beyond. We will have to investigate these in the vetting phase. Harmonics are also not obvious, but this is not enough to discard this candidate.

Neither candidate exhibited any major red flag that would immediately discard them, so I moved to the next step.

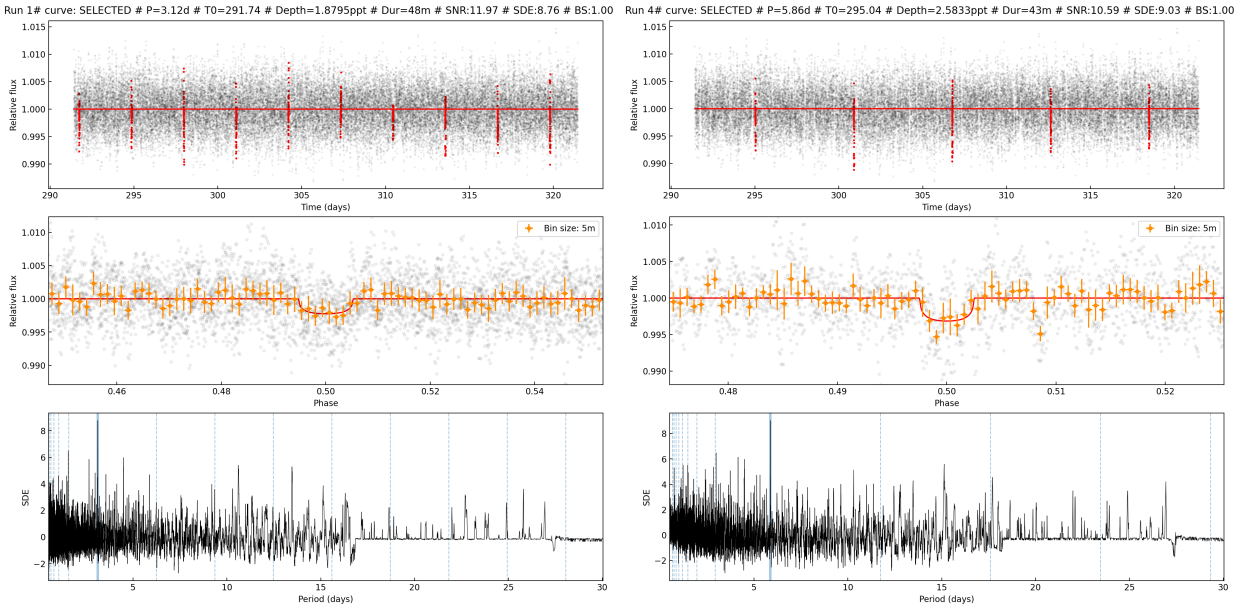

Fig. 90: KIC6522967, results for the first signal (left) and the fourth (right).

Results from the vetting are satisfactory for both candidates, as seen in Fig. 91. There are no red flags in sight. This is especially encouraging since we suspected a subharmonic in both candidates' power spectra, but no signal was detected at half the periods. See snr_p2_t0 and snr_p2_t02, which investigate signals at half the period for the transit epoch and the transit epoch + P/2, respectively. As usual, we now have to check the source offset to see if the vetting was fully passed for both candidates.

T0 (d)	Period (d)	Duration (h)	Depth (ppt)
291.7413	3.117	0.79	1.88

Table 2: The candidate parameters.

T0 (d)	Period (d)	Duration (h)	Depth (ppt)
295.0385	5.8629	0.71	2.583

Table 2: The candidate parameters.

Metric	Value	Passed
snr_p_t0	11.855	True
snr_p_2t0	1.52	True
snr_2p_t0	8.164	True
snr_2p_2t0	8.597	True
snr_p2_t0	1.52	True
snr_p2_t02	0.33	True
snr_p_score	0.128	True
snr_2p_score	0.433	True
snr_p2_score	0.1	True
transit_offset_ra	291.994	True
transit_offset_dec	41.984	True
transit_offset_err	0.0	True
transit_offset_pos	0.0	False
core_flux_snr	2.176	nan
halo_flux_snr	-0.426	nan
og_score	-0.196	nan
centroids_ra_snr	-2.407	True
centroids_dec_snr	-2.873	True

Table 3: The results of the numerical tests.

Metric	Value	Passed
snr_p_t0	10.718	True
snr_p_2t0	0.001	True
snr_2p_t0	7.218	True
snr_2p_2t0	9.796	True
snr_p2_t0	0.001	True
snr_p2_t02	1.307	True
snr_p_score	0.0	True
snr_2p_score	2.578	True
snr_p2_score	0.122	True
transit_offset_ra	291.994	True
transit_offset_dec	41.984	True
transit_offset_err	0.0	True
transit_offset_pos	0.0	False
core_flux_snr	0.532	nan
halo_flux_snr	0.385	nan
og_score	0.723	nan
centroids_ra_snr	1.284	True
centroids_dec_snr	1.272	True

Table 3: The results of the numerical tests.

Fig. 91: KIC6522967, vetting's numerical test results for the first signal (left) and the fourth (right).

As shown in Fig. 92, the source offset for both candidates seems satisfactory. The two methods are in good agreement, and the computed source is close to our actual target. This is another green flag for these candidates.

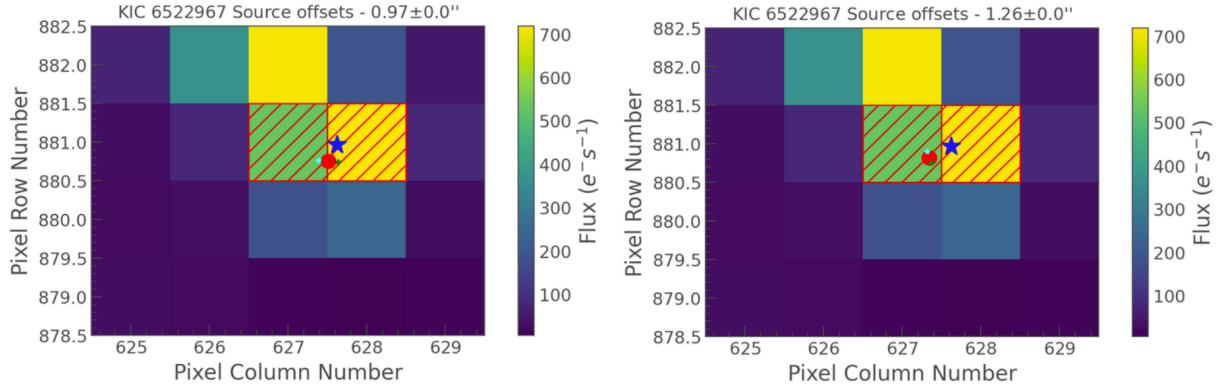

Fig. 92: KIC6522967, source offsets for the first signal (left) and the fourth (right).

Sadly, KIC6522967 was not present in the star catalog used by TRICERATOPS, and we couldn't perform the statistical validation or get the stellar neighborhood as we usually would. This forces us to stop our investigation here. None of the two candidates we discussed show any major red flags and can still be considered relatively promising.

5.13 KIC7799884 (sdB)

KIC7799884 is an sdB star observed in Q4.2 in short cadence by Kepler. I selected the first and second candidates as promising for our search in this work.

With a period of 1.74d, the first candidate was spotted in 10 detrends and in the PDCSAP flux. Values of SNR and SDE are satisfactory (SNR=11.79, SDE=8.23). Harmonics are relatively obvious in the power spectrum, especially the second, third, and fourth. However, the transit is not very deep, and the error bars in the folded light curve call for caution.

The second signal, with a period of 8.73d, was spotted in 7 detrends and the PDCSAP Flux. Values of SNR and SDE are also satisfactory (SNR=10.72, SDE=7.65). The transit is deep and quite obvious in the folded light curve. That being said, it is worth keeping in mind that the curve exhibits some variations before and after transit. The third harmonic is easily spotted in the power spectrum, while the second is less obvious.

Both these candidates seem promising enough for further investigation.

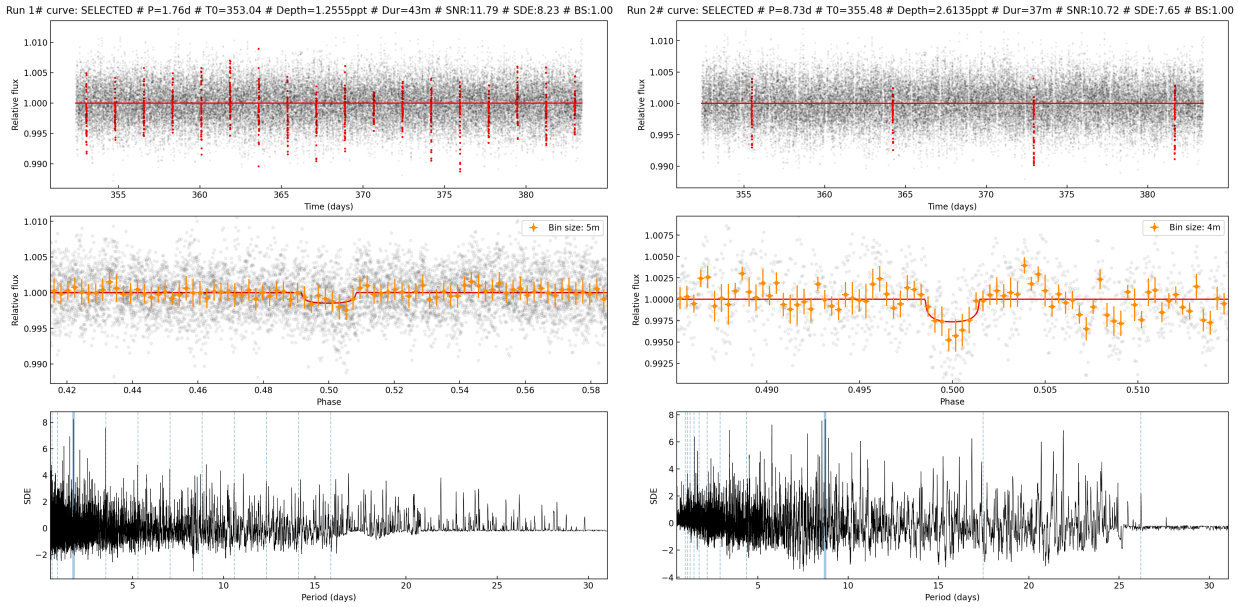

Fig. 93: KIC779984, results for the first signal (left) and the second (right).

As shown in Fig. 94, the vetting didn't raise any red flags for either candidate. AS always, the source offset has to be checked manually.

T0 (d)	Period (d)	Duration (h)	Depth (ppt)
353.0363	1.7618	0.72	1.256

Table 2: The candidate parameters.

Metric	Value	Passed
snr_p_t0	13.026	True
snr_p_2t0	0.001	True
snr_2p_t0	12.439	True
snr_2p_2t0	5.891	True
snr_p2_t0	0.001	True
snr_p2_t02	0.686	True
snr_p_score	0.0	True
snr_2p_score	6.548	True
snr_p2_score	0.053	True
transit_offset_ra	281.404	True
transit_offset_dec	43.589	True
transit_offset_err	0.0	True
transit_offset_pos	0.001	False
core_flux_snr	2.387	nan
halo_flux_snr	-0.873	nan
og_score	-0.366	nan
centroids_ra_snr	0.039	True
centroids_dec_snr	-0.698	True

Table 3: The results of the numerical tests.

T0 (d)	Period (d)	Duration (h)	Depth (ppt)
355.4841	8.7279	0.62	2.613

Table 2: The candidate parameters.

Metric	Value	Passed
snr_p_t0	7.027	True
snr_p_2t0	0.001	True
snr_2p_t0	6.024	True
snr_2p_2t0	4.407	True
snr_p2_t0	0.001	True
snr_p2_t02	0.001	True
snr_p_score	0.0	True
snr_2p_score	1.617	True
snr_p2_score	0.0	True
transit_offset_ra	281.404	True
transit_offset_dec	43.591	True
transit_offset_err	0.0	True
transit_offset_pos	0.001	False
core_flux_snr	0.096	nan
halo_flux_snr	0.217	nan
og_score	2.247	nan
centroids_ra_snr	-0.284	True
centroids_dec_snr	0.331	True

Table 3: The results of the numerical tests.

Fig. 94: KIC779984, vetting's numerical test results for the first signal (right) and the second (left).

Figure 95 shows the source offset for both candidates. The first plot might be worrying since the source is 3.93" away from our target, a shy cry from Kepler's pixel size of 3.98". So although the test is passed, the margin is still very low. Furthermore, the two methods don't agree much, creating high uncertainty. This first candidate is to be taken with a grain of salt.

The second plot is more reassuring, with a distance of only 1.85" and a much better agreement between the two methods.

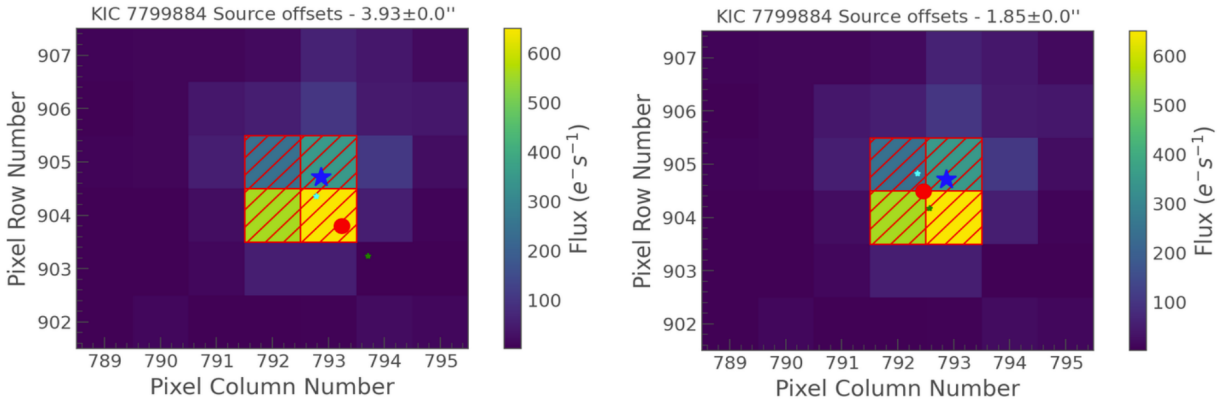

Fig. 95: KIC779984, source offsets for the first signal (right) and the second (left).

Sadly KIC779984 was not in the TRICERATOPS catalog, and the statistical validation could not be performed. Hence we have to stop our investigation here.

Overall both candidates remain relatively promising since we could not isolate any obvious reason to discard them.

5.14 KIC10961070 (sdOB)

KIC10961070 is an sdOB star observed in Q4.2 SC by Kepler. I selected the first and fourth candidates as promising in this work.

With a period of 2.19d, the first signal was spotted in 11 detrends. Values of SNR and SDE are good (SNR=12.11, SDE=7.49). It is relatively deep, with the second and third harmonics relatively easy to spot in the power spectrum, as shown in Fig. 96.

The fourth signal, with a period of 12.01 days, was spotted in 5 detrends. SNR and SDE are also satisfactory (SNR=11.84, SDE=6.45), even if the SDE is on the lower side. No harmonics can be seen in Fig. 96, which is expected for such a long-period candidate. The transit is one of the deepest we have detected, but the fact only two transits were retrieved calls for caution.

Both candidates are promising enough to be investigated further.

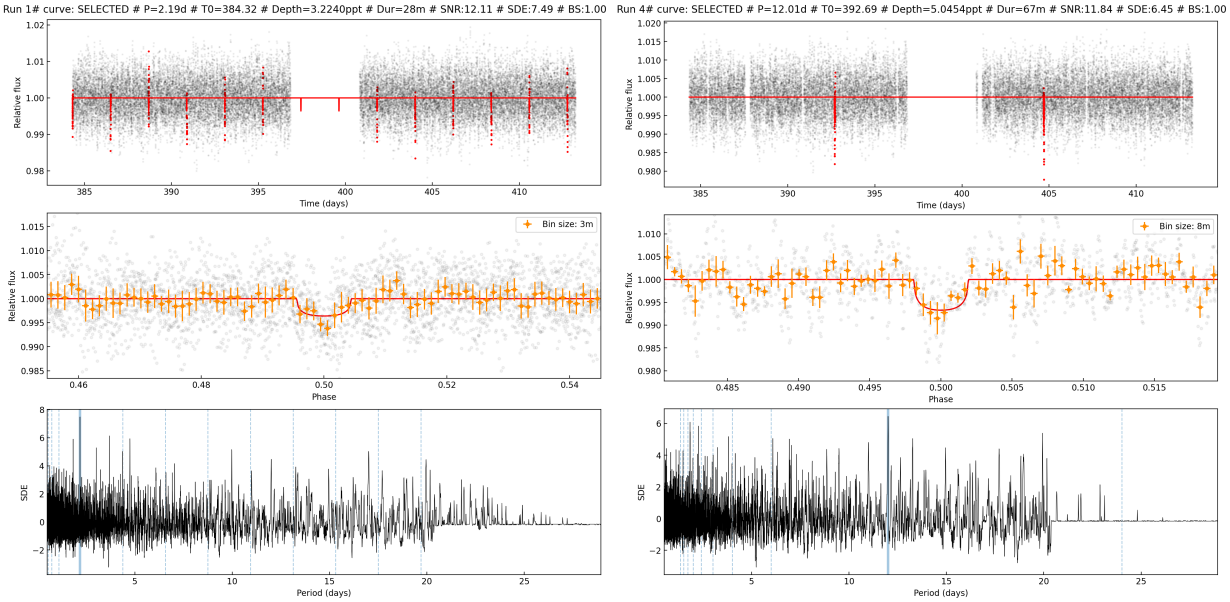

Fig. 96: KIC10961070, results for the first signal (left) and the fourth (right).

The vetting is promising for both candidates, with no red flags raised, as shown in Fig. 97

T0 (d)	Period (d)	Duration (h)	Depth (ppt)
384.3175	2.1878	0.47	3.224

Table 2: The candidate parameters.

Metric	Value	Passed
snr_p_t0	12.726	True
snr_p_2t0	0.391	True
snr_2p_t0	6.218	True
snr_2p_2t0	12.894	True
snr_p2_t0	0.391	True
snr_p2_t02	0.514	True
snr_p_score	0.031	True
snr_2p_score	6.675	True
snr_p2_score	0.01	True
transit_offset_ra	283.373	True
transit_offset_dec	48.465	True
transit_offset_err	0.0	True
transit_offset_pos	0.001	False
core_flux_snr	1.935	nan
halo_flux_snr	0.161	nan
og_score	0.083	nan
centroids_ra_snr	1.209	True
centroids_dec_snr	1.781	True

Table 3: The results of the numerical tests.

T0 (d)	Period (d)	Duration (h)	Depth (ppt)
392.695	12.0055	1.12	5.045

Table 2: The candidate parameters.

Metric	Value	Passed
snr_p_t0	9.754	True
snr_p_2t0	0.001	True
snr_2p_t0	6.382	True
snr_2p_2t0	7.392	True
snr_p2_t0	0.001	True
snr_p2_t02	0.001	True
snr_p_score	0.0	True
snr_2p_score	1.011	True
snr_p2_score	0.0	True
transit_offset_ra	283.374	True
transit_offset_dec	48.465	True
transit_offset_err	0.0	True
transit_offset_pos	0.001	False
core_flux_snr	0.145	nan
halo_flux_snr	-0.192	nan
og_score	-1.325	nan
centroids_ra_snr	1.654	True
centroids_dec_snr	0.447	True

Table 3: The results of the numerical tests.

Fig. 97: KIC10961070, numerical test results for the first signal (left) and the fourth (right).

The source offset is satisfactory for both candidates, with both computation methods in relative agreement. The source is not further away than Kepler's pixel size of 3.98", but it gets close, especially for the first candidate, whose source is 3.74" away from our target.

Furthermore, a high flux is obvious in the top left corner. This is not a bad thing, but it could hint toward contamination by a nearby star in this region. To investigate this possibility, we look at the flux per pixel to see if this region exhibits any variability that could be causing our detection.

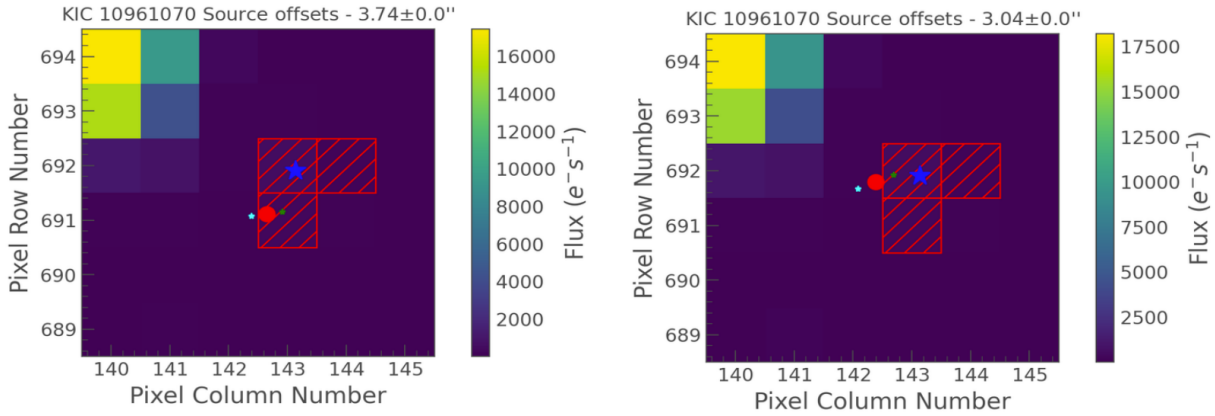

Fig. 98: KIC10961070, source offsets for the first signal (left) and the fourth (right).

Figure 99 shows the flux received for each pixel. Target pixels are highlighted in purple. This figure can easily be compared with Fig. 98, and we see that the problematic region in the top left corner doesn't exhibit any obvious variability that could impact our signals. This is a reassuring sight. Contamination from nearby stars is less likely.

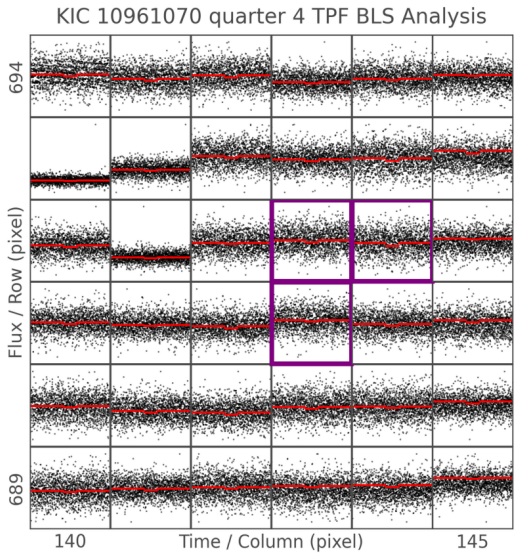

Fig. 99: KIC10961070, per pixel light curves around target

Sadly KIC10961070 is not present in the TRICERATOPS star catalog, and the statistical validation could not be performed.

These two candidates remain promising, even though further investigation would have been appreciated.

5.15 KIC5340370 (sdB+?)

KIC5340370 is an sdB star observed in Q4.2 SC by Kepler. This target exhibits unusual behavior, with a periodicity varying between 0.20 and 0.73 days in Q4.2.

This behavior was discussed in Østensen et al. 2011 [29], where a wavelet transform (WFT) was performed and can be seen in Fig. 100. In this figure, we see periodicities at around 0.55 and 0.73d in the first half of the data. They then seem to disappear and are replaced by small peaks at 0.20 and 0.23d and a strong and broad structure between 0.31 and 0.39d at the very end of this subquarter.

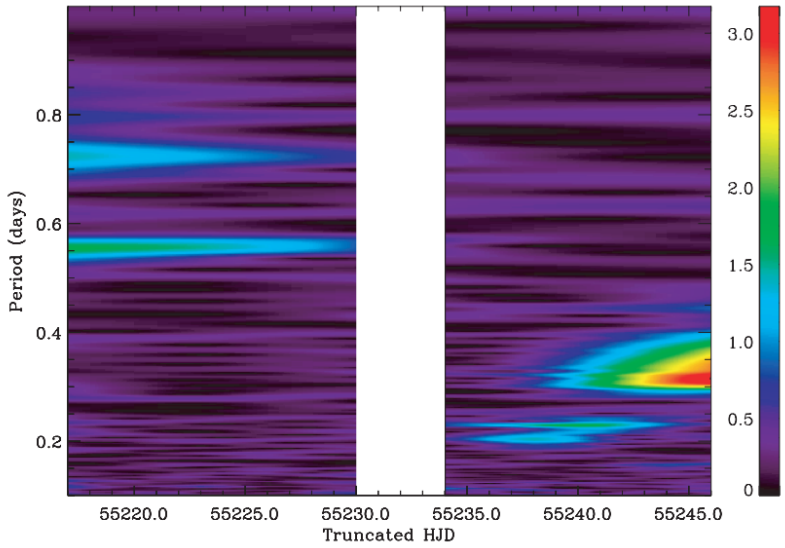

Fig. 100: KIC5340370, WFT for Q4.2 from Østensen et al. 2011

We ran SHERLOCK with the autodetrend. It removed a periodicity of 0.35d, which seems to correspond to this strong structure toward the end of the data. Note that SHERLOCK removes all period above this 0.35d value as well, so the structure at 0.55 and 0.73d are also removed, as evident in Fig. 101.

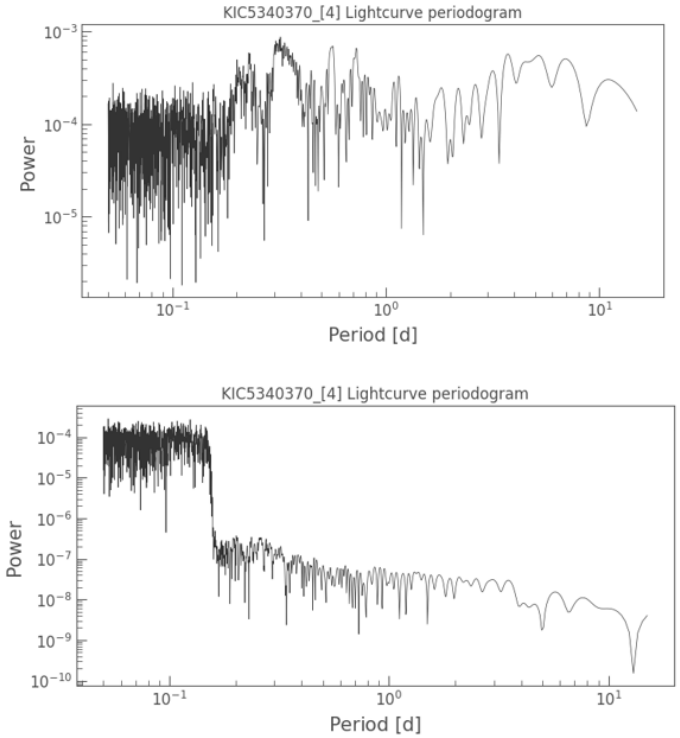

Fig. 101: KIC5340370, initial (above) and final (below) periodograms, showing the effect of autodetrend

We used Felix to investigate this behavior further in Q4 and Q10. The results seen in Fig. 102 show the same behavior for Q4, and a period of around 0.5d appears three times in Q10, for a duration of 7-8 days each time. Since this target shows this strange behavior in both quarters, we rule out an instrumental issue.

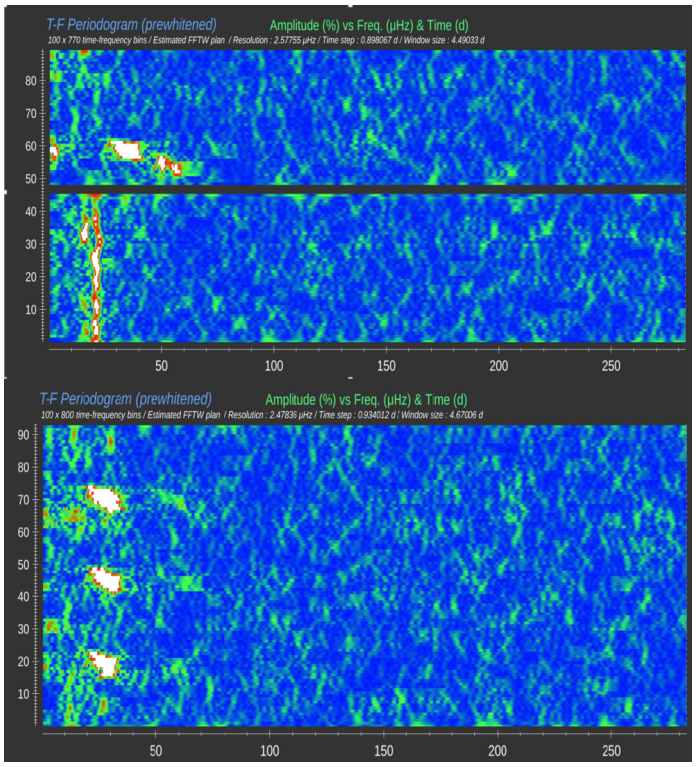

Fig. 102: KIC5340370, time-frequency plots for Q4 (above) and Q10 (below) in LC data performed using Felix. x-axis: frequency in Hz, y-axis: Time in days

After further discussions with Østensen, it appears the "sdB+?" classification is based entirely on the light curve, with no real hint of a companion in any spectra. However, a K-star companion cannot be ruled out completely. The periodic ripples seen in Q10 could be due to magnetic behavior in a K-star companion, but we would expect flares and a significant brightening, which doesn't seem to be the case here.

The nature of this behavior is, therefore, unclear as of now. Due to the unique nature of this target, any potential transit detection made in this work is to be taken with a grain of salt.

5.16 KIC8889318 (sdB)

KIC8889318 is an sdB star observed in Q2.3 SC by Kepler. SHERLOCK stopped the search after run 3 for this target, and all three selected candidates are promising enough to undergo further investigations.

With a period of 4.42d, the first candidate was spotted in 9 detrends. SNR and SDE are satisfactory (SNR=12.04, SDE=7.00) although the SDE is on the lower side. Figure 103 shows a relatively deep transit, but no obvious harmonics can be seen. It is worth noting that a subharmonic might be present at half the period, something to investigate further in the vetting.

The second signal, with a period of 5.35 days, was spotted in 8 detrends. Values of SNR and SDE are equally acceptable (SNR=12.73, SDE=6.92). The transit is about the same depth as the first signal, and the first harmonic can be spotted relatively easily. The bin size is a bit high and the resulting error bars in our folded light curve call for caution.

Finally, the third signal was spotted in 8 detrends, with a period of 3.43d. Values of SNR and SDE are also acceptable (SNR=8.41, SDE=8.13), although the SNR is on the lower side this time. The transit is easily spotted in our folded light curve and the first harmonic can be seen, even though it does not stick out.

Overall, none of these three candidates are particularly exciting, but they are all promising enough for further investigation.

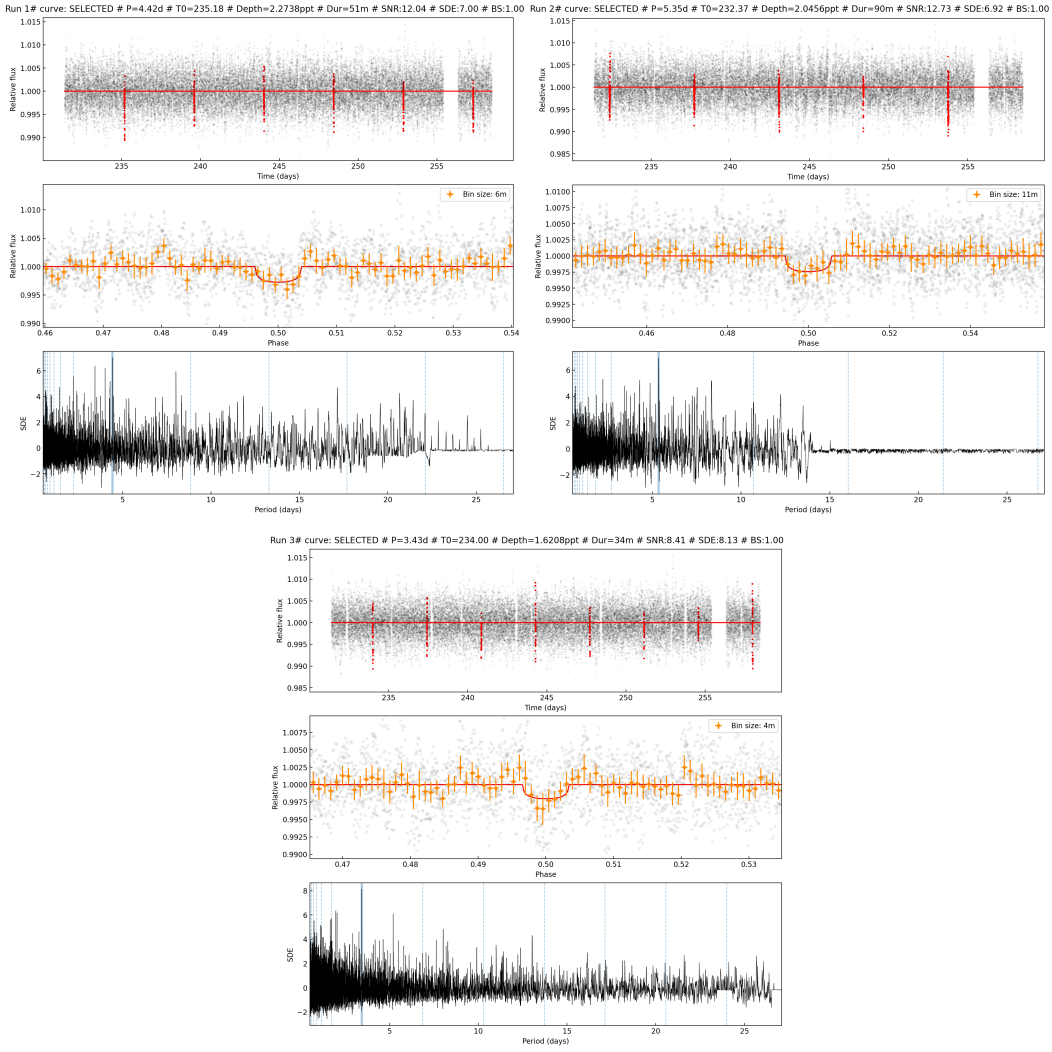

Fig. 103: KIC8889318, results for the first (top left), second (top right), and third (bottom) candidates.

The numerical tests performed during the vetting seem promising for all three candidates, as shown in Fig. 104.

T0 (d)	Period (d)	Duration (h)	Depth (ppt)
235.1826	4.4215	0.86	2.274

Table 2: The candidate parameters.

Metric	Value	Passed
snr_p_t0	12.014	True
snr_p_2t0	0.001	True
snr_2p_t0	9.999	True
snr_2p_2t0	7.735	True
snr_p2_t0	0.001	True
snr_p2_t02	0.001	True
snr_p_score	0.0	True
snr_2p_score	2.264	True
snr_p2_score	0.0	True
transit_offset_ra	293.21	True
transit_offset_dec	45.172	True
transit_offset_err	0.0	True
transit_offset_pos	0.001	False
core_flux_snr	0.587	nan
halo_flux_snr	-0.026	nan
og_score	-0.044	nan
centroids_ra_snr	0.126	True
centroids_dec_snr	1.377	True

Table 3: The results of the numerical tests.

T0 (d)	Period (d)	Duration (h)	Depth (ppt)
232.3695	5.3474	1.5	2.046

Table 2: The candidate parameters.

Metric	Value	Passed
snr_p_t0	11.705	True
snr_p_2t0	0.001	True
snr_2p_t0	10.781	True
snr_2p_2t0	4.539	True
snr_p2_t0	0.001	True
snr_p2_t02	0.001	True
snr_p_score	0.0	True
snr_2p_score	6.242	True
snr_p2_score	0.0	True
transit_offset_ra	293.211	True
transit_offset_dec	45.173	True
transit_offset_err	0.0	True
transit_offset_pos	0.0	False
core_flux_snr	0.647	nan
halo_flux_snr	-0.241	nan
og_score	-0.372	nan
centroids_ra_snr	0.385	True
centroids_dec_snr	-1.085	True

Table 3: The results of the numerical tests.

T0 (d)	Period (d)	Duration (h)	Depth (ppt)
233.9995	3.4285	0.57	1.621

Table 2: The candidate parameters.

Metric	Value	Passed
snr_p_t0	8.218	True
snr_p_2t0	0.001	True
snr_2p_t0	7.882	True
snr_2p_2t0	4.369	True
snr_p2_t0	0.001	True
snr_p2_t02	0.001	True
snr_p_score	0.0	True
snr_2p_score	3.513	True
snr_p2_score	0.0	True
transit_offset_ra	293.211	True
transit_offset_dec	45.172	True
transit_offset_err	0.0	True
transit_offset_pos	0.001	False
core_flux_snr	1.347	nan
halo_flux_snr	-0.283	nan
og_score	-0.21	nan
centroids_ra_snr	-2.249	True
centroids_dec_snr	-0.156	True

Table 3: The results of the numerical tests.

Fig. 104: KIC8889318, results for the vetting's numerical tests the first (top left), second (top right), and third (bottom) candidates.

The source offsets shown in Fig. 105 are also satisfactory. The relatively high uncertainty on the first candidate, due to the poor agreement between the two methods has to be taken into account, however. No issue arises from these source offsets for the two other candidates.

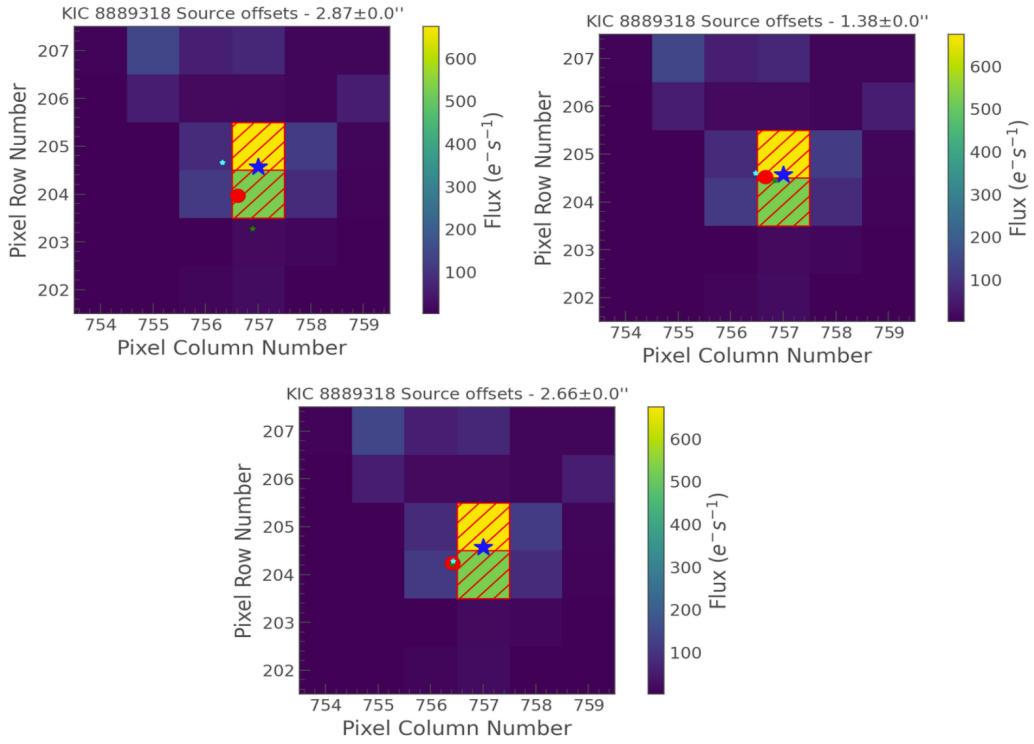

Fig. 105: KIC8889318, source offsets for the first (top left), second (top right), and third (bottom) candidates.

Sadly KIC8889318 was not in the TRICERATOPS star catalog, and we couldn't perform the statistical validation. Therefore we are forced to stop the investigation at this stage.

None of these three candidates could be formerly discarded from the aforementioned results.

5.17 KIC3527617 (He-sdOB)

KIC3527617 is an He-sdOB star observed in Q2.2 in SC data. In this work, the third signal selected by SHERLOCK will be investigated.

This third signal, with a period of 5.73d, was spotted in 9 detrends and the PDCSAP flux. SNR is on the lower side, but nothing disqualifying, and the SDE is good (SNR=9.84, SDE=9.26). The transit is relatively deep, and harmonics can be seen in the power spectrum, although not obvious (see Fig. 106).

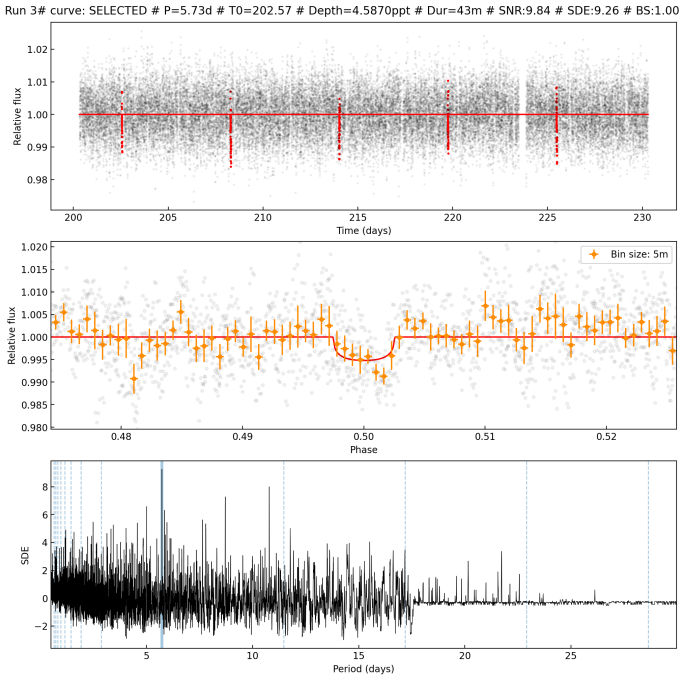

Fig. 106: KIC3527617, results for the third candidates.

The results from the vetting are satisfactory for the most part, as seen in Fig. 107, with the obvious exception of the centroids DEC SNR. Let us investigate this red flag a bit further.

T0 (d)	Period (d)	Duration (h)	Depth (ppt)
202.5689	5.7268	0.71	4.587

Table 2: The candidate parameters.

Metric	Value	Passed
snr_p_t0	11.298	True
snr_p_2t0	1.11	True
snr_2p_t0	7.869	True
snr_2p_2t0	8.098	True
snr_p2_t0	1.11	True
snr_p2_t02	0.001	True
snr_p_score	0.098	True
snr_2p_score	0.228	True
snr_p2_score	0.098	True
transit_offset_ra	285.854	True
transit_offset_dec	38.689	True
transit_offset_err	0.0	True
transit_offset_pos	0.001	False
core_flux_snr	1.643	nan
halo_flux_snr	-0.043	nan
og_score	-0.026	nan
centroids_ra_snr	-0.552	True
centroids_dec_snr	-4.621	False

Table 3: The results of the numerical tests.

Fig. 107: KIC3527617, numerical test results from the vetting

Figure 108 doesn't exhibit a clear transit shape, something we would expect in case of contamination. This red flag still calls for caution, but this alone cannot be used to fully discard our candidate just yet.

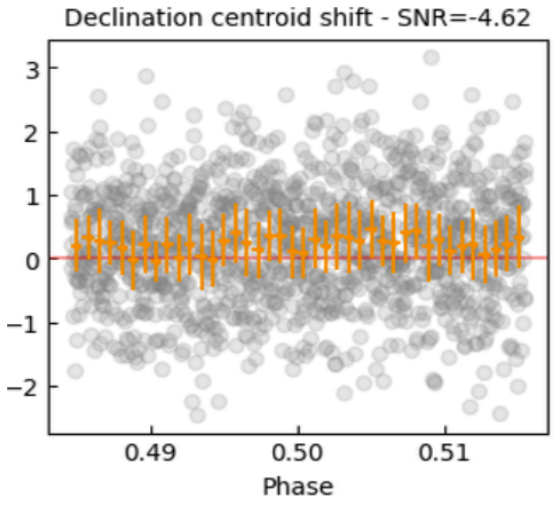

Fig. 108: KIC3527617, DEC centroid shift plot.

The source offset shown in Fig. 109 is satisfactory, the source is only 2.12" away from the target, and the two methods to compute this value seem in relative agreement. However, the higher flux in the upper region hints toward a nearby star, which could contaminate our detection.

KIC3527617 was not in the TRICERATOPS star catalog, and we could not perform the statistical validation or check bright stars around our target using this package. This forces us to stop our investigation here.

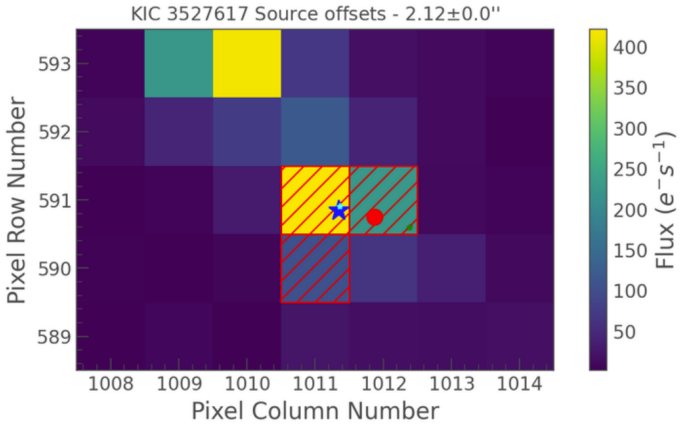

Fig. 109: KIC3527617, source offset.

Overall this candidate remains promising, with a word of caution due to the centroids,

the presence of a high flux from a close pixel, and the inability to use TRICERATOPS for further investigation.

5.18 KIC9095594 (sdB)

KIC9095594 is an sdB star observed in Q3.2, SC. I took the first selected candidate as promising.

With a period of 5.20d, this first candidate was spotted in 4 detrends. Although the number of detrends the signal was spotted in is quite low, the SNR and SDE values are good (SNR=11.33, SDE=8.10), the transit is relatively deep, and some harmonics can be seen in the power spectrum in Fig. 110. Apart from the low number of detrends in which the signal was spotted, it seems initially promising.

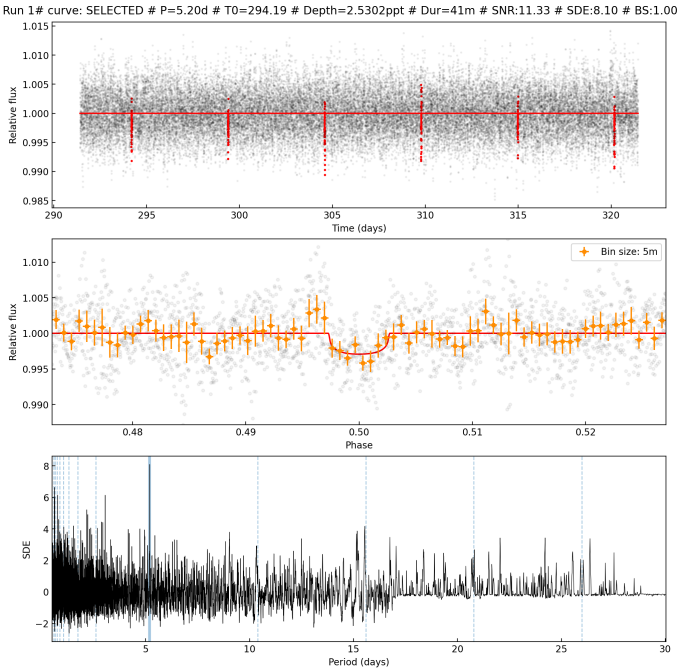

Fig. 110: KIC9095594, results for the first selected candidate

The first vetting results in Fig. 111 are also promising, with no red flags. All tests are passed with a relatively high margin.

T0 (d)	Period (d)	Duration (h)	Depth (ppt)
294.1917	5.196	0.68	2.53

Table 2: The candidate parameters.

Metric	Value	Passed
snr_p_t0	11.226	True
snr_p_2t0	0.001	True
snr_2p_t0	8.654	True
snr_2p_2t0	7.546	True
snr_p2_t0	0.001	True
snr_p2_t02	2.101	True
snr_p_score	0.0	True
snr_2p_score	1.108	True
snr_p2_score	0.187	True
transit_offset_ra	294.247	True
transit_offset_dec	45.441	True
transit_offset_err	0.0	True
transit_offset_pos	0.0	False
core_flux_snr	1.089	nan
halo_flux_snr	0.579	nan
og_score	0.532	nan
centroids_ra_snr	1.083	True
centroids_dec_snr	0.51	True

Table 3: The results of the numerical tests.

Fig. 111: KIC9095594, results for the numerical tests from the vetting

The source offset is also a green flag, as seen in Fig. 112. The source computed location is only 1.25" away from the target, on the same pixel, and both methods agree.

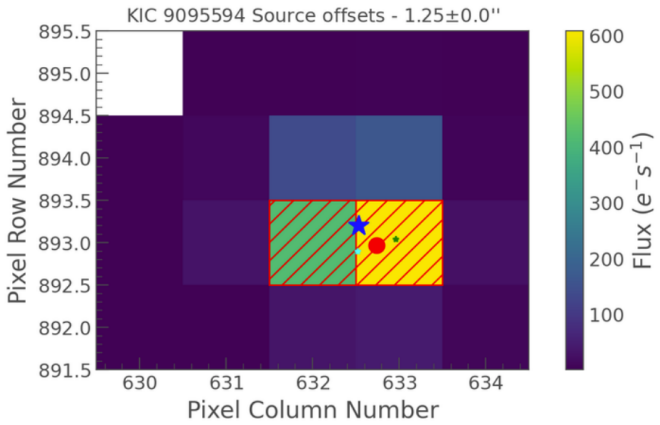

Fig. 112: KIC9095594, source offset for the first candidate

This target was not in the TRICERATOPS star catalog and could not be investigated much further. From our results, we have no reason to discard this candidate.

6 Conclusion

Throughout this work, I systematically investigated 54 hot subdwarfs, aiming to retrieve transits from close planets. Such objects could help us better understand the formation of single hot-subdwarfs, the fate of planetary systems post RGB phase and the survival of engulfed planets. Since all these questions are still open and the focus of active research fields, any such detection would prove to be an exciting step forward. It has been proved from previous injection-and-recovery tests that planets down to Earth-size and even below can be detected through the transit method on short orbital periods.

I used data from the Kepler Space Telescope to perform this search, using four years of light curves. I typically investigated a target for a quarter of 90 days or a subquarter of 30 days in short cadence. Using SHERLOCK as my main tool to search for transits, I was able to retrieve many signals, 17 of which were selected for further investigation via vetting and statistical validation. We don't have any clear candidate of a planetary transit, with the vast majority of our signals being "in-between ", i.e., not strong enough to have any certainty but not bad enough to be discarded with a valid reason. Note that the inability to use the TRICERATOPS module for some candidates restrained our interpretation of the results since the statistical validation could not be performed. Moreover, most of the targets were not bright stars (Kp >15.0), and none of our candidates could be observed from ground-based telescopes, constraining follow-up observations.

The most promising candidate from this search is from the sdB + WD binary KIC1202174. Although this signal passed every test successfully, a planet so close to such a binary system (P=3.50d for the planetary candidate) is unexpected, and this promising result is to be taken with great caution.

This work focuses on non-pulsating hot subdwarfs in Kepler's short cadence. The long cadence data were left untouched, as well as hot subdwarfs pulsators. These data are also to be investigated by any who would wish to pursue this work.

7 Thanks

First, I would like to thanks my two supervisors, Dr. Valérie Van Grootel and Dr. Francisco J. Pozuelos, for accepting me in their team and making this work possible. Their advice and patience was of tremendous help. I would also like to thank Antoine Thuillier and Martín Devora-Pajares from our team, who took time to guide me when needed. I am thankful to Mathieu Motte, who also worked in this team as a master student, for the mutual help we gave each other. Finally, I have to thank all my friends and family for their unyielding moral support which carried me through this entire project.

8 References

[1] Ulrich Heber. "Hot Subdwarf Stars". In: *Annual Review of Astronomy and Astrophysics* 47.1 (Sept. 1, 2009), pp. 211–251. ISSN: 0066-4146, 1545-4282. DOI: 10.1146/annurev-astro-082708-101836. URL: https://www.annualreviews.org/doi/10.1146/annurev-astro-082708-101836 (visited on 07/03/2023).

[2] R F Maldonado et al. "Do instabilities in high-multiplicity systems explain the existence of close-in white dwarf planets?" In: *Monthly Notices of the Royal Astronomical Society: Letters* 501.1 (Dec. 15, 2020), pp. L43–L48. ISSN: 1745-3925, 1745-3933. DOI: 10.1093/mnrasl/slaa193. URL: https://academic.oup.com/mnrasl/article/501/1/L43/6019876 (visited on 07/14/2023).

[3] E. M. Green et al. "Systematics of Hot Subdwarfs Obtained from a Large Low Resolution Survey". In: *Hot Subdwarf Stars and Related Objects*. Ed. by U. Heber, C. S. Jeffery, and R. Napiwotzki. Vol. 392. Astronomical Society of the Pacific Conference Series. Jan. 2008, p. 75.

[4] V. Van Grootel et al. "Third generation stellar models for asteroseismology of hot B subdwarf stars: A test of accuracy with the pulsating eclipsing binary PG 1336–018". In: *Astronomy & Astrophysics* 553 (May 2013), A97. ISSN: 0004-6361, 1432-0746. DOI: 10.1051/0004-6361/201220896. URL: http://www.aanda.org/10.1051/0004-6361/201220896 (visited on 08/08/2023).

[5] Zhenxin Lei et al. "New Hot Subdwarf Stars Identified in *Gaia* DR2 with LAMOST DR5 Spectra". In: *The Astrophysical Journal* 868.1 (Nov. 21, 2018), p. 70. ISSN: 1538-4357. DOI: 10.3847/1538-4357/aae82b. URL: https://iopscience.iop.org/article/10.3847/1538-4357/aae82b (visited on 07/03/2023).

[6] N. Ivanova et al. "Common envelope evolution: where we stand and how we can move forward". In: *The Astronomy and Astrophysics Review* 21.1 (Nov. 2013), p. 59. ISSN: 0935-4956, 1432-0754. DOI: 10.1007/s00159-013-0059-2. URL: https://link.springer.com/10.1007/s00159-013-0059-2 (visited on 07/31/2023).

[7] P_f.L. Maxted et al. "The binary fraction of extreme horizontal branch stars". In: *Monthly Notices of the Royal Astronomical Society* 326.4 (Oct. 2001), pp. 1391–1402. ISSN: 00358711, 13652966. DOI: 10.1111/j.1365-2966.2001.04714.x. URL: https://academic.oup.com/mnras/article-lookup/doi/10.1111/j.1365-2966.2001.04714.x (visited on 07/31/2023).

[8] S. Yu and L. Li. "Hot subdwarfs from the stable Roche lobe overflow channel". In: *Astronomy & Astrophysics* 503.1 (Aug. 1, 2009), pp. 151–163. ISSN: 0004-6361, 1432-0746. DOI: 10.1051/0004-6361/200809454. URL: https://www.aanda.org/articles/aa/abs/2009/31/aa09454-08/aa09454-08.html (visited on 07/31/2023).

[9] Icko Iben Jr. and Alexander V. Tutukov. "On the Number-Mass Distribution of Degenerate Dwarfs Produced by the Interacting Binaries and Evidence for Mergers of Low-Mass Helium Dwarfs". In: *The Astrophysical Journal* 311 (Dec. 1, 1986). ADS Bibcode: 1986ApJ...311..753I, p. 753. ISSN: 0004-637X. DOI: 10.1086/164813. URL: https://ui.adsabs.harvard.edu/abs/1986ApJ...311..753I (visited on 07/31/2023).

[10] V. Schaffenroth et al. "Two candidate brown dwarf companions around core helium-burning stars". In: *Astronomy & Astrophysics* 570 (Oct. 2014), A70. ISSN: 0004-6361,

1432-0746. DOI: 10.1051/0004-6361/201424616. URL: http://www.aanda.org/10.1051/0004-6361/201424616 (visited on 07/14/2023).

[11] Jean-Claude Passy, Mordecai-Mark Mac Low, and Orsola De Marco. "ON THE SURVIVAL OF BROWN DWARFS AND PLANETS ENGULFED BY THEIR GIANT HOST STAR". In: *The Astrophysical Journal Letters* 759.2 (Oct. 2012), p. L30. ISSN: 2041-8205. DOI: 10.1088/2041-8205/759/2/L30. URL: https://dx.doi.org/10.1088/2041-8205/759/2/L30 (visited on 07/14/2023).

[12] M. Livio and N. Soker. "Star-planet systems as possible progenitors of cataclysmic binaries". In: *Monthly Notices of the Royal Astronomical Society* 208.4 (June 1, 1984), pp. 763–781. ISSN: 0035-8711, 1365-2966. DOI: 10.1093/mnras/208.4.763. URL: https://academic.oup.com/mnras/article-lookup/doi/10.1093/mnras/208.4.763 (visited on 07/14/2023).

[13] Eva Villaver and Mario Livio. "The Orbital Evolution of Gas Giant Planets Around Giant Stars". In: 705.1 (Nov. 2009), pp. L81–L85. DOI: 10.1088/0004-637X/705/1/L81. arXiv: 0910.2396 [astro-ph.EP].

[14] Eva Villaver et al. "Hot Jupiters and Cool Stars". In: 794.1, 3 (Oct. 2014), p. 3. DOI: 10.1088/0004-637X/794/1/3. arXiv: 1407.7879 [astro-ph.EP].

[15] Eliza M. R. Kempton. "The ultimate fate of planets". In: *Nature* 480.7378 (Dec. 2011), pp. 460–461. ISSN: 0028-0836, 1476-4687. DOI: 10.1038/480460a. URL: https://www.nature.com/articles/480460a (visited on 07/14/2023).

[16] R. H. Østensen et al. "First Kepler results on compact pulsators - I. Survey target selection and the first pulsators: First Kepler results on compact pulsators". In: *Monthly Notices of the Royal Astronomical Society* 409.4 (Dec. 21, 2010), pp. 1470–1486. ISSN: 00358711. DOI: 10.1111/j.1365-2966.2010.17366.x. URL: https://academic.oup.com/mnras/article-lookup/doi/10.1111/j.1365-2966.2010.17366.x (visited on 07/20/2023).

[17] B. -Q. For et al. "KBS 13 – a Rare Reflection Effect sdB Binary with an M Dwarf Secondary". In: (2008). DOI: 10.48550/ARXIV.0809.4517. URL: https://arxiv.org/abs/0809.4517 (visited on 07/20/2023).

[18] S. Bloemen et al. "Kepler observations of the beaming binary KPD 1946+4340: Kepler observations of KPD 1946+4340". In: *Monthly Notices of the Royal Astronomical Society* (Oct. 2010), no–no. ISSN: 00358711. DOI: 10.1111/j.1365-2966.2010.17559.x. URL: https://academic.oup.com/mnras/article-lookup/doi/10.1111/j.1365-2966.2010.17559.x (visited on 07/29/2023).

[19] Jeffrey C. Smith et al. "*Kepler* Presearch Data Conditioning II - A Bayesian Approach to Systematic Error Correction". In: *Publications of the Astronomical Society of the Pacific* 124.919 (Sept. 2012), pp. 1000–1014. ISSN: 00046280, 15383873. DOI: 10.1086/667697. URL: http://iopscience.iop.org/article/10.1086/667697 (visited on 07/25/2023).

[20] Joshua N. Winn. "Transits and Occultations". In: (2010). DOI: 10.48550/ARXIV.1001.2010. URL: https://arxiv.org/abs/1001.2010 (visited on 07/25/2023).

[21] V. Van Grootel et al. "A search for transiting planets around hot subdwarfs: I. Methods and performance tests on light curves from *Kepler* , K2, TESS, and CHEOPS". In: *Astronomy & Astrophysics* 650 (June 2021), A205. ISSN: 0004-6361, 1432-0746. DOI:

10.1051/0004-6361/202140381. URL: https://www.aanda.org/10.1051/0004-6361/202140381 (visited on 03/10/2023).

[22] Francisco J. Pozuelos et al. "GJ 273: on the formation, dynamical evolution, and habitability of a planetary system hosted by an M dwarf at 3.75 parsec". In: *Astronomy & Astrophysics* 641 (Sept. 2020), A23. ISSN: 0004-6361, 1432-0746. DOI: 10.1051/0004-6361/202038047. URL: https://www.aanda.org/10.1051/0004-6361/202038047 (visited on 08/03/2023).

[23] Lightkurve Collaboration et al. "Lightkurve: Kepler and TESS time series analysis in Python". In: *Astrophysics Source Code Library* (Dec. 1, 2018). ADS Bibcode: 2018ascl.soft12013L, ascl:1812.013. URL: https://ui.adsabs.harvard.edu/abs/2018ascl.soft12013L (visited on 07/18/2023).

[24] Michael Hippke et al. "Wōtan : Comprehensive Time-series Detrending in Python". In: *The Astronomical Journal* 158.4 (Sept. 11, 2019), p. 143. ISSN: 1538-3881. DOI: 10.3847/1538-3881/ab3984. URL: https://iopscience.iop.org/article/10.3847/1538-3881/ab3984 (visited on 07/19/2023).

[25] Michael Hippke and René Heller. "Optimized transit detection algorithm to search for periodic transits of small planets". In: 623, A39 (Mar. 2019), A39. DOI: 10.1051/0004-6361/201834672. arXiv: 1901.02015 [astro-ph.EP].

[26] G. Kovács, S. Zucker, and T. Mazeh. "A box-fitting algorithm in the search for periodic transits". In: (2002). DOI: 10.48550/ARXIV.ASTRO-PH/0206099. URL: https://arxiv.org/abs/astro-ph/0206099 (visited on 07/19/2023).

[27] Steven Giacalone et al. "Vetting of 384 TESS Objects of Interest with TRICERATOPS and Statistical Validation of 12 Planet Candidates". In: *The Astronomical Journal* 161.1 (Dec. 11, 2020), p. 24. ISSN: 1538-3881. DOI: 10.3847/1538-3881/abc6af. URL: https://iopscience.iop.org/article/10.3847/1538-3881/abc6af (visited on 07/11/2023).

[28] Maximilian N. Günther and Tansu Daylan. "Allesfitter: Flexible Star and Exoplanet Inference from Photometry and Radial Velocity". In: *The Astrophysical Journal Supplement Series* 254.1 (May 1, 2021), p. 13. ISSN: 0067-0049, 1538-4365. DOI: 10.3847/1538-4365/abe70e. URL: https://iopscience.iop.org/article/10.3847/1538-4365/abe70e (visited on 07/31/2023).

[29] R. H. Østensen et al. "First Kepler results on compact pulsators - VI. Targets in the final half of the survey phase: First Kepler results on compact pulsators - VI". In: *Monthly Notices of the Royal Astronomical Society* 414.4 (July 11, 2011), pp. 2860–2870. ISSN: 00358711. DOI: 10.1111/j.1365-2966.2011.18405.x. URL: https://academic.oup.com/mnras/article-lookup/doi/10.1111/j.1365-2966.2011.18405.x (visited on 08/09/2023).

9 Annexes

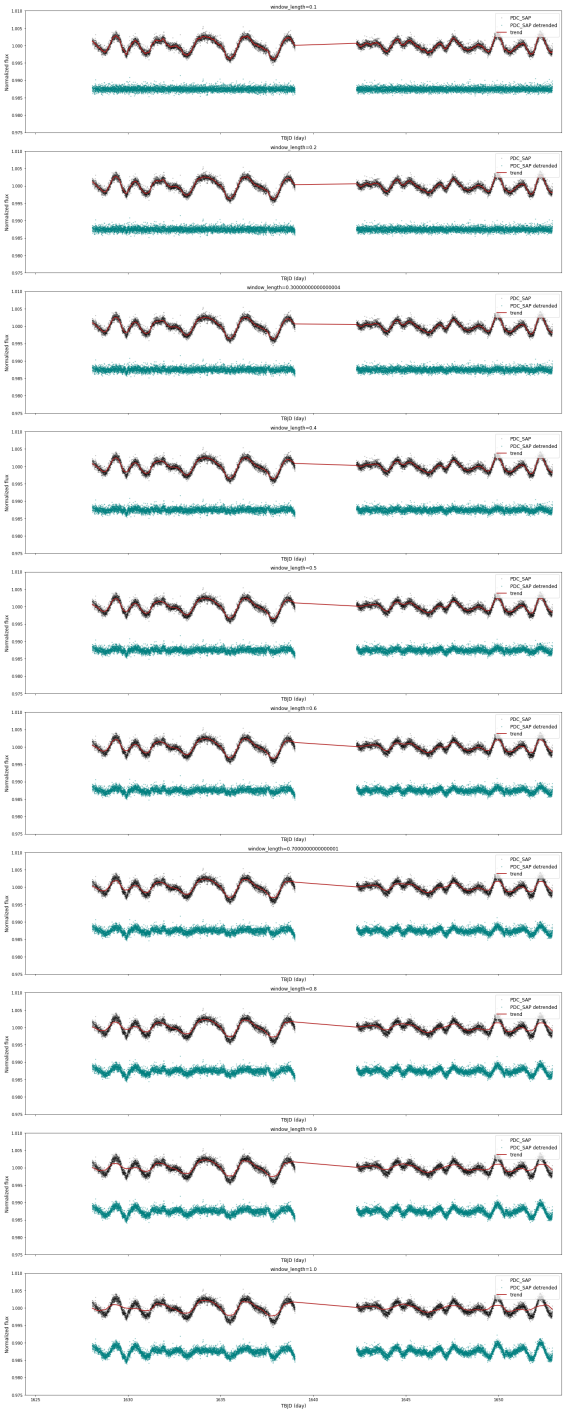

Fig. 113: Multi-detrend with increasing window size performed by SHERLOCK

Target List for sdB/sdOB stars				
KIC	Class	Kp	Data SC	Data LC
6848529	sdB+?	10.7	Q0	Q0-Q17
1868650	sdB+dM	13.4	Q1	Q0-Q17
9543660	sdOB	13.8	Q1	Q1-Q17 except Q7&Q11
10982905	sdB+F/G	14.1	Q2.1	Q2-Q10
6188286	sdOB	14.2	Q2.3	Q2, Q6-Q8, Q14-Q16
8054179	He-sdOB	14.4	Q3.1, Q6	Q3.1, Q4-Q17 execpt Q11&Q12
7975824	sdOB+WD	14.6	Q1, Q5-Q12	Q1, Q5-Q17.2
10449976	He-sdOB	14.9	Q3.2	Q3, Q5-Q9
3353239	sdB	15.2	Q4.1	Q4-Q5, Q7-Q9, Q13-Q17
10593239	sdB+F/G	15.3	Q2.3	Q2, Q5-Q17.2
2569583	sdB	15.4	Q11.2	Q11
7104168	sdB	15.5	Q3.1	Q3, Q5-Q9
10149211	sdB+?	15.5	Q4.2	Q4-Q17.2
10789011	sdOB	15.5	Q3.2	Q3, Q5-Q10
11350152	sdB+F/G	15.5	Q3.1	Q3, Q5-Q10
7434250	sdB+?	15.5	Q2.3	Q2, Q5-Q17.2
2020175	sdB	15.5	Q3.1	Q3, Q5-Q10, Q13-Q17.2
12021724	sdB+WD?	15.6	Q4.2	Q4-Q10
3343613	He-sdOB	15.7	Q3.2	Q3, Q5-Q10
5938349	sdB	16.1	Q3.2	Q3, Q10
6614501	sdB+WD?	16.1	Q3.3, Q5, Q6, Q8-Q10	Q3.3, Q5-Q17.2
9211123	sdB	16.1	Q3.3	Q3, Q5-Q10, Q13-Q17.2
9957741	He-sdOB	16.1	Q2.1	Q2, Q6-Q9
2304943	sdB	16.2	Q3.3	Q3, Q10
8496196	sdOB	16.4	Q2.3	Q2, Q6-10
8874184	sdB+?	16.5	Q4.1	Q4-Q10, Q13-Q17.2
8022110	sdB	16.5	Q2.3	Q2, Q6-Q10, Q13-Q17.2
6878288	he-sdOB+?	16.7	Q3.1	Q3, Q5-Q10
6522967	sdB	16.9	Q3.2	Q3, Q10
7799884	sdB	16.9	Q4.1	Q4.1
10462707	sdB+WD?	16.9	Q4.1	Q4.1, Q10
11400959	sdB	16.9	Q4.1	Q4.1
10784623	sdB	17.0	Q10	Q4-Q10, except Q8
10961070	sdOB	17.0	Q4.2	Q4.2
3527028	sdB+?	17.1	Q4.2	Q4-Q10
5340370	sdB+?	17.1	Q4.2	Q4, Q10
9569458	sdB	17.2	Q1	Q1
8889318	sdB	17.2	Q2.3	Q2.3, Q13-Q17.2
9408967	He-sdOB	17.2	Q2.3	Q2.3, Q10
4244427	sdB	17.3	Q2.1, Q6-Q10	Q2.1, Q6-Q17.2 except Q12
8142623	sdB+?	17.3	Q1	Q1, Q5-Q17.2
11357853	sdOB	17.4	Q2.1	Q2.1
3527617	He-sdOB	17.5	Q2.2	Q2.2
3729024	sdB	17.6	Q2.2	Q2.2
9095594	sdB	17.7	Q3.2	Q3.2
5342213	sdOB	17.7	Q2.2	Q2.2, Q14-Q16
10661778	sdB	17.7	Q2.3, Q6-Q10	Q2.3, Q6-Q17.2 except Q11&Q12

Table 4: List of sdB/sdOB targets investigated in this report.

Target List for sdO stars				
KIC	Class	Kp	Data SC	Data LC
7755741	sdO	13.7	Q1	Q1-Q17
9822180	sdO+F/G	14.6	Q2.1, Q6	Q2.1, Q6-Q10
7353409	sdO	14.7	Q2.2, Q5	Q2.2, Q5-Q9
10207025	He-sdO	15.0	Q3.3	Q3.3, Q5-Q9
7335517	sdO+dM	15.7	Q3.2, Q6	Q3.2, Q5-Q17.2
2297488	sdO+F/G	17.2	Q1	Q1
2303576	He-sdO+?	17.4	Q3.3, Q6	Q3.3, Q6-Q17.2

Table 5: List of sdO stars investigated in this work